Ministry of Higher Education and Scientific Research
Kasdi Merbah University of Ouargla
Faculty of Hydrocarbons, Renewable Energies, Earth and Universe Sciences
Department of Earth and UniverseSciences

Serial number: ……/2024

Thesis to Obtain the Master's Degree

Option: Petroleum Geology

THEME

A study and analysis of petrophysical parameters in zone 20a (Hassi Messaoud)

Presented by:
HAFIANE SID AHMED
ZIGHEM IYAD

Publicly defended on 23/06/2024
Jury members:

President :	Bensir fateh	MCA Univ. Ouargla
Supervisor :	Fellah Lahcene	MCA Univ. Ouargla
Co-supervisor :	Merad Mohamed Zakaria	PhD. St. Univ. Ouargla
Examiner :	Sahraoui salah	MCA Univ. Ouargla

Academic Year 2023-2024

DEDICACE

Last but not least, I want to thank me for believing in me. I want to thank me for doing all this hard work. I wanna thank me for having no days off. I wanna thank me for never quitting. I wanna thank me for always being a giver and trying to give more than I receive. I wanna thank me for trying to do more right than wrong. I wanna thank me for being me at all times.

Sid Ahmed Hafiane

DEDICACE

I dedicate this work to all those who guided me in my life journey and showed me the right path, to those who provided me with love, encouragement, and understanding that helped me successfully complete my studies.

To my dear family: You are the source of my courage and inspiration."

ZIGHIM IYAD

Contents

List of Figures

List of tables

General introduction

Since its first discovery, oil has played a pivotal role as one of the most important global energy sources, often referred to as "black gold." Despite ongoing efforts to reduce reliance on this fossil fuel in daily life, its dominance remains steadfast. Algeria, endowed with significant oil production capabilities, considers this resource cornerstone to economic growth and social development. Among Algeria's oil fields, the Hassi Messaoud field near the Tunisian border stands out as the country's largest oil reserve. This has garnered considerable interest, including our study focusing on analyzing petrophysical properties within Zone 20A of the reservoir.

Characterizing and correlating petrophysical properties of reservoir rocks are critical steps in justifying drilling activities by identifying potential extension areas. This knowledge is fundamental for understanding geological formations shaping the reservoir and their behavior during various drilling stages.

Our study comprises distinct parts. Initially, the theoretical section provides a comprehensive introduction to the Hassi Messaoud field, highlighting its strategic importance as an oil resource in Chapter One. Chapter Two presents a detailed structural analysis of Study Area 20A, delineating both engineering and structural characteristics of the reservoir and conducting stratigraphic and lithological studies of the area, meticulously identifying and describing its geological layers. Chapter Three focuses on evaluating specific petrophysical parameters of Zone 20A in the Hassi Messaoud reservoir, including permeability, porosity, oil saturation, and gas saturation, establishing relationships to enhance understanding of reservoir dynamics and improve oil extraction techniques.

In conclusion, our study offers valuable insights into the rock formations and their behavior through petrophysical analyses of Zone 20A in the Hassi Messaoud reservoir. These insights are essential for making informed decisions regarding planning and executing oil exploration and extraction efforts. Based on our findings, we provide recommendations aimed at improving oil recovery in this specific area. Ultimately, this study significantly contributes to enhancing knowledge about oil reservoirs, offering practical insights to support economic development and energy independence in Algeria.

Chapter 01:
GENERALITIES

Chapter 01:

Generalities

Section one: Generalities about the Hassi Messaoud field

1. Introduction

The Hassi Messaoud oil field is classified among the largest and most complex in the world. With an area of approximately 2200 km² and substantial reserves, it remains the primary oil field in Algeria. Its formation results from a complex geological and paleotectonic history, marked by several successive tectonic phases. The heterogeneous nature of the reservoir rock, both horizontally and vertically, is a consequence of its deposition process and has undergone significant diagenetic modifications throughout its structural and tectonic evolution. These include Hercynian erosion and eruptive and intrusive intra-Cambrian volcanism. The selection of this site for this study stems from several factors [1]:

1. The substantial erosion of the Cambrian Ra reservoir, situated at a high structural position within zone 20a, is a notable phenomenon.

2. Production issues have arisen due to the declining yield of older oil wells and the depletion of the reservoir, which has led to gas breakthrough problems.

Consequently, the objective of this study is to enhance production efficiency in this area by characterizing petrophysics and identifying zones of higher quality reservoirs. This will facilitate new drilling or potential conversion of old vertical wells into horizontal wells in specific reservoir zones.

1. Historical Discovery of the Field

The Hassi Messaoud oil field was discovered on January 16, 1956, by SN-REPAL, which initiated the initial drilling operation (MD1) following a refraction seismic survey on June 15 of the same year. The drilling, which reached a depth of 3,338 meters, identified Cambrian sandstones as oil producers. In May 1957, CFPA drilled a well, OM1, approximately 7 km northwest of MD1. This well confirmed the existence of the oil reservoir. The reservoir in question has a thickness of up to 200 meters and an estimated initial pressure of 482 kilograms per centimeter squared [2-4]

The Hassi Messaoud field was divided into two distinct concessions; the northern part of the field was assigned to CFPA, while the southern part was allocated to SN-REPAL [2-4].

The field commenced production in 1958 with 20 operational wells. Initially, the primary method of drainage was through the expansion of dissolved gases. However, in the present era, secondary recovery drainage is the predominant approach, achieved through the injection of water or miscible gases. Subsequently, the number of drilling operations increased significantly, particularly following the nationalization of hydrocarbons on February 24, 1971.

The Hassi Messaoud field has continued to provide Algeria with its natural resource of crude oil for nearly 48 years.

2. Field Location

The Hassi Messaoud field is recognized as one of the largest deposits in the world, forming an integral part of the Triassic province in its northern region. The field's primary attribute is its notable heterogeneity, where a uniform lithological identification has not yet been established between wells due to the presence of lithological faults.

2.1- Geographic Location (Fig.1 and 2)

The Hassi Messaoud field is situated approximately 850 km southeast of Algiers, 280 km southeast of the Hassi R'Mel gas field, and 350 km west of the Tunisian border. The area covered by the field is 2,500 km². The Lambert coordinates (LSA) for the area in question are as follows:

X	790 000 – 840 000 East
Y	110 000 – 150 000North

Figure 1:Geographic Coordinates of the Hassi Messaoud Field. (1996) [5]

Figure 2: Geological Setting of the Hassi Messaoud Field (Wec 2007). [6]

2.2- Geological Location (Fig. 2)

The Hassi Messaoud field occupies the central part of the Triassic province. With its area and reserves, it is the largest oil field in Algeria.

It is bordered by:

- Northwest by the Ouargla fields [Gellala, Ben Kahla, and Haoud Berkaoui].

- Southwest by the El Gassi, Zotti, and El Agreb fields.

- Southeast by the Rhourde El Baguel and Mesdar fields.

Geologically, it is bordered by:

- West by the Oued M'ya depression.

- South by the Amguid El Biod ridge.

- North by the Djammaa-Touggourt structure.

- East by the Dahar highlands, Rhourde El Baguel, and the Ghadamès depression.

Fig. 3 - Map of Various Basins in Algeria (Wec 2007). [6]

3- Stratigraphy of the Field (Fig3)

On the Hassi Messaoud ridge, a large part of the stratigraphic sequence is missing. Paleozoic deposits rest on a granitic basement and were eroded in the center of the structure during the Hercynian phase. Therefore, Mesozoic deposits rest unconformably on the Cambro-Ordovician. Moving away from the center towards the periphery of the field, the stratigraphic sequence becomes more complete.

From base to top, we distinguish:

3.1. Crystalline Basement

The crystalline basement is encountered at a depth of approximately 4,000 meters and is essentially formed of pink porphyroid granite.

3.2. Infracambrian

This is the oldest lithological unit encountered by drilling in the region, especially north of the structure. It consists of red clayey sandstones.

3.3. Paleozoic

Ordovician formations are only present on the periphery of the field where they have undergone differential erosion.

3.3.1. Cambrian

Mainly composed of heterogeneous sandstones, ranging from fine to very coarse, interspersed with clayey, micaceous siltstone beds. It is divided into four (04) litho-zones Ra, Ri, R2, and R3.

- **Ra litho-zone**: Composed of medium to coarse-grained feldspathic and micaceous sandstones at the base, with abundant clayey cement, admitting passes of ferruginous sandstones and silty clay.

-Ri litho-zone: Consists of medium to coarse micaceous sandstones, poorly sorted, with abundant clayey cement and intercalations of silts. Stratifications are often oblique.

- **R2 litho-zone**: Comprised of medium to coarse micaceous sandstones, poorly sorted, with abundant clayey cement, and admitting intercalations of silts. Stratifications are often oblique.

- **R3 litho-zone:**Made up of coarse-grained feldspathic and micaceous sandstones, conglomeratic at the base, with abundant clayey cement, admitting passes of ferruginous sandstones and silty clay. Stratifications are often oblique to cross-bedded, sometimes horizontal. Tigillites are present in the upper part of the series.

3.3.2. Ordovician:

Four (04) lithological units are distinguished from base to top:

- **Alternation Zone**: Characterized by the presence of numerous intercalated hardened clays alternating with fine isometric quartzite beds.

- **El-Gassi Clay:**Consists of indurated schistose clay, presenting a green to black color, rarely red. It can be glauconitic or carbonate, with a fauna (graptolites) indicating a marine deposition environment. This formation is mainly encountered on the western periphery of the Hassi Messaoud field.

- **El Atchane Sandstone**: Comprised of fine to very fine sandstones, gray-beige to dark gray. These sandstones can be clayey or glauconitic, admitting numerous clayey and silty intercalations.

- **Hamra Quartzites:**Consists of fine quartzitic sandstones, with rare clay intercalations.

3.4. Mesozoic:

It is subdivided as follows:

3.4.1. Triassic: It rests unconformably on Cambrian in the center and on the Ordovician on the flanks of the structure. It is subdivided into three (03) units:

- **Sandy Trias**: Its thickness varies from 0 to 75m. It constitutes the first filling of the Paleozoic relief and is divided into several units differing in lithology's and logging responses. It locally rests on an eruptive flow filling the deep Hercynian erosion valleys.

- **Clayey Trias:**Consists of more or less silty clays, red-brown to variegated, dolomitic and anhydritic, with layers of slightly silty and dolomitic clay.

- **Saliferous Trias**: It consists of massive salt beds with intercalations of anhydrite and slightly silty and dolomitic clay.

3.4.2. Jurassic:

Its thickness averages 340m. Jurassic consists of clayey sandstones with intercalations of limestone at the top (Malm) and alternating marine lagoon facies at the base (Dogger and Lias).

3.4.3. Cretaceous:

Its thickness averages 1670m. It is clayey sandstone at the base with marl and dolomite interbeds, becoming entirely lagoon and carbonate at the top.

3.5. Cenozoic:

Its thickness averages 360m.

Eocene:(average thickness 118m) Dolomitic limestone with flint.

- Mio-Pliocene:(average thickness 230m) Continuous sand with alternations of clay, sandy marl, dark or red-brown sandstone, and coarse sand.

ERE	SYST	ETAGES		Ep moy	DESCRIPTION
CENO-ZOIQUE	NEOGENE	MIO-PLIOCENE discordance alpine		240	Sable, calcaire, marne sableuse
		EOCENE		120	Sable, calcaire à silex
MESOZOIQUE	CRETACE	SENONIEN	CARBONATE	107	Calcaire, dolomie, anhydrite
			ANHYDRITIQUE	219	Anhydrite, marne, dolomie
			SALIFERE	140	Sel massif et traces d'anhydrite
		TURONIEN		90	Calcaire crayeux avec quelques niveaux argileux
		CENOMANIEN		145	Anhydrite, marne, dolomie
		ALBIEN		350	Grés, sable avec intercalations d'argile silteuse
		APTIEN		25	Dolomie cristalline avec niveau argileux, calcaire
		BARREMIEN		280	Argile, grés, dolomie
		NEOCOMIEN		180	Argile, marne, dolomie, grés
	JURASSIQUE	MALM		225	Argile, marne, calcaire, grés et traces d'anhydrite
		DOGGER	ARGILEUX	105	Argile silteuse, marne dolomitique avec fines passées de grés
			LAGUNAIRE	210	Anhydrite, marne dolomitique, marne grise
		LIAS	L.D 1	65	Dolomie, anhydrite, argile
			L.S 1	90	Alternances sel, anhydrite et argile
			L.D 2	55	Anhydrite et dolomie cristalline
			L.S 2	60	Alternances sel et argile
			L.D 3	30	Alternances de dolomie et de marne
	TRIAS	SALIFERE	TS 1	46	Alternances de sel, d'anhydrite et de dolomie
			TS 2	189	Sel massif à intercalations d'anhydrite et argile gypsifère
			TS 3	202	Sel massif et traces d'argile
		ARGILEUX		113	Argile rouge dolomitique ou silteuse injectée de sel et d'anhydrite
		GRESEUX		35	Grés, argile
		ERUPTIF discordance hercynienne		0-92	Andésites altérées
PALEOZOIQUE	ORDOVICIEN	QUARTZITES D'EL HAMRA		75	Quartzites fines avec traces de tigillites
		GRES D'EL ATCHANE		25	Grés fins à ciment argileux, bitumineux
		ARGILES D'EL GASSI		50	Argiles schisteuses, vertes ou noires, glauconieuses à graptolithes
		ZONE DES ALTERNANCES		20	Alternance de grés et argile. Présence de tigillites
	CAMBRIEN	Ri		50	Grés isométriques, fins, silteux
		Ra		120	Grés à grés quartzitiques anisométriques à niveaux de silts
		R2		100	Grés moyens à grossiers à ciment argileux illitique
		R3		300	Grés grossier à ciment argileux, argile silteuse
	INFRA-CAMBRIEN			45	Grés argileux rouges
SOCLE					Granite porphyroïde rose

Fig. 4 - Description of the Sedimentary Series [7].

4- Historical Structuring of the Field

The structure of the Hassi Messaoud field appears as a vast flattened anticlinal dome, with a general NE-SW direction. The faults affecting the reservoir are of two types:

- Faults of N.NE - S.SO sub-meridian directions and others perpendicular faults of NO-SE direction, emphasizing the Horst and Graben tectonic character.

- Faults without displacement, which had a significant effect on the reservoir fracturing.

4.1. Structuring of the Hassi Messaoud Field

The structural evolution of the field is the result of several tectonic phases that can be summarized chronologically as follows:

4.1.1. Ante-Triassic Structuring

- Panafrican Phase: This phase, compressive in an E-W direction, resulted from a continental collision between the rigid West African craton and the plastic East African block. It was followed by intense erosion leading to a paleo-plain called the intra-tassilian surface. This marked the end of a major basement tectonic phase. At the Cambrian-Ordovician boundary, there was a change from compressive to distensive regime, with a NO-SE direction, causing normal faulting and volcanic activity. This resulted in tectonic instability of the Cambrian-Ordovician sequences.
- Early Caledonian Phase: Approximately 500 million years ago, this phase was characterized by the transgression of isometric sandstones (Ri) known on the field's flanks after the reservoir (Ra) deposition.
- Caledonian Phase: Around 400 million years ago, this phase is regionally recognized by the absence of Devonian and Carboniferous sediments over the entire El Biod high plateau surface.
- Hercynian Phase: Dated from 225 to 280 million years ago, this phase caused a significant NE-SW directional bulge accompanied by faulting of the same orientations, compartmentalizing the reservoir into blocks with their own behavior (Horst, Graben). There was erosion of the entire Paleozoic cover above the reservoir and radial arrangement of large erosion valleys. During this phase, there was a tightening in the NW-SE direction, perpendicular to the major faults.

4.1.2. Post-Triassic Structuring

The effects of this phase are relatively weak and correspond to only 50 to 100m of structural closure (2950-3050m). These deformations are accompanied by a 200m northwestward tilt between the SE and NW parts, which occurred during the Mesozoic.

The N-S closure is much more significant than the E-W closure and could be due to movements in the Eocene, an Atlas tectonic phase with a NNO-SSE compression direction.

- Austrian Phase: Dated approximately 100 million years ago, this phase involved an E-W shortening, accentuating structural closure and causing fractures along ancient faults, which likely reactivated.
- Atlas Phase: This phase, with a NNE-SSW compression direction, occurred after hydrocarbon formation, likely causing permeability barriers due to reservoir level shifts.

4.1.3. Current Structuring:

This structuring shows a closure of 300m between the edges and the top of the reservoir. It is compressive with N-S shortening and has undergone slight epeirogenic readjustment. The current structuring has a general NE-SW elongation and shows local culminations with amplitudes of several hundred meters; the known fault throw does not exceed 70 to 80 meters.

5- Cambrian-Ordovician Reservoir

5.1. Reservoir Subdivision

5.1.1. Introduction

According to data from CFP (A) and SN.REPAL [3,4,8]:, the Cambrian-Ordovician reservoir has been subdivided into drainage units based on well logs (Gamma Ray, Neutron) and petrophysical criteria.

5.1.2. Description of Drains and Drain Concept

The drain concept refers to sedimentological, log, and reservoir quality data, characterizing reservoir petrophysical properties both vertically and horizontally. "Drain" refers to loosely cemented zones that coincide with the three preferred reservoir zones.

- Drain D1 (R170 - R200): Composed of coarse sandstones with dominant, well-defined, and often micro-conglomeratic trough cross-bedding at the base, with an absence of Tigillites.

- Inter Drain ID (R150 - R170): Represents a very gradual transition between D1 and D2, thinner with a greater abundance of silty levels, sometimes accompanied by local Tigillites.

- Drain D2 (R140-R150): Well-sorted coarse sandstones with dominant tabular cross-bedding, forming megabeds, with intercalations of silt levels accompanied by fine bioturbation.

- Drain D3 (R130-R140): Corresponds to the middle fine part of the Homer, characterized by finer grain size, abundance of silty beds and fine grains with numerous bioturbations (especially Tigillites).

- Drain D4 (R100-R130): Represents the upper coarse part of the Homer, with sandstones presenting abundant tabular cross-bedding forming megabeds. Its significant thickness variation is due to significant facies variations. Its westward development is caused by the progradation of an estuarine environment (formation of tidal sandbars).

- Drain D5: This marine depositional environment is characterized by significant lateral continuity of silts, composed of finer and better-sorted materials than Ra, with frequent Tigillites bioturbations. Stratifications are often horizontal.

According to sedimentological subdivision according to Homer (1967) [9]:

- Lower coarse zone or Lower Ra (R190-R140): This zone shows remarkably uniform thickness, ranging from 78m to 86m on average. It can be subdivided into three coarse masses (G1, G2, G3), with respective thicknesses of 30m, 8 to 12m, and 24 to 28m. G2 is often surrounded by several meters of coarse sandstones accompanied by silty passes.

- Middle fine zone or Middle Ra (R140 - R130): This zone has a less coarse grain size than the Lower Ra, with numerous silty intercalations.

- Upper coarse zone or Upper Ra (R 130 - R95): This zone, with variable thickness often affected by erosion, is similar to the Lower Ra in terms of materials.

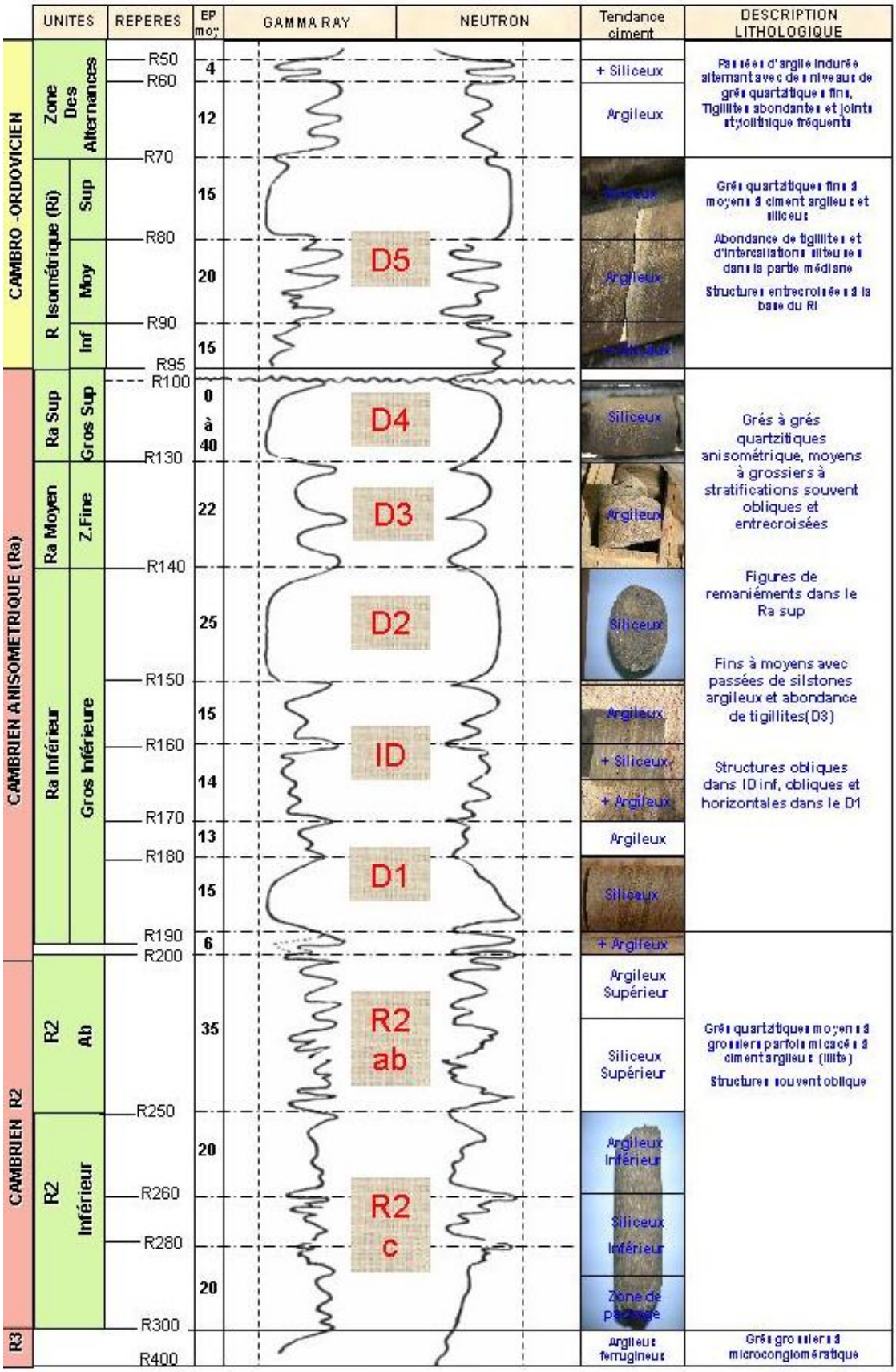

Fig. 5- Cambrian Drainage Division of Hassi Messaoud [10].

6- Depositional Environments

Sedimentological studies comparing the sedimentary series of Hassi Messaoud with those outcropping in the Tassili reveal that Cambrian deposits are characterized by a regular succession of detrital cycles ranging from very coarse levels at the base to clayey-sandy facies of the Ri.

The sands of Ra and R2 are distinguished by their coarse grain size, granulometry, and oblique and cross-bedded stratifications. These deposits are typical of braided fluvial sedimentation, where phases of sandy input are interrupted by calm periods with clayey-silty facies, which filled topographic irregularities. Conversely, the finer intercalations of the middle Ra, with their frequent clayey-silty and Tigillites layers, suggest shallow marine sedimentation.

The coarse zone of Ra exhibits sedimentation instability, with oscillations between a fluvial regime (micro-conglomeratic sandy deposition) and a shallow marine regime. The isometric sands of the Ri reflect shallow marine sedimentation characterized by a calm hydrodynamic regime.

A study conducted by BEICIP in 1995 suggests that the Cambrian deposition at Hassi Messaoud occurred in three phases [11]:

- Infilling by R3 deposits under a proximal high-energy regime.
- A phase characterized by unidirectional "channels" extending several meters, typical of a fluvial environment.
- A phase typical of shallow marine sedimentation, characteristic of the Ri.

7- Geometry of Sand Bodies

Detailed field studies conducted by the IFP along the entire Hoggar border have defined the deposition mode and geometry of the Cambrian sands. The litho-elementary unit, called a "channel," consists of a set of centimeter-thick sheets arranged obliquely, which is a characteristic of the Cambrian.

Obliquely stratified sands are predominant and extend only a few tens of meters. Their extension is controlled by the particular shape of these "channel" sand bodies, as well as by erosion processes occurring after their emplacement.

These stratifications are often interrupted by impermeable clay-silt discontinuities. At these discontinuity levels, coarser sands devoid of stratifications are frequently observed.

8- Source Rock and Deposition Genesis

8.1. Source Rock

Silurian:

Silurian clays constitute the source rock, the hydrocarbon-generating source, on the scale of the entire Saharan platform. These black, carbonate-rich and radioactive clays are organic-rich, with a thickness generally ranging between 20 and 70 meters. The present organic matter is mainly amorphous, and the presence of Tasmanian confirms its marine origin, thus highlighting its petroleum potential.

It is currently established that after the dissipation of hydrocarbons generated in the Paleozoic, a second, more significant generation phase occurred, ending at the end of the Cretaceous due to subsidence reduction.

The Silurian is preserved north of the Hassi Messaoud field, as well as west (in the Oued Mya basin), southwest (in the Moydir basin), and east (in the Ghadames basin). These preserved areas play a crucial role as potential hydrocarbon sources in the region [6,12].

Section two: Section two: characteristics of the "zone 20a" study area

1- Introduction

Zone 20a is positioned intermediate between the center and the periphery of the Hassi Messaoud field. Its boundaries with neighboring zones are not clearly defined from a structural perspective. The southeast boundary seems to correspond to the MD55-MD272 Graben and is affected by a main fault crossing the field from southwest to northeast.

In terms of production, this zone is in a depletion phase. The reservoir pressure ranges from 110 kg/cm² to 320 kg/cm². Hence, it is subject to a pressure maintenance program through gas injection.

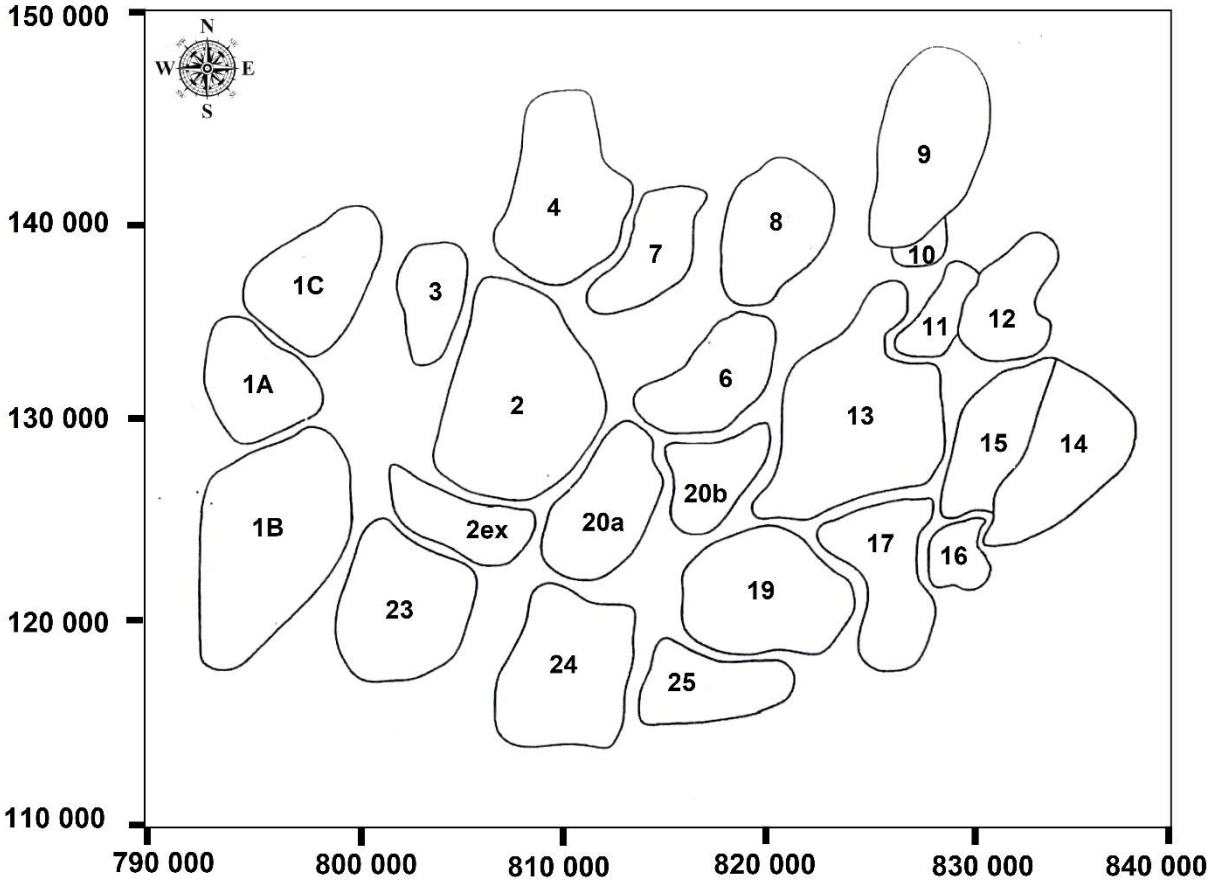

Fig.6: Representation of the different production zones of the Hassi Messaoud field (WEC2007) [6]

2- Geographic Location

Zone 20a is located on the Hassi Messaoud field with the following coordinates, according to the Lambert South Algeria (LSA) projection system:

Xmin: 808625 Ymin: 117813

Xmax: 816575 Ymax: 128839

Zone 20a is bounded by (Fig. 6):

• Zone 6 and Zone 2 to the north.

• Zone 24 to the south.

• Zone 20b, 19 to the east.

• Zone 2ex, 2 to the west.

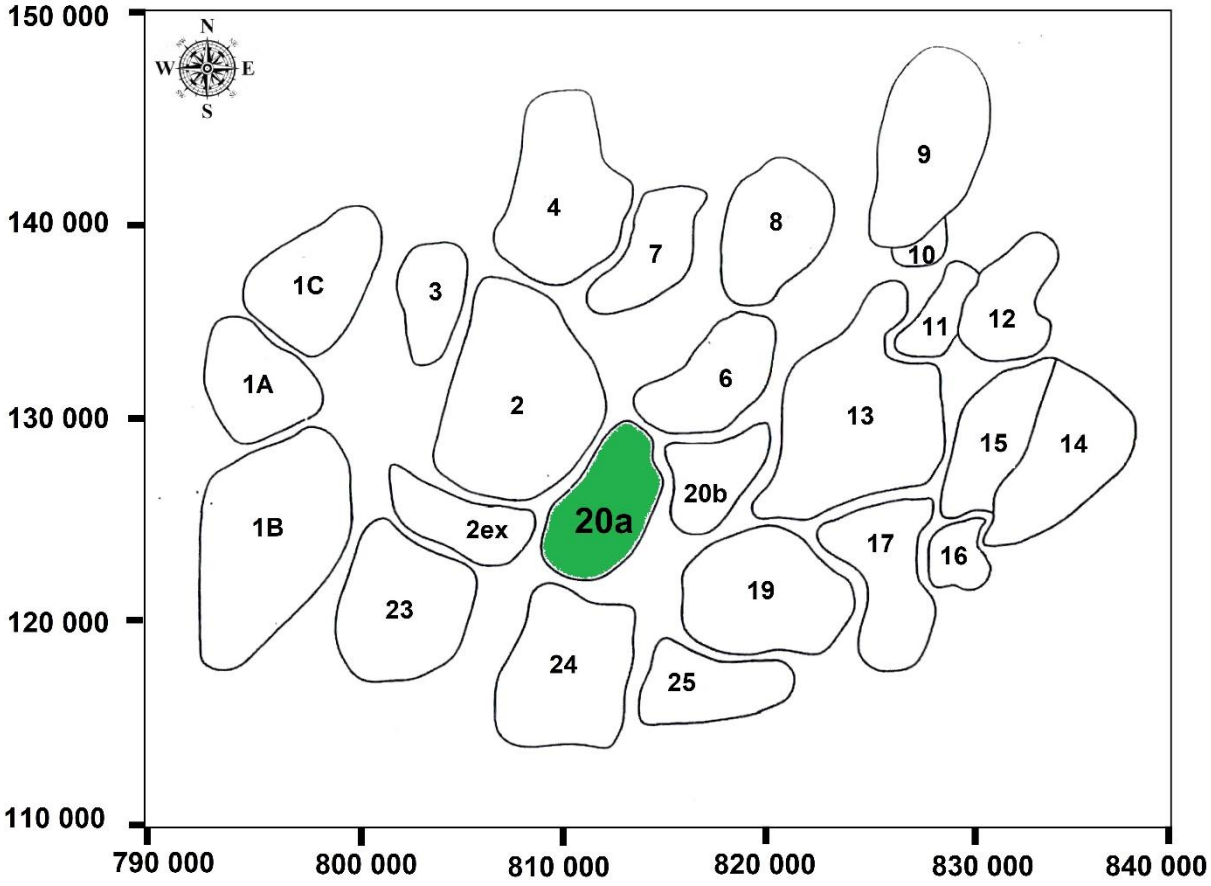

Fig.7 Geographical location of Zone 25 [6]

3- Geological Setting

3.1 Structural and Tectonic Aspects

Zone 20a does not correspond to a single structural entity. It is situated on both sides of the major fault oriented North 30 degrees, which traverses the field from southwest to northeast. The northern half of Zone 20a is thus located on the high side of the fault and corresponds to the southern end of the horst oriented North 120 degrees, affecting Paleozoic series. Conversely, the southern half of Zone 20a and Zone 20b are situated at the foot of this major fault.

This zone is affected by several faults of different directions and magnitudes:

- A major regional fault oriented northeast - southwest with a throw of 10 to 20 meters.
- Two low throw faults oriented southwest - northeast passing through the center of the zone.
- A sub-meridional fault intersecting the two preceding faults.

At the level of the discordance surface, the geological cross-section revealed the presence of deep erosion valleys, crossing Zone 20a from northeast to southwest along its central part. The magnitude of erosion varies from the south where Drain D5 is partially present, to the north where Drains D3 and D2 outcrop at the surface of the Hercynian discordance. There is also the presence of eruptive valleys affecting the reservoir, notably in the southwest.

The drains involved in the reservoir of Zone 20a are mainly Drains D2, ID, D1, and R2ab, encountered by 98% of the wells. Drains D5 and D4 are only present in the south of the zone and are crossed respectively by 9% and 17% of the wells. Drain D3 is present in the south and center of the zone, crossed by 39% of the wells.

3.2 Interpretation of Structural Maps

- Isobaths at the top of the Hercynian Unconformity (Fig. 9):

The structural map clearly highlights the uplifted part of the major fault located on the north side and the depressed part on the south side of the fault. Erosion valleys are also visible to the southwest, south, and southeast, generally following the axis of the faults.

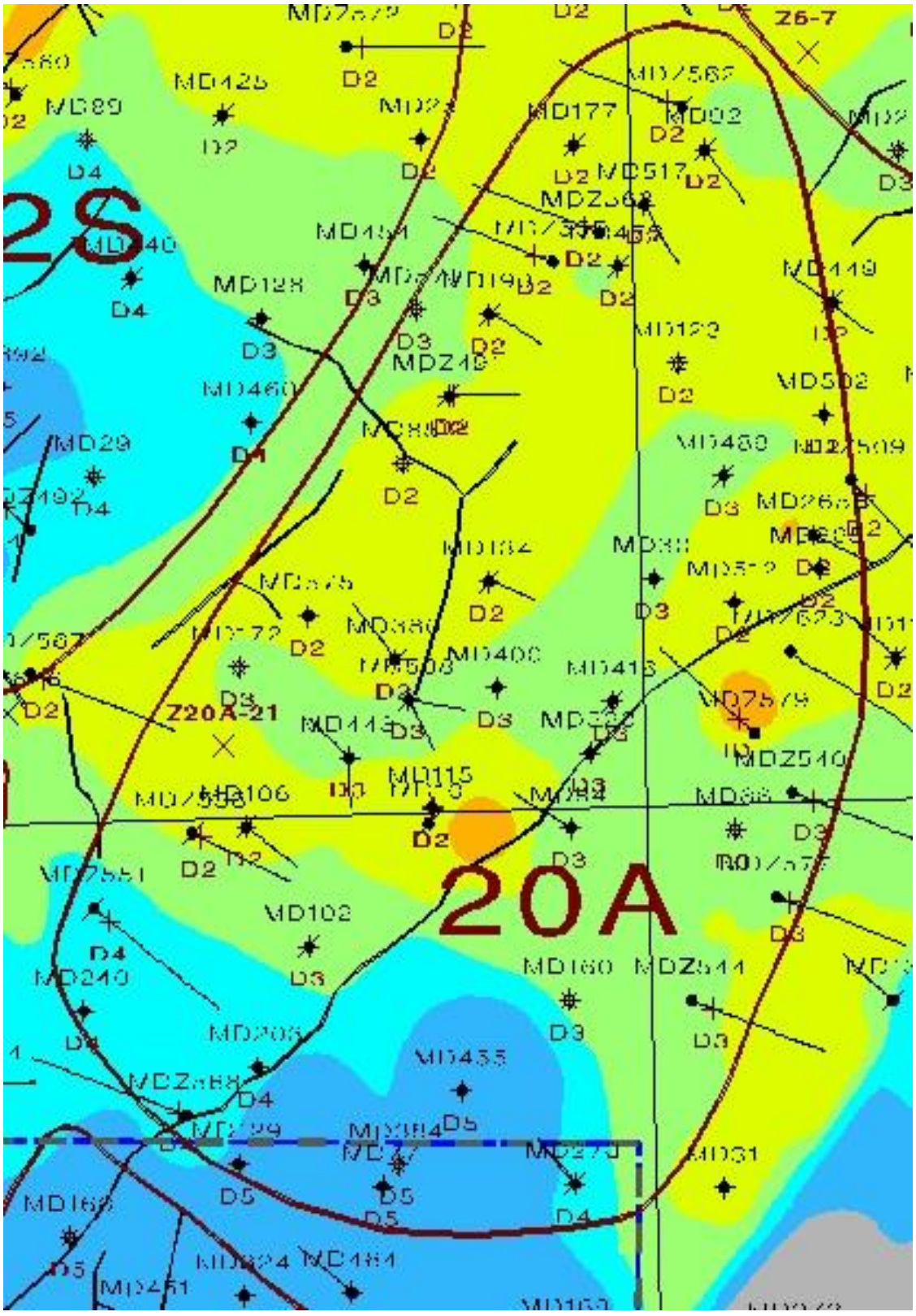

Fig. 8. Geological cross-section at the Hercynian unconformity. [13]

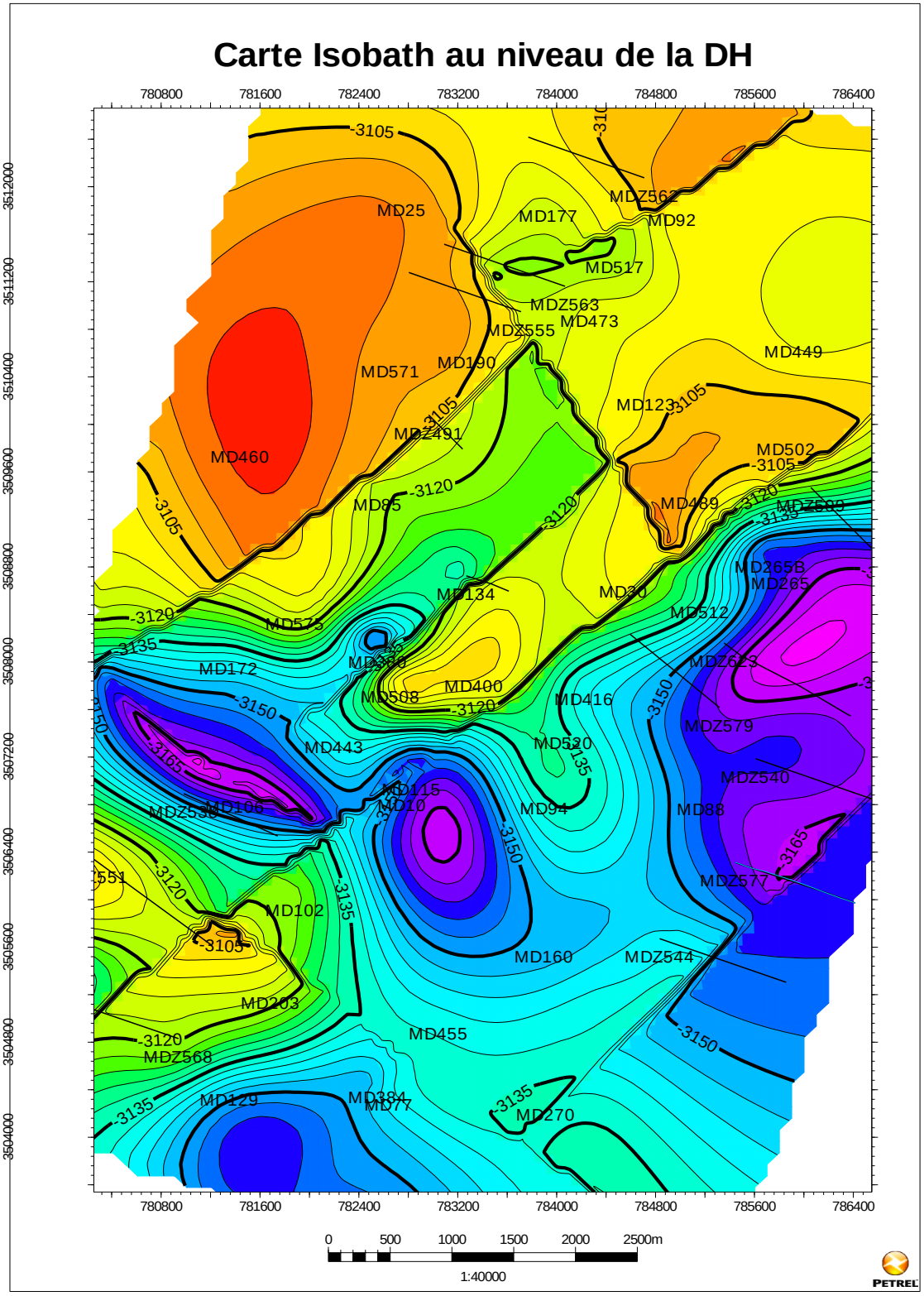

Figure 8. Geological cross-section at the Hercynian unconformity. [13]

- Isobaths at the top of Drain D1 (Fig. 10):

The configuration of the reservoir in Zone 20a is depicted by the top of Drain D1, as this area has not been eroded. The cartographic representation at this top level (see Fig. 11) reveals a flattened structure north of the elevated part of the main fault, with a southwest-oriented inclination. In the area of the fault that has been depressed, the structure exhibits a southward inclination. In the upper reaches of the drains, the original structural configuration is obscured by the effects of erosion, which have reached the ID.

- Structural cross-sections through zone 20a:

North - South Section (Fig. 11)

This figure illustrates the flattened nature of the structure to the north of the uplifted side of the major fault where the structure has undergone maximum erosion. In the southern part of the fault where the structure has been less affected by erosion, it dips in the same direction, i.e., towards the south.

Cross-section analysis:

This cross-section, cutting across zone 20a from east to west, shows the existence of 03 structural blocks in this direction. The structural dip is not very pronounced.

3.3 Structural Position of The Water Level (SW=65%):

The precise determination of the water level is essential for the optimal exploitation of hydrocarbon reserves. In zone 20a, four wells have reached the SW=65% surface, marking the beginning of the transition zone. These wells are as follows: MD134, where this surface was reached at a depth of 3401m (or -3239m in absolute elevation); MD380, at 3467m (or -3289m in absolute elevation); MD571, at 3436m (or -3270m in absolute elevation); and MD575, at 3476m (or -3296m in absolute elevation). Therefore, it is estimated that the SW=65% surface would be at an average elevation of approximately -3273m.

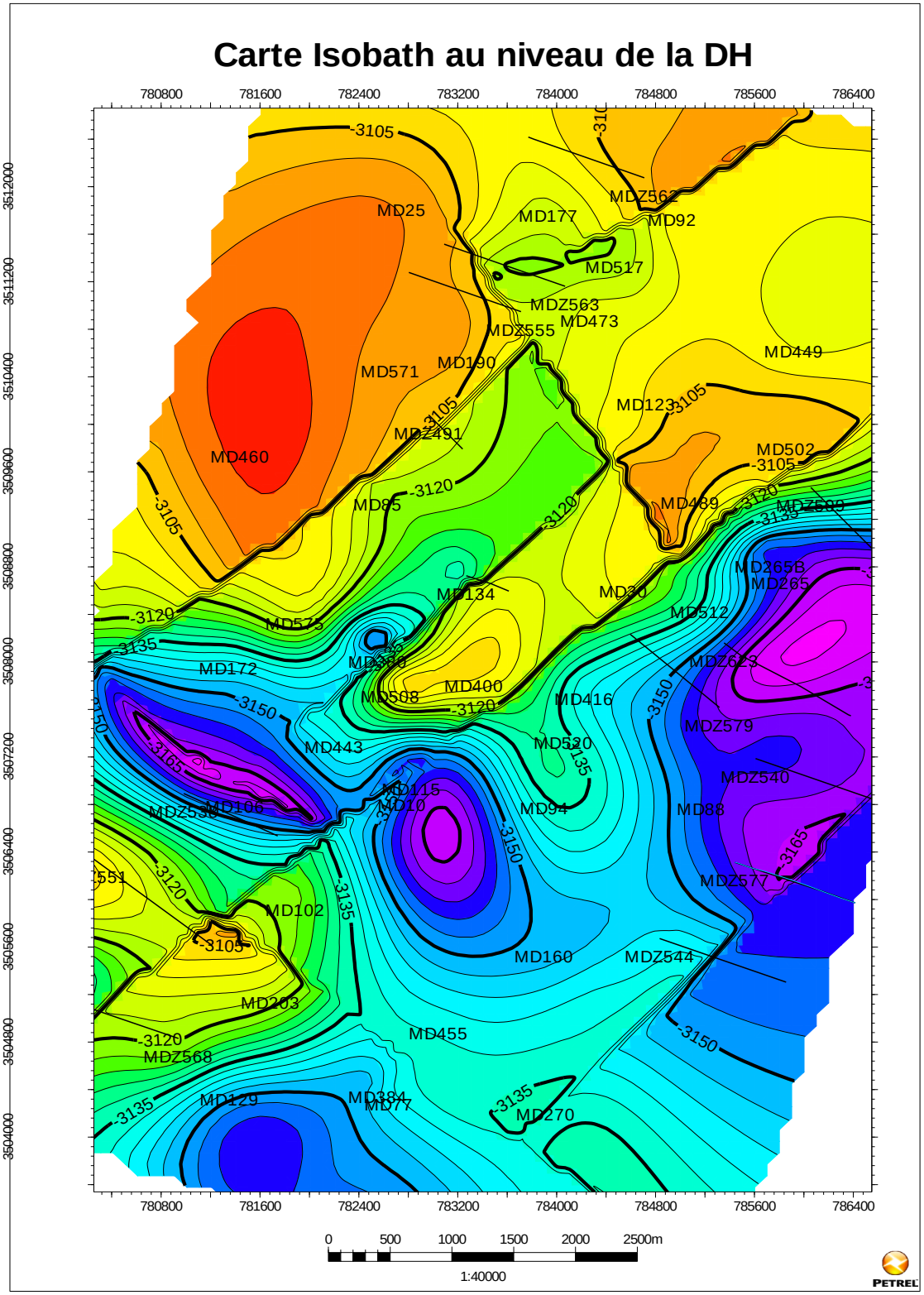

Fig. 9. Isobaths at the top of the Hercynian Unconformity.

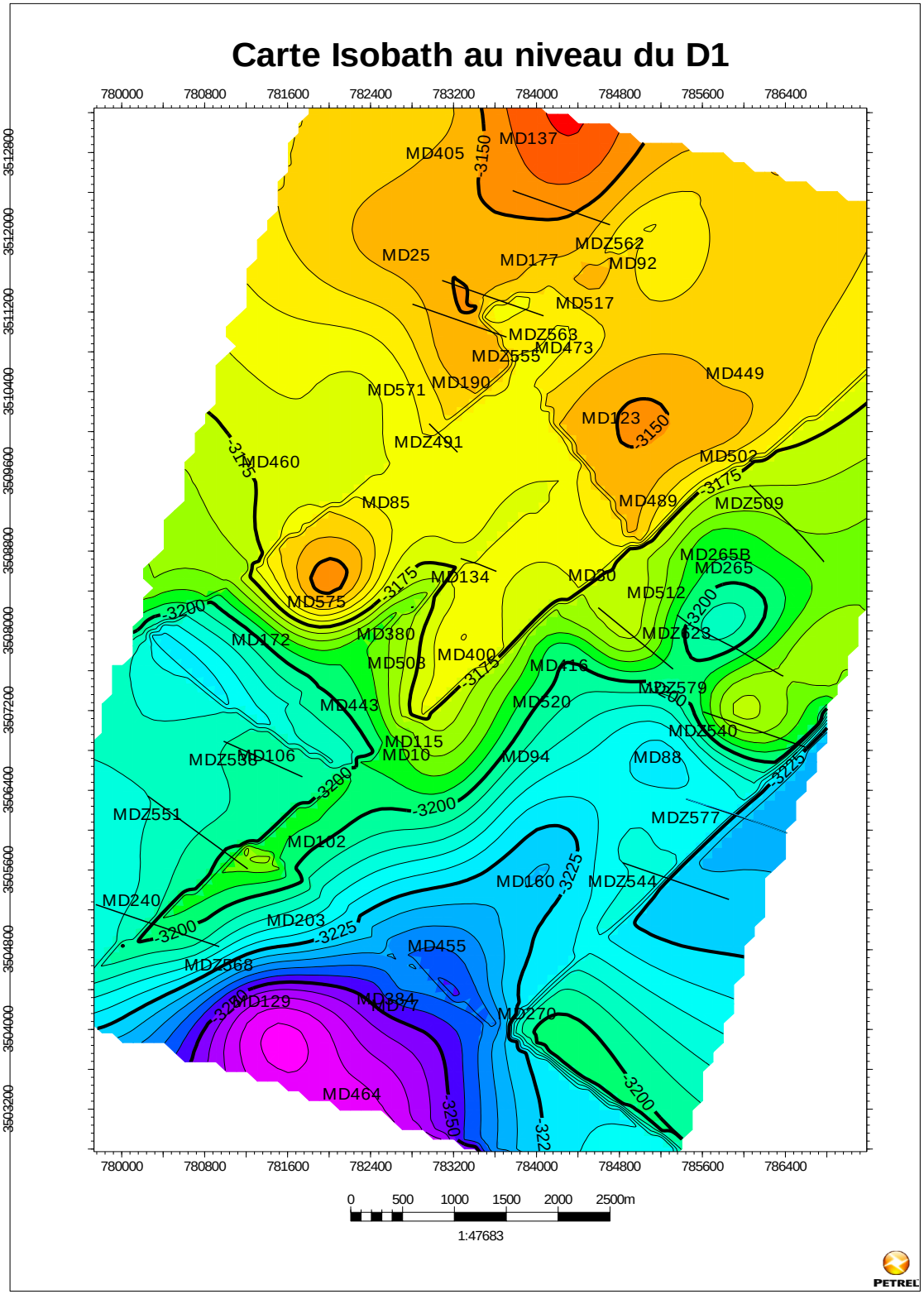

Fig.10. Isobaths at the top of Drain D1.

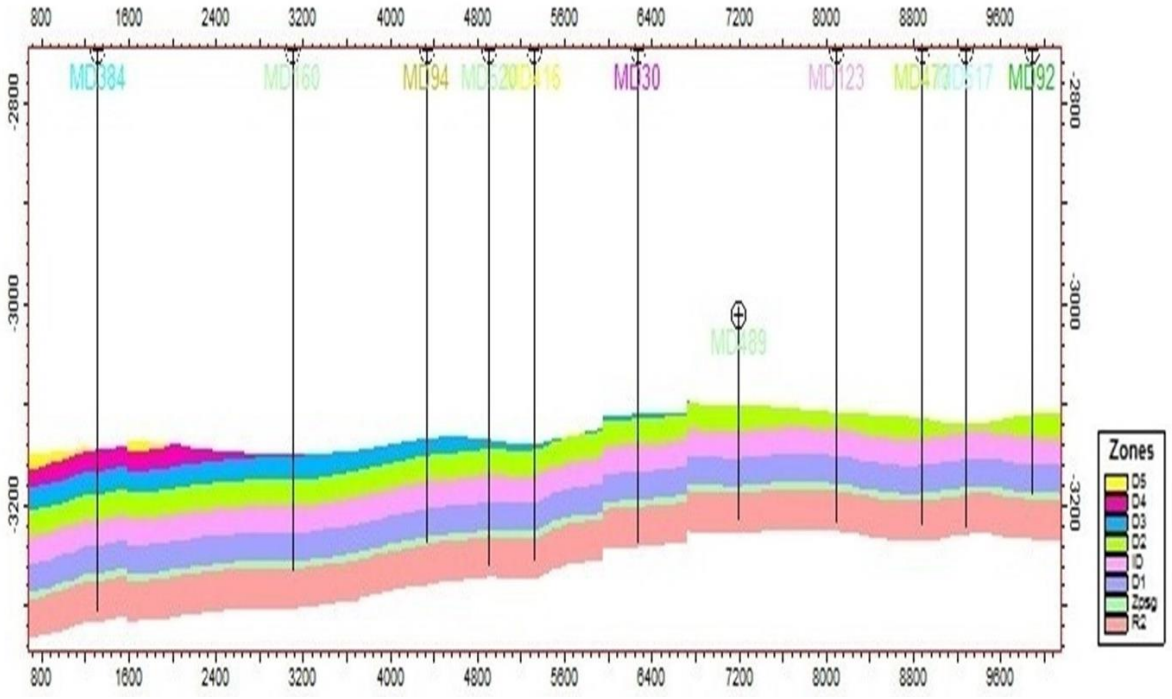

Fig. 11. North-South cross- section.

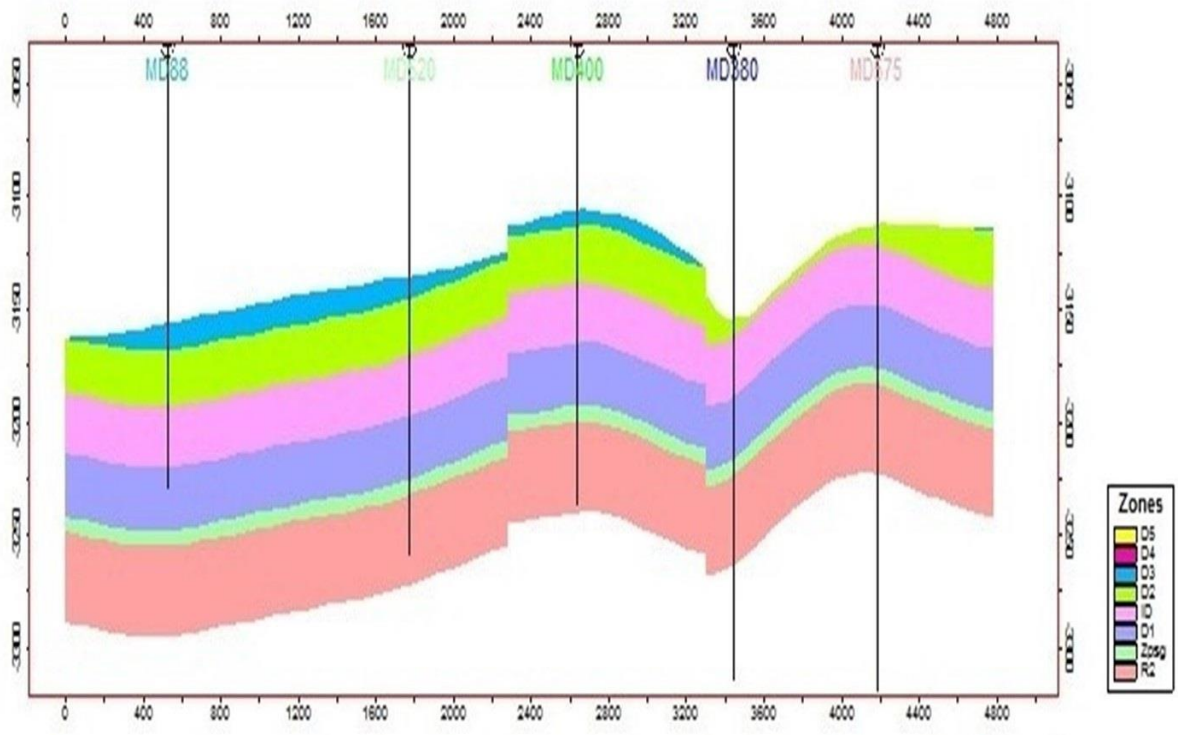

Fig. 12.NW-SE cross- section.

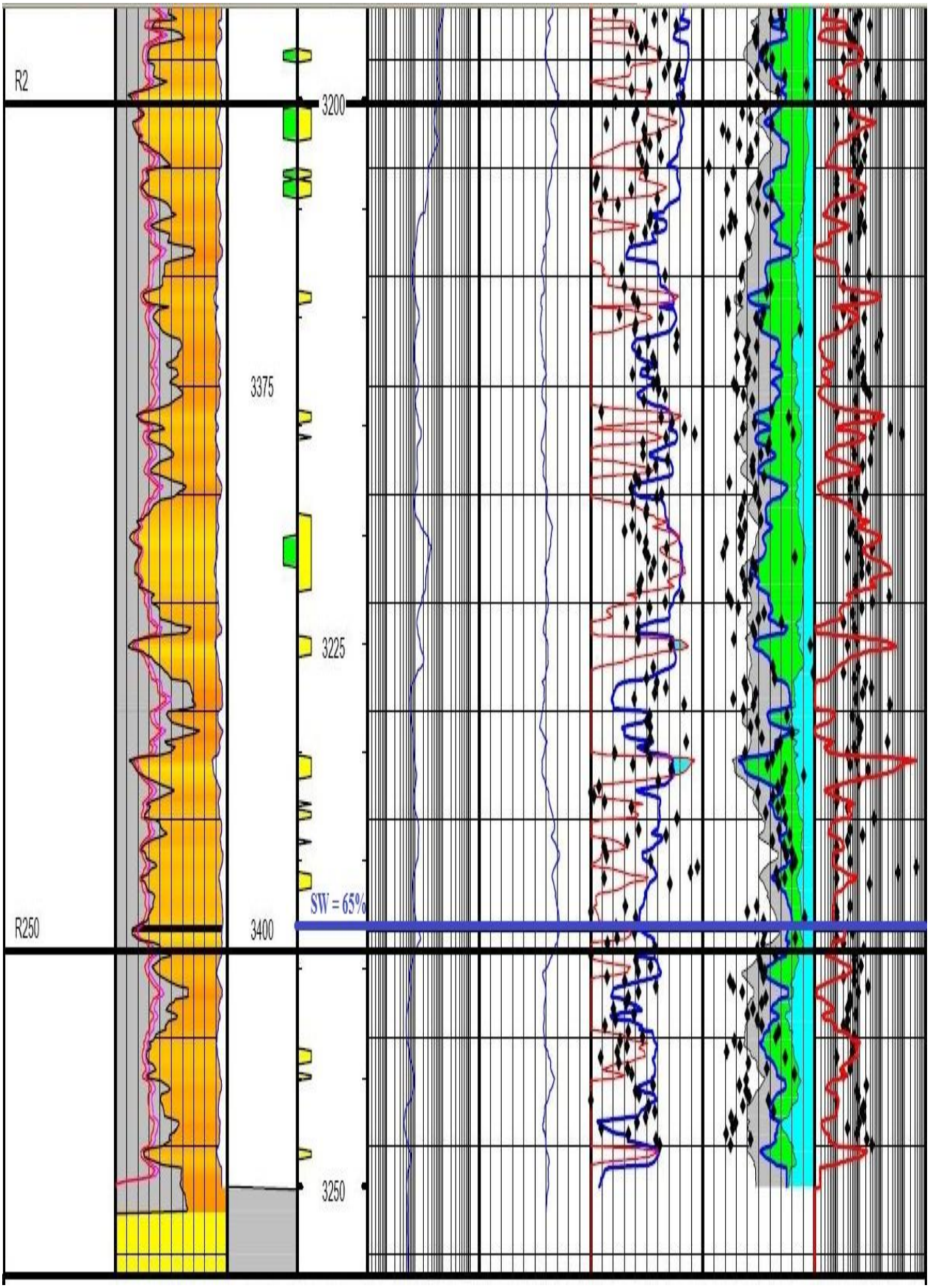

Fig.13. MD134.

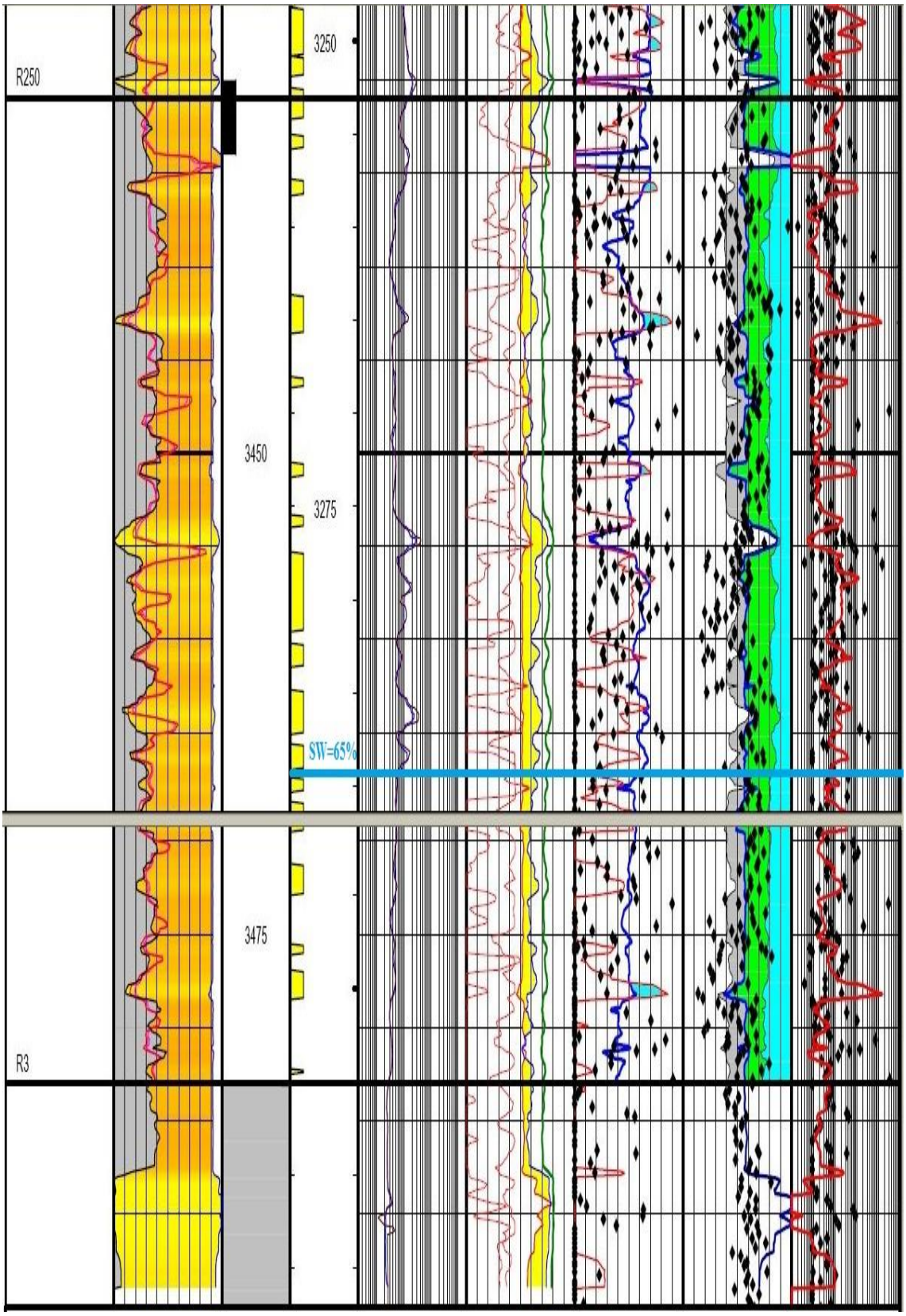

Fig.14. MD380.

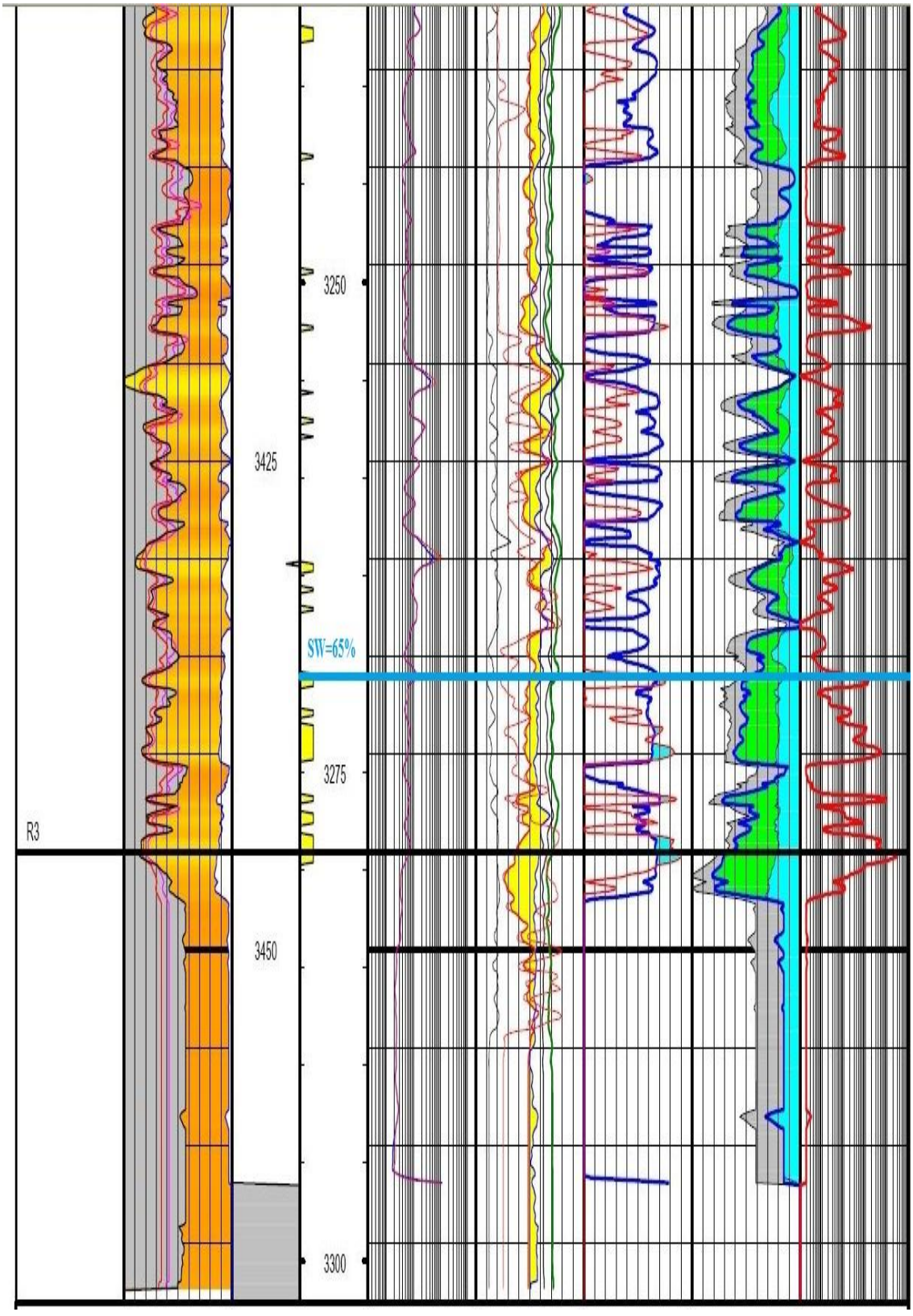

Fig.14. MD571

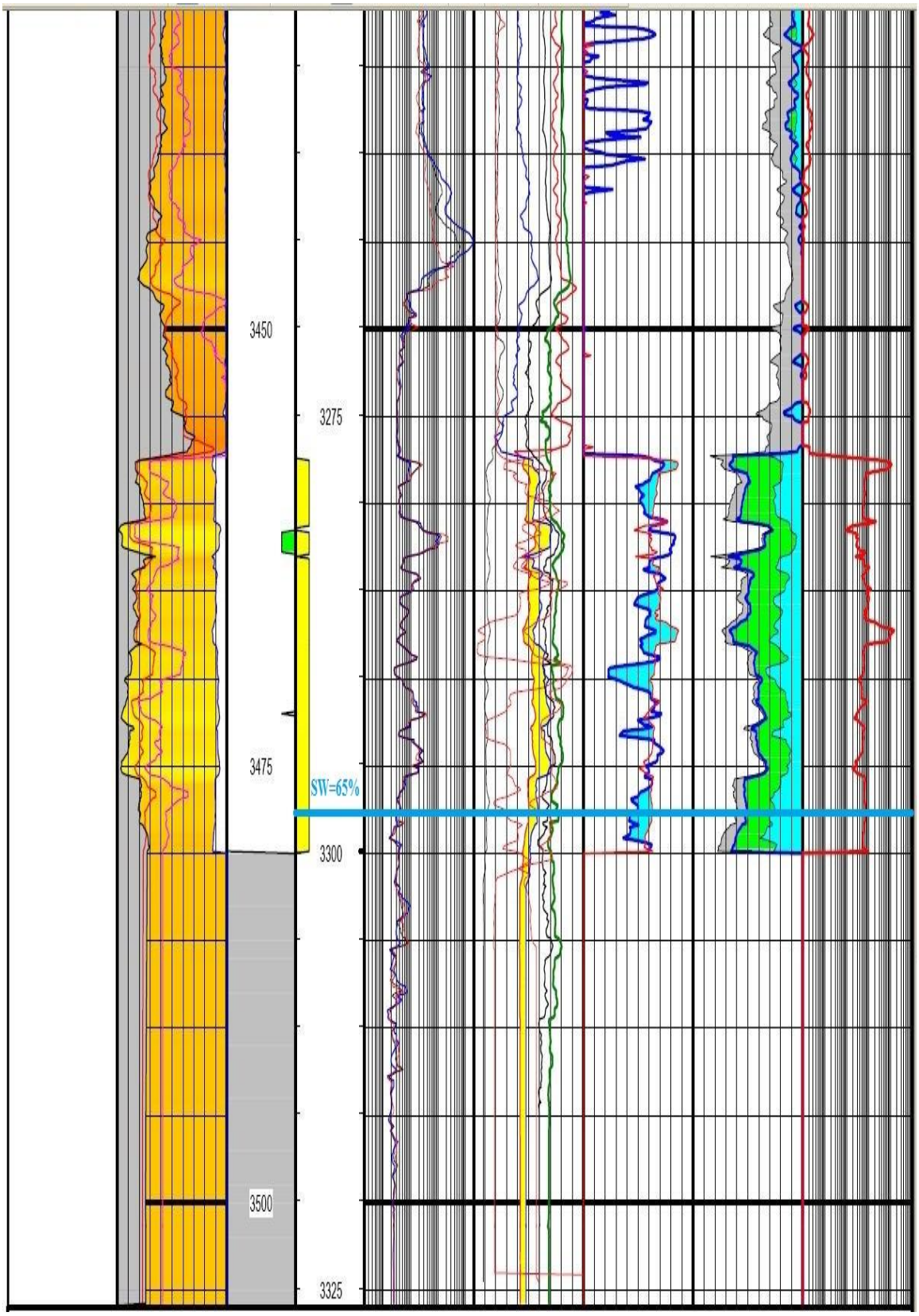

Fig.15. MD575.

4- Stratigraphy:

Due to their reservoir characteristics, thickness, and the number of wells that have intersected them, the main drains constituting the reservoir in this zone are as follows, from bottom to top:

- R2ab: Considered as a secondary reservoir, it has been encountered by 79% of the boreholes. Its thickness varies from 6m on MD270 to 86m on MD380 and 89m on MD575, with an average penetration of 31m. It consists of coarse sandstone with micro-conglomerates, sub-angular, with abundant illitic clay cement and generally present oblique stratifications.

- Drain D1: Not affected by erosion, its average thickness is 30m, and it has been intersected by 98% of the boreholes in this zone. It consists of coarse sandstone with dominant arched oblique stratifications, often micro-conglomeratic at the base. The transition zone thickness is included in that of D1.

- Inter-Drain (I-D): Crossed by all wells in zone 20a, its average thickness is 28m. It constitutes a progressive transition between D1 and D2, with a greater abundance of silty levels and locally traces of tigillites.

- Drain D2: Encountered by 98% of the wells, it consists of well-sorted coarse sandstone with dominant tabular oblique stratifications, forming megaplates and marked by intercalation of silt levels with fine bioturbations. Its average thickness is 24m.

- Drain D3: Crossed by 39% of the wells, it has an average thickness of 24m. Composed of fine to medium well-sorted sandstone, it is characterized by the abundance of silt beds and bioturbations, with generally sub-horizontal stratifications.

- Drains D4 and D5: Represented minimally in zone 20a, their presence is very localized, mainly in the extreme south of the zone. D4 is recognized in 17% of the wells with a thickness of 11m, while D5 is identified in 9% of the wells with a thickness of 9m.

Diagraphic Correlations:

NW-SE Correlation (Fig. 15):

This correlation across zone 20a highlights the progressive erosion evolution from SE to NW, consequently to the structural uplift observed in the same direction. Laterally, no thickness variation was observed on the drains unaffected by erosion.

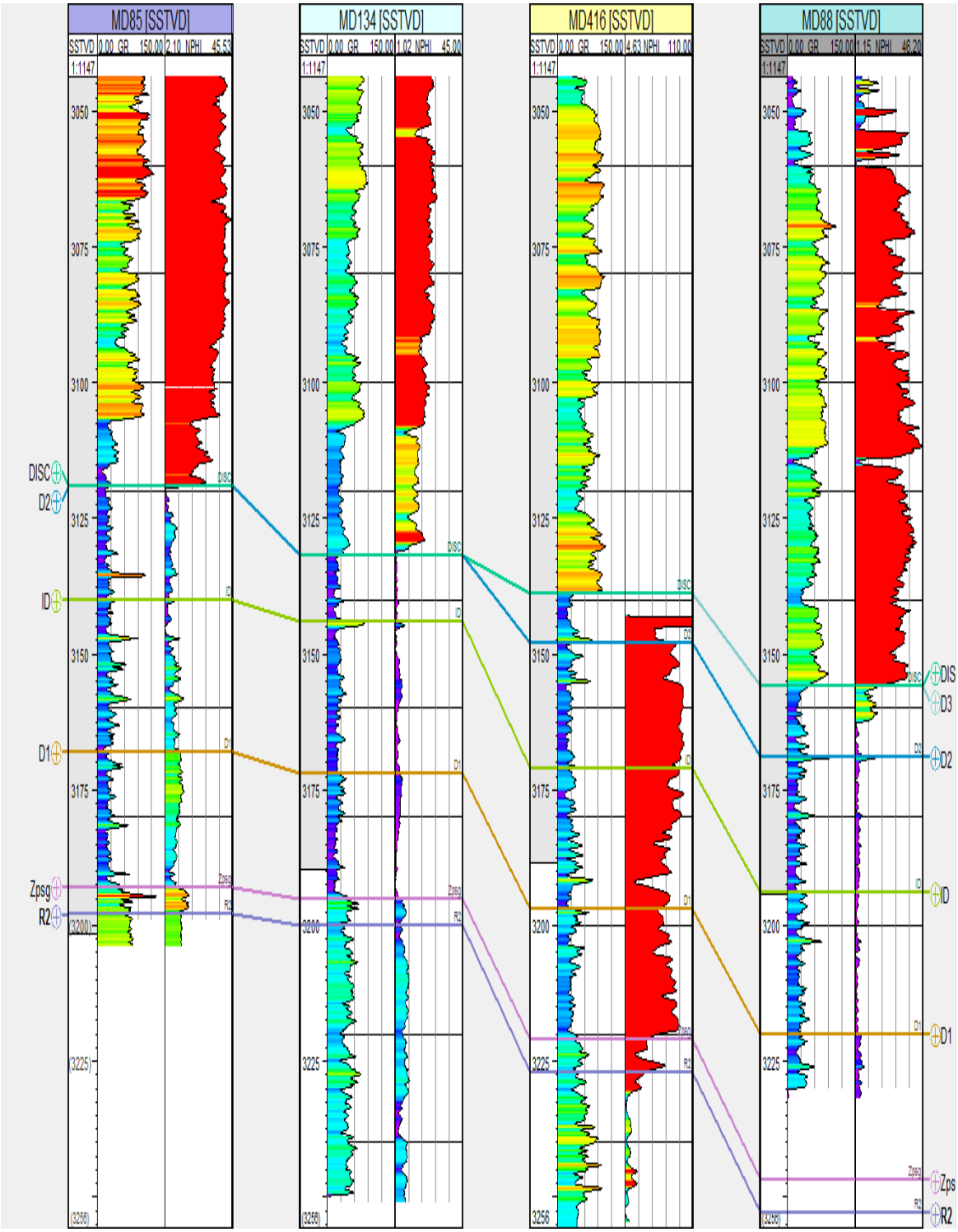

Fig.16. NW-SE Correlation.

Corrélation SW-NE (Fig. 17):

This correlation clearly shows significant reservoir erosion from south to north with an amplitude of approximately 120m. The uneroded drains exhibit some lateral isopachy.

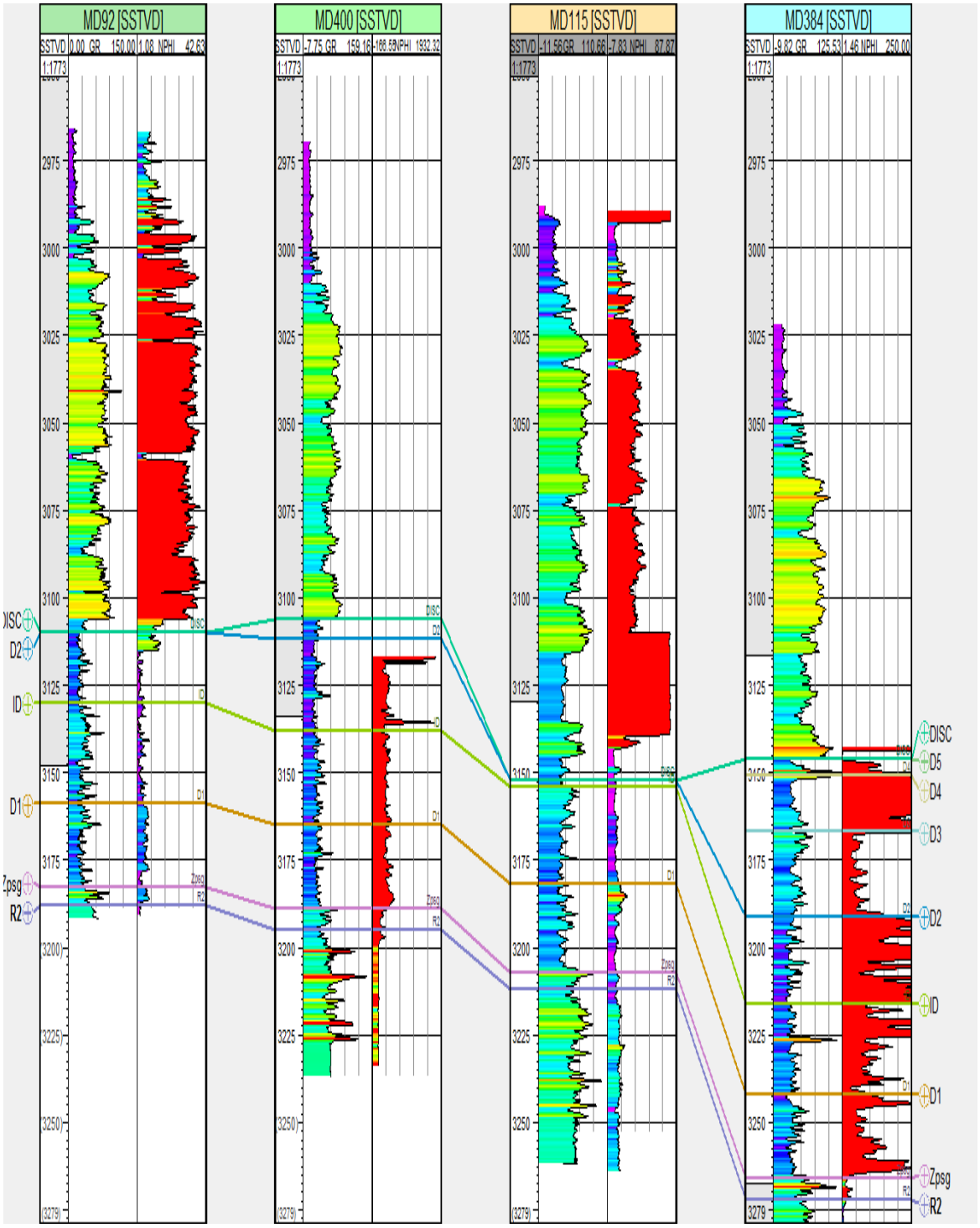

Fig. 17. Correlation SW-NE.

In the HMD field, a water saturation of 65% or more is generally considered a water zone. Water saturation is lower in the west and north of the zone, increasing towards the center (MD416) and southeast of the zone, as shown in the water saturation isopleth maps.

Regarding production, zone 20a has 51 wells distributed as follows, based on their status (see Annex No. 2):

- 40 oil-producing wells, including 6 wells equipped with gas lift.

- 9 gas injection wells.

- 2 water injection wells.

- 1 abandoned well.

Out of the 52 wells in the zone, 14 were drilled horizontally and 15 were converted to low-radius wells, commonly known as "short radius" wells.

Gas injection for pressure maintenance began in 1977 with wells MD123, MD160, and MD88, and in 1978 with well MD172, which was closed in 1986 due to zero injectivity, along with well MD384 in 1991.

The cumulative oil production until 19/05/2013 amounts to 47.965 million cubic meters.

The production status of zone 20a (Fig. 18) visualizes the production status of the wells and the cumulative production of each well in the zone. It is evident that the best wells are located in the center of the zone, oriented along a SW-NE axis, indicating a probable channel of better petrophysical facies.

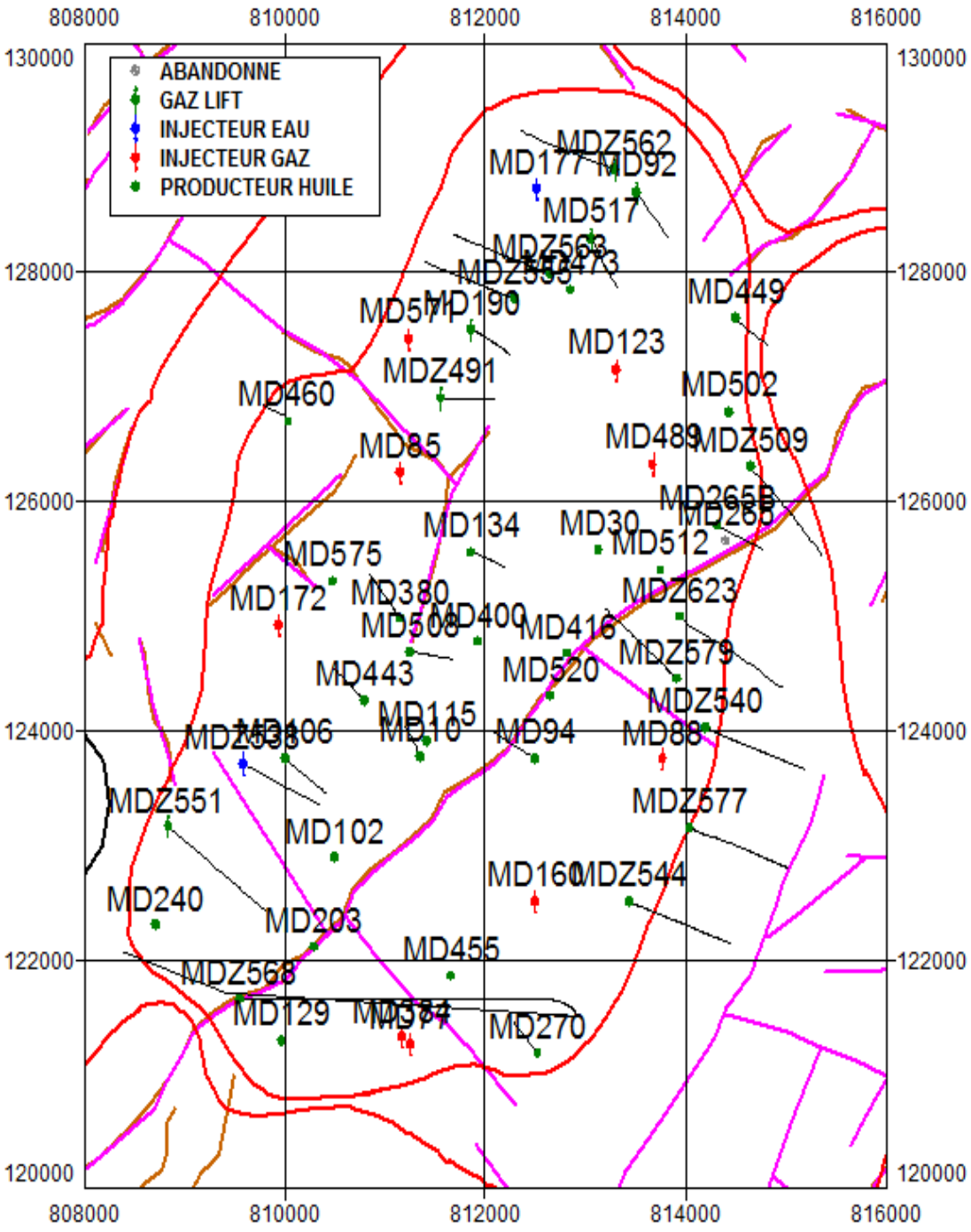

Fig. 18. Well Status in Zone 20a.

Chapter 2: Sedimentological Study

Chapter 2:
Sedimentological Study

Introduction

The objective of this study is to provide geological information about the study area. It is based on several elements: (1) a sedimentological analysis of facies from six core drillings, (2) a lithostratigraphic and sedimentological subdivision at the reservoir scale, (3) correlations at the same scale, and (4) finally, the reconstruction of depositional environments.

1Description of Cores:

They committed to describing the different characteristics observed in the cores. A precise description of these characteristics and their interpretation in terms of hydrodynamic regime allows for deducing associations between these characteristics and depositional environments. The description of characteristics is made using several criteria: lithological composition, grain size, nature of grains, and the presence of specific elements. Finally, one of the most important aspects is the recognition of sedimentary structures.

1.1 MD88 Well:

Description of R2 between 3329m and 3330m

The reservoir presents fine to medium-grained sandstones, compact, highly clayey, reddish-brown or gray in color, locally containing quartzite inclusions. The presence of veins and nodules of pink anhydrite at a depth of 3330.80 meters mark these sandstones. Numerous closed fractures also appear.

This description indicates the characteristics of the encountered rocks, notably the grain size of the sandstones, their clayey composition, color, as well as the presence of quartzite and anhydrite. The mention of closed fractures suggests a detailed analysis of the internal structure of these rocks.

COMBRIEN Ra ROOF at 3330.50m

Description of R2 between 3329m and 3330m

The Cambrian sandstones consist of quartzite, with medium-sized grains and rarely coarse, anisometric, gray, and light gray in color. They exhibit numerous millimeter to centimeter-

scale joints filled with gray-greenish clay. The presence of numerous strongly silicified whitish zones is also observed.

From 3331.60 meters, the fracturing becomes very developed, giving the core the appearance of highly tectonized rock.

This description highlights the characteristics of Cambrian sandstones, detailing the composition, grain size, types of joints, and present mineral alterations. The mention of increased fracturing from 3331.60 meters suggests a tectonized zone marked by intense fracturing.

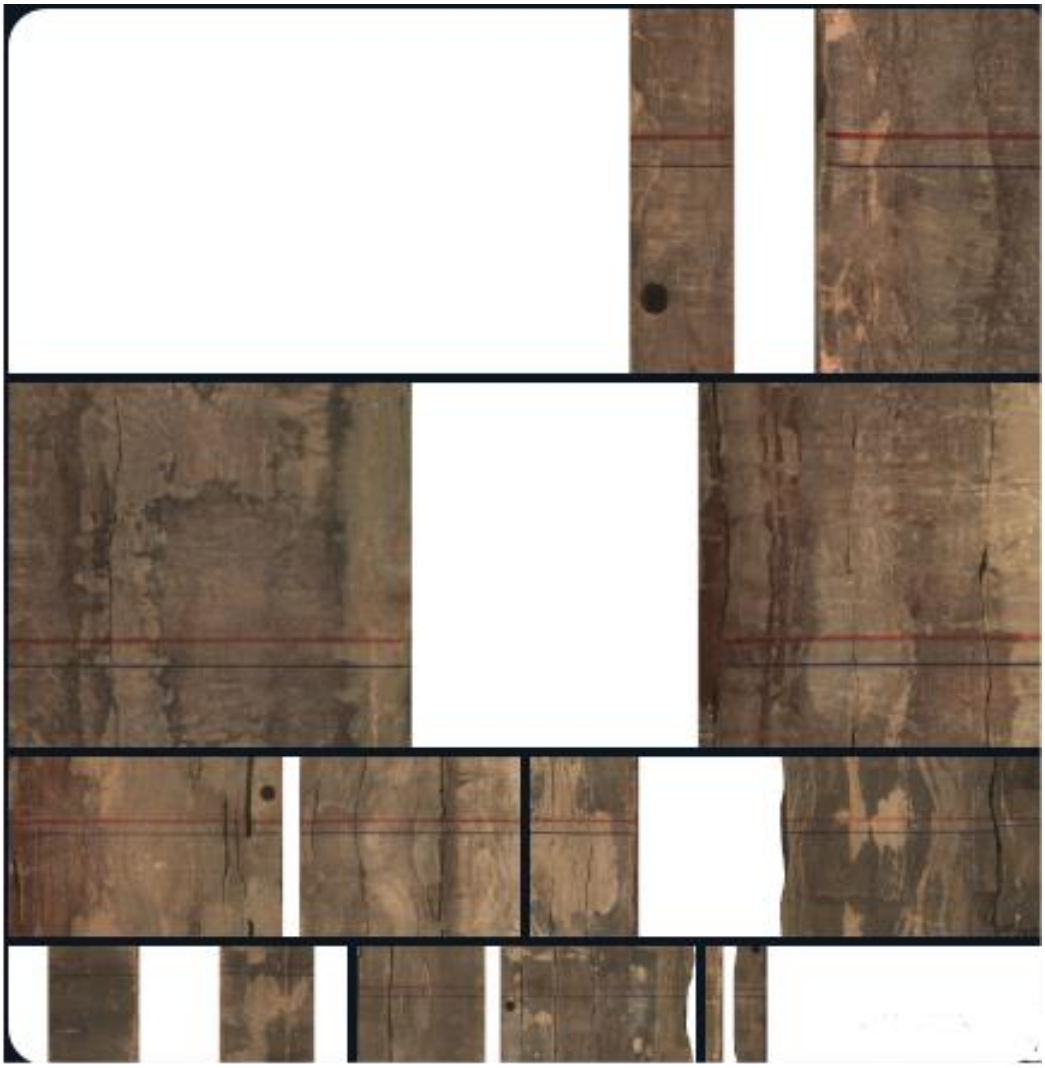

Figure 19: Core 1 from Well (MD_88) 3333.008_3335.00

1.2 MD92 Well:

Description of Ra between 3263.00m and 3264.00m

The sandstones are highly clayey, with medium to coarse grains, and sometimes very coarse. They are reddish and reddish-gray in color.

This description highlights the main characteristics of the sandstones, including their clayey composition, grain size, and color variations.

Description of Ra between 3264.00m and 3264.00m

The quartzites, and more rarely gritty quartzites, exhibit medium to very coarse grains, anisometric, light gray to dark gray in color. Some areas with intense silicification are noted around 3266.70 meters, as well as rare gray-greenish siltmicaceous patches.

Vertical fracturing is highly developed from 3264.50 meters. The Cambrian roof is located at a depth below 3264.50 meters.

This description specifies the characteristics of the quartzites, their composition, grain size, color variations, and the presence of silicified and siltmicaceous zones. It also emphasizes the marked vertical fracturing and locates the Cambrian roof.

Figure 20: Core 2 from Well (MD_92) 3263.00_3369.00

1.3 Well MD115 Core 2

Description of Ra-R2 between 3364.70 and 3391.30m

- Dark gray, medium to coarse-grained anisometric quartzite sandstones, often microconglomeratic.
- The core exhibits a brecciated appearance in some areas.
- In the coarse and microconglomeratic levels, there are wide incisions ranging from 1 to 3 mm wide and 2 to 10 mm deep.
- Numerous vertical cracks with closed lips are present and filled with sulfates (anhydrite) or clay.
- Rare decimeter-scale passes of gray-greenish clay-micaceous siltstones.
- Centimeter-scale passes of gray-green or black clays are few.
- Many quartz grains are disseminated in the rock (2 to 5 mm).

Subhorizontal stratification from 3391.30 to 3420.10 m

- Pale, fine to medium-grained, often coarse, anisometric quartzite sandstones, with frequent microconglomeratic passes.
- The rock cement is abundant.
- Centimeter-scale passes of gray-green clay-micaceous siltstones are frequent, one of them reaching 35 cm (from 3415.50 to 3415.85 m).
- Numerous centimeter-scale passes of black clays.
- The stratification is subhorizontal, marked by numerous yellowish clayey films without an air limit at RA-R2: 3391.30 m.

Figure 21: Core 1 from Well (MD_115) 3320.30_3342.00

1.4 Well MD134:

From 3288.40 to 3288.80

Compact black-gray clay admitting some lustrous joints.

From 3288.80 to 3290.30

Tectonic breccias with elements of fine to medium gray-white to black-gray quartzites and black-gray clay-bituminous cement, locally becoming clayey-sandy.

- The elements, ranging from millimeters to decimeters, are sub-angular to angular in shape.

- Presence of numerous gray-pink to gray-white quartz grains.

From 3290.30 to 3303.20

Medium to coarse-grained quartzite sandstones, light gray to black-gray, with numerous microconglomeratic beds admitting 6 centimeter-scale passes and 3 decimeter-scale passes of gray-greenish clay-micaceous siltstones.

From 3303.20 to 3308.50

Quartzite-sandstones, compact, medium to coarse-grained, gray-white to dark gray, with intercalated silicification and 4 passes of gray-greenish clay-micaceous siltstones.

From 3308.50 to 3311.20

Medium to coarse-grained quartzite sandstones, light gray to dark gray, admitting 5 passes of gray-greenish clay-micaceous siltstones.

- Rare nodules of beige clay.

- Highly developed sub-vertical fracturing, mostly filled with pyrite, bituminous clay, and rarely core.

Remarks:

From 3288.40 to 3290.30: Remaniated Cambro-Ordovician - probable.

- Roof of Cambro-Ordovician Ra at 3290.30.

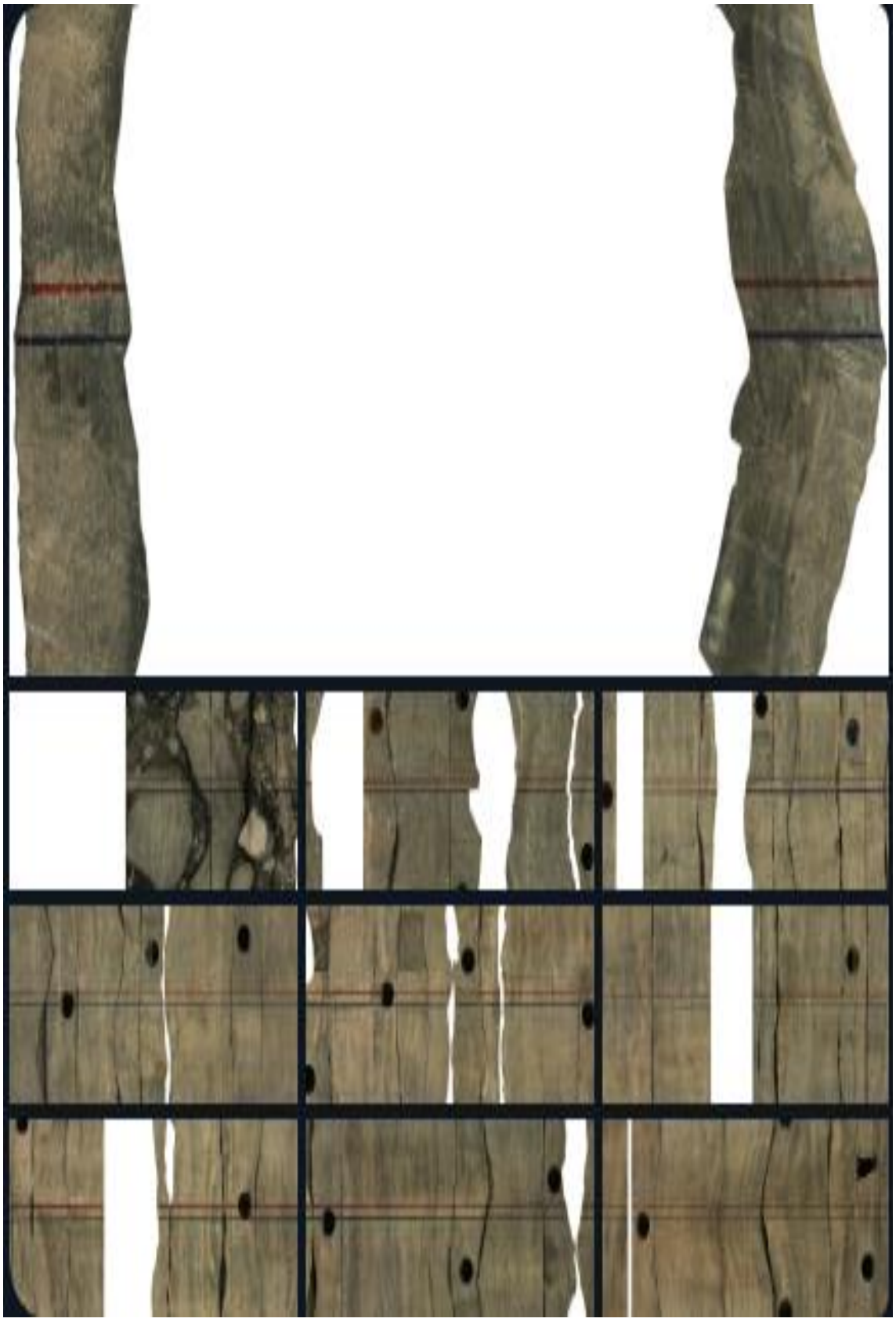

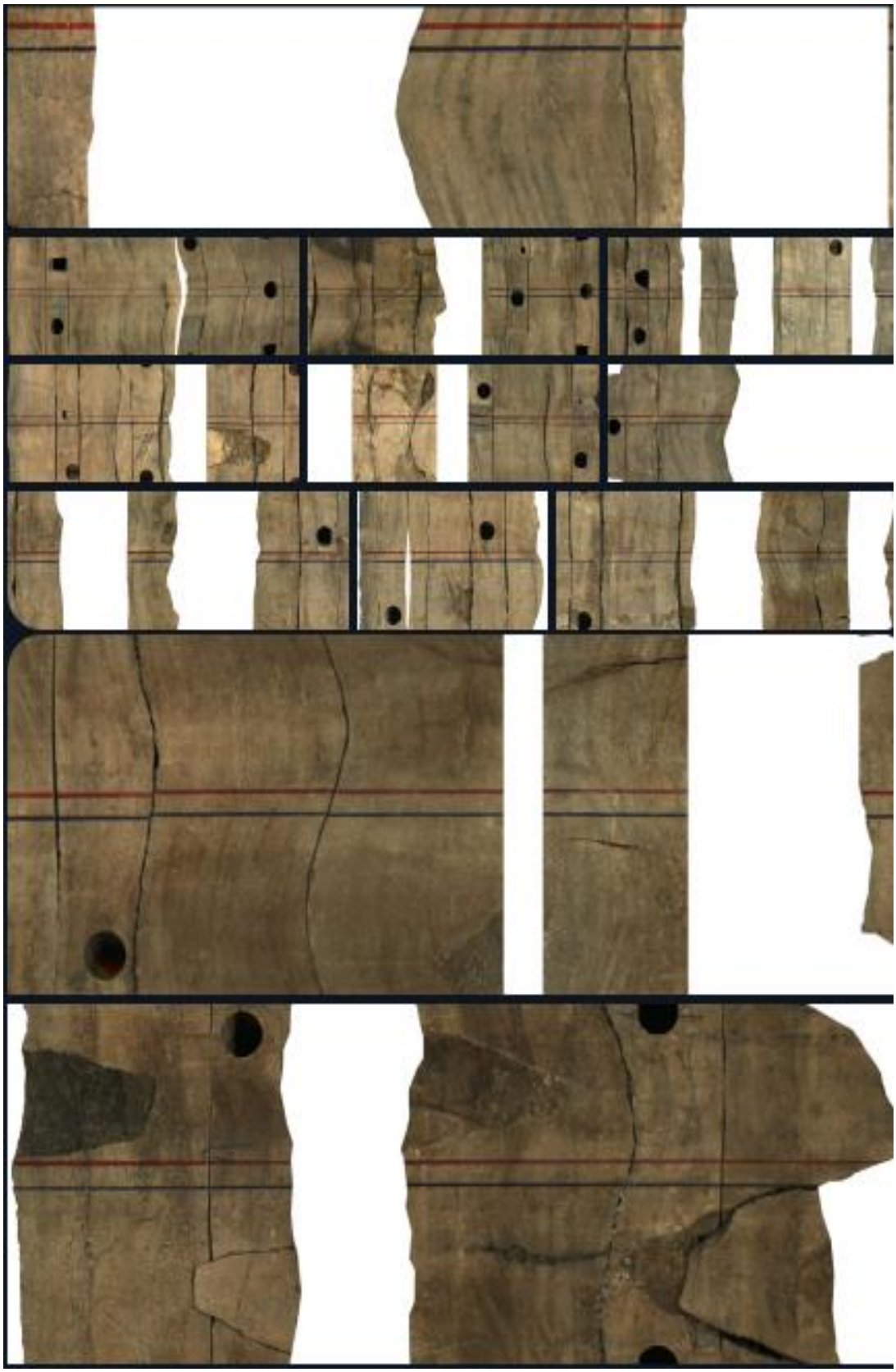

Figure 22: Core 1 from Well (MD_134) 3288.30 - 3311.00m.

6- Interpretation Results of PLT (Production Logging Tool):

Zone 20a is distinguished by the prevalence of numerous wells exhibiting a high Gas-Oil Ratio (GOR), a phenomenon commonly observed in wells with a reservoir of superior quality. The results of permanent downhole gauges (PLT) interpretation conducted on certain wells indicate that oil production is primarily derived from Drain D1 in the majority of cases. Conversely, instances of gas breakthroughs are frequently observed in Drains D2 and Inter-Drain (ID).

It is notable that wells situated in the central region of Zone 20a on the northern side, exhibiting elevated elevations relative to the major fault, exhibit high GORs. Moreover, these wells correspond to those with good reservoir quality.

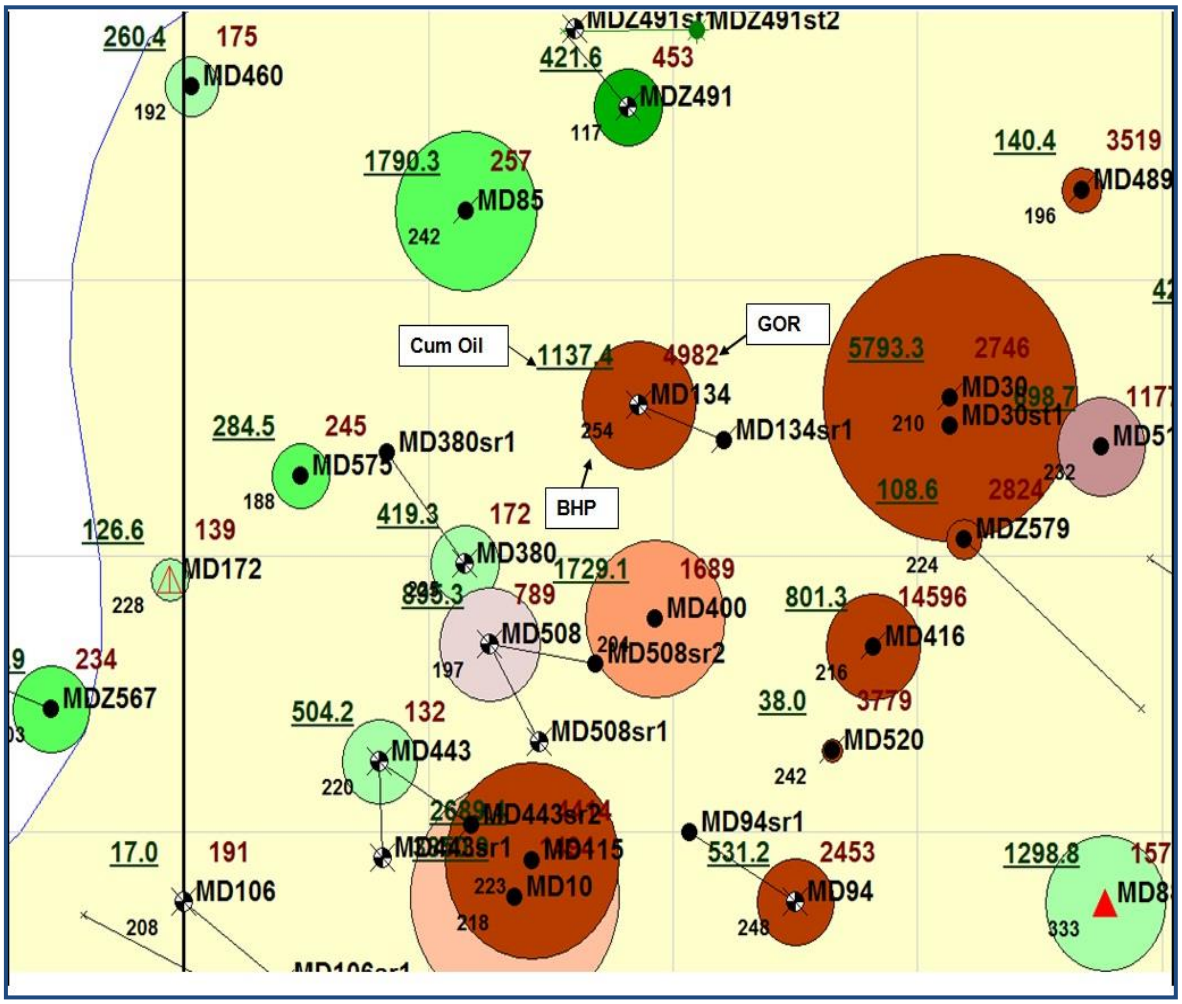

Figure 23. Map representing cumulative production, Gas-Oil Ratio (GOR), and reservoir pressure by well.

CHAPTER 3: PETROPHYSICAL PARAMETERS AND LOGGING STUDY

Chapter 3:

Petrophysical Parameters and Logging Study

Introduction

In the oil and gas industry, maximizing hydrocarbon recovery relies on both measuring the rock and fluid properties (petrophysical parameters) and understanding the larger geological context (reservoir characteristics). Petrophysical parameters, like porosity and permeability, tell us how much oil and gas a rock can store and how easily it can flow. Reservoir characteristics, like rock type and presence of fractures, provide context for interpreting this data. Sandstone, for example, typically has higher porosity and permeability than shale. By understanding these factors together, we can identify promising areas for drilling (exploration), estimate the amount of recoverable resources (reservoir evaluation), plan well development (production planning), and manage the reservoir over time to maximize extraction (reservoir management). In essence, these measurements and geological insights work together as a roadmap for efficiently finding, evaluating, and developing oil and gas reserves.

2- Concepts and Definitions

2.1. Porosity

Porosity is a crucial petrophysical parameter measured in the oil and gas industry. It refers to the percentage of empty space within a rock that can store fluids like oil, gas, or water. Imagine a sponge – the holes in the sponge represent porosity, with the more holes, the higher the porosity. In rocks, these empty spaces are called pores, and they can vary in size, shape, and how well they are connected. The porosityis measured in the laboratory: this is the direct method or calculated using well logs: this is the indirect method.

It is the ratio of the volume of void spaces (pores) in a rock sample to the total volume of the same rock sample (Plug). The porosity unit isin m^3/m^3or (%) .

$$\Phi = \frac{\text{Volume of pores}}{\text{Total volume}} \qquad [\%] \text{ or } [m^3/m^3] \qquad \text{Eq.01}$$

2.1.1. Types of Pores

We can distinguish several types of pores, such as:

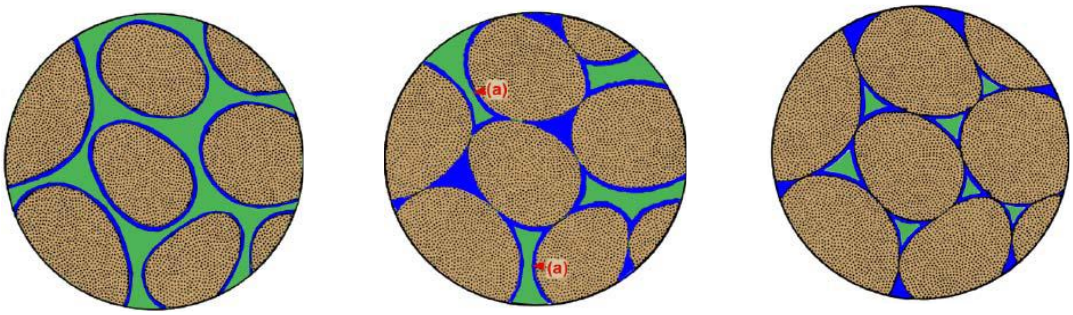

a-Connected pores b-Dead-end pores c-Isolated pores

Fig.24. Les Types de Pores.

2.1.2. Classification Based on Pore Types

$$\text{Total porosity (absolute)} = \frac{\text{Volume of (connected + dead ends + isolated)pores}}{\text{Total volume}} \qquad \text{Eq.02}$$

$$\text{Effective porosity (effiace)} = \frac{\text{Volume of (connected + dead ends)pores}}{\text{Total volume}} \qquad \text{Eq.03}$$

$$\text{Ineffective porosity} = \frac{\text{Volume of isolated pores}}{\text{Total volume}} \qquad \text{Eq.04}$$

2.2. Permeability

Permeability is the ability of rock to allow fluid flow.

The primary method for determining permeability is laboratory measurement. It is expressed in milli-Darcy (mD).

1mD = 10^{-3} Darcy

1 Darcy $\approx 10^{-12}$ m^2

Darcy's law

Consider a sample of length dx and section A, saturated with a fluid of dynamic viscosity μ, horizontally traversed by a flow rate Q (measured under conditions of the dx slice; in steady-

state, the upstream pressure is P, the downstream pressure is P-dp. The seal is made on the lateral faces.

If there is no reaction of the fluid with the rock, which is the general case, we have:

$$K = \frac{Q \cdot \mu \cdot dx}{A \quad dp} \qquad [mD] \qquad \text{Eq.05}$$

2.2.1. Permeability Classification:

- Absolute Permeability (K)
- Effective Permeability (Ke)
- Relative Permeability (Kr)

2.3. Water Saturation:

In soil and rock mechanics, the definition of water content is by weight:

- Ww: weight of water
- Ws: weight of grains, or dry fraction of soil.

2.4. Basic Notions

In addition to determining porosity and water saturation, logging tools have various applications, including:

Sonic Toolis used to:

- Identify lithology in association with the Neutron.
- Evaluate secondary porosity in carbonate reservoirs.
- Perform log correlations to determine interfaces and lateral extensions of different geological layers.

Neutron Toolis used to:

- Determine useful porosity.
- Identify gas and oil zones in association with the density log.
- Determine lithology in combination with other logs.

Density Toolis used to:

- Calculates rock density (g/cm³) by induced radiation emitted from a source. It has the same applications as the Neutron tool.

Gamma Ray Toolis used to:

Measures the natural radioactivity of rocks caused by the presence of radioactive minerals such as potassium (K), thorium (Th), and uranium (U). The Spectral Gamma Ray or NGT allows measuring the concentration rate of each of these elements relative to the other two. It is very useful in correlation and lithology characterization work.

***Magnetic Resonance Tool*:** Measures permeability.

3- MEASUREMENT METHODS

3.1. Porosity Measurement Methods:

3.1.1. Direct or Laboratory Methods:

The methods for measuring porosity differ depending on the nature of the sample and its dimensions. Among these methods is the one used by the CRD laboratory in Hassi Messaoud.

This method consists of measuring the solid volume using a mercury immersion porosimeter of the CORELAB type.

The volume of solid phase (Vs) is obtained by measuring the Archimedean push in xylene after saturation of the samples by this liquid.

The total volume (Vt) is obtained by measuring the Archimedean push on the sample by calculating the specific point of the solid phase.

$$\Phi = \frac{V_{vaccum}}{V_{Total}} = \frac{V_{Total} - V_{solid}}{V_{Total}} \qquad [\%] \qquad \text{Eq.06}$$

Where:

Vv: void (vaccum) volume

Vs: solid volume

Vt: total volume.

Figure 25: TR AP100 Gas/Helium Porosimeter (Tryte Technologies) [14].

3.1.2. Indirect Methods:

This method is based on the use of logging tools, electrical, nuclear, acoustic, and magnetic resonance tools such as GR-Neutron, Density, Sonic, Resistivity, etc.

To determine effective porosity, we follow these steps:

1-Determination of clay volume using the following formula:

$$V_{sh} = \frac{GR_{\log} - GR_{\min}}{GR_{\max} - GR_{\min}} \qquad \text{Eq.07}$$

Where: Vsh = volume of clay (Volume of shale).

2- Calculation of Effective Porosity

$$\Phi_u = \Phi_{Total} - \Phi_{sh} \times V_{sh} \qquad \text{Eq.08}$$

Where:

Øu = Effective porosity

Øtotal = porosity read on Neutron log,

Øsh = porosity of clay,

Vsh = volume of clay.

3.2. Permeability Measurement Method

3.2.1. Laboratory Permeability Measurement

Two types of devices are commonly used in the laboratory:

Variable charge permeameter, type IFP.

Constant charge permeameter, type CORELAB.

Determination of permeability from well tests:

Knowing the value of transmissivity HK obtained during a well test by the relation:

$$HK = 526.7 \times \frac{Q \cdot \delta \cdot B_0}{m} \qquad \text{Eq.09}$$

Q = Flow rate in m^3/h

δ = viscosity of oil in cp

B_0 = slope deduced from the graph p = (logT + T/t)

Figure 26: AG2P-700 Automatic Gas Permeameter 700 bar (Weatherford) [15].

3.2.2. Indirect Method

There are logging tools for permeability determination. The operation of these tools is based on magnetic resonance, but their use is not very common in the Hassi Messaoud field.

3.3. Methods of Water Saturation Measurements

Direct method in the laboratory

Indirect method using well logs

To determine water saturation, it is essential to know the formation resistivity. The tools that allow its measurement are:

The laterolog, used in water-based mud.

The induction tool, used in oil-based mud.

a- Water saturation

The calculation method of Swis based on Archie's formula given by the following relation:

$$S_w = F \times \frac{R_w}{R_t} \qquad \text{Eq.10}$$

Where:

F = formation factor which is equal to: F = 0.62/Ø2

Rw = resistivity read on resistivity log,

Rt = resistivity of formation water (known for each reservoir).

b- Oil saturation

- By direct measurement in the laboratory
- By deduction from the indirect method

$$S_o = 1 - S_w \qquad \text{Eq.11}$$

Figure 27: An image illustrating a water saturation measurement device (Soxhlet) [16].

4- Distribution of Petrophysical Parameters:

- Statistical Approach:

To refine the study of the distribution of petrophysical parameters, we found it useful to complement the classical analysis with geostatistical approach.

4.1. Useful reminders:

Mode:

The mode, generally designated by Mo, is defined as the value of the random variable that has the highest frequency in a statistical series. A statistical series can be unimodal (single mode) or multimodal (multiple modes).

The number of modes in a statistical series can provide information about the homogeneity or heterogeneity of the sample or statistical population. However, in the case of grouping the statistical series into classes, the number of modes may depend on the number of classes and the class interval used.

Median:

The median of a statistical series is the value of the variable that corresponds to a cumulative frequency of 50%.

Arithmetic Mean:

The arithmetic mean, often denoted by M or $\bar{x}$, is calculated by dividing the sum of the statistical series by the total number N. If N is the sample size and n is the number of classes, with n_i representing the size of the i-th class, then we can write $N = n_1 + n_2 + ... + n_i + ... + n_n$.

If X is a continuous variable, then the arithmetic mean is calculated by multiplying each value of the variable by its frequency and dividing the sum of these products by the total frequency N.

If X is a discrete variable and X_i represents the center of class i and n_i/N represents its frequency f_i, then:

The arithmetic mean plays the role of a certain midpoint between extremes. It is analogous to a center of gravity.

Relative Frequency and Cumulative Frequency:

If n_i is the size of the ith class and N is the total size,

n_i/N is called the relative frequency of class i. If $n_{\text{cum}} = n_1 + n_2 + ...+ n_i$, then n_{cum} is called the cumulative frequency and n_{cum}/N is called the cumulative frequency.

If k is the number of classes:

Geometric Mean:

The geometric mean is defined as follows:

Variance:

It is denoted by S^2. In the case of a continuous variable, it is equal to:

N - total size; $\bar{x}$ - arithmetic mean; x_i - variable

In the case of a discrete variable:

n' - number of classes, X_i - class center, f_i - relative frequency of class i.

The calculation of the variance already assumes knowledge of the arithmetic mean. The variance of a statistical sample is generally denoted by S^2 and that of the entire population by σ^2.

Standard Deviation S or σ:

This is the square root of the variance.

Coefficient of Variation:

This is the ratio of the standard deviation to the mean multiplied by 100:

- The coefficient of variation measures relative dispersion.

Standard Deviation:

The Standard Deviation is a statistical measure of the volatility of a value compared to its Arithmetic Moving Average (over a period P), characterizing the dispersion of prices.

Generally, the Standard Deviation is used as a component of another indicator rather than alone. For example, Bollinger Bands are calculated by adding the Standard Deviation to the Moving Average.

The formula for Standard Deviation is:

$$\text{Standard Deviation} = \sqrt{\frac{S}{P}}$$

Where:

- P is the period,

- S is the sum, for each session of the period, of the difference between the closing price of the session and the Moving Average over the period, all squared.

Histograms:

These are graphical representations of the distribution of a given parameter, obtained by plotting the relative frequencies (F) of each class against the cumulative frequency. The best choice of class intervals will yield the best distribution of parameters.

$F = n_i/N$

F: frequency of class i

n_i: total sample number

The essential purpose of these histograms is to give the shape of the distribution curve.

5. Petrophysical Study by Drains

The methodology adopted to start this study is the geostatistical approach to porosity and permeability supported by a cartographic basis.

Due to their thickness and presence across the zone, the drains chosen as the basis of the study are: D2, ID D1, and R2ab.

5.1. D2 Drain.

- Porosity:

The frequency histogram (Fig28), drawn from 1461 samples, shows that the distribution of porosity is unimodal, indicating that the distribution of porosity is homogeneous. The arithmetic mean is 6.8931%.

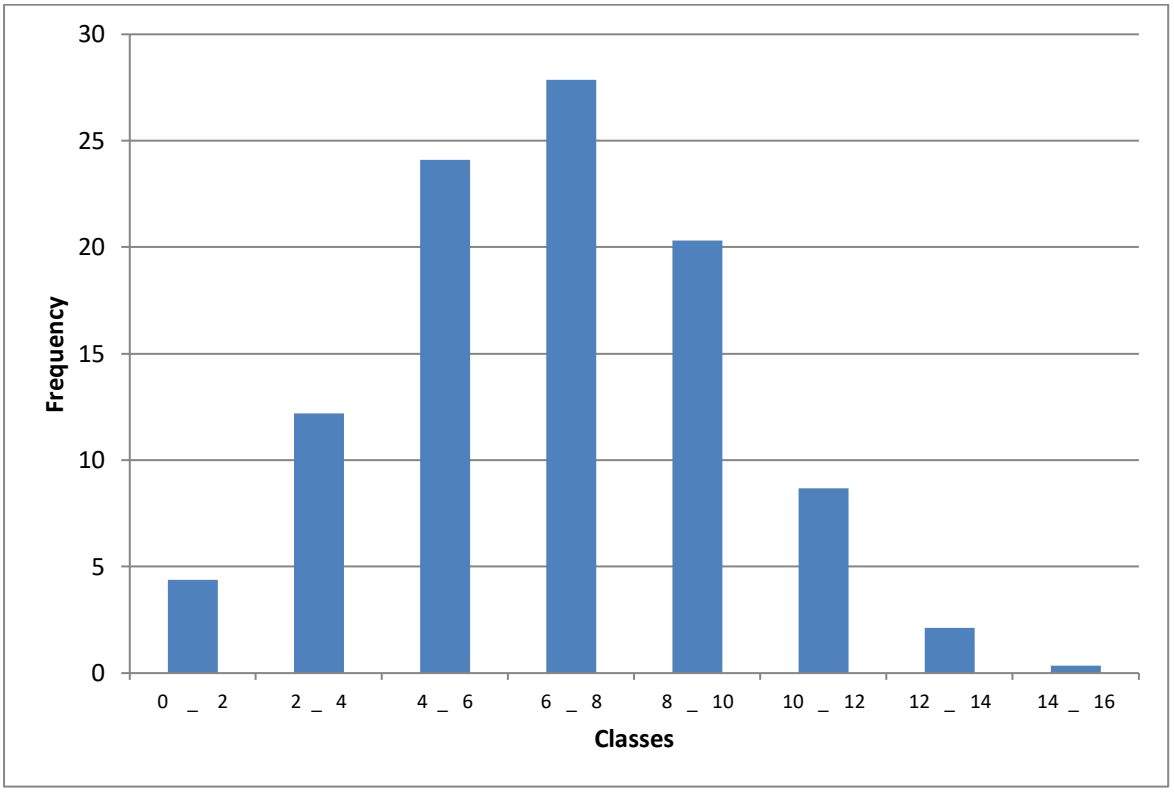

Figure 28. Histogram of the porosity distribution of D2.

Table 1: Summary of statistical calculationsof D2 porosity

Observations	Minimum	Maximum	Moyenne	Ecart-type
1461	0,200	47,980	6,898	3,324

Table 2: Porosity distribution histogram parameters of D2.

Classes	0-2	2-4	4-6	6-8	8-10	10-12	12-14	14-16	**Total**
Samples Nb.	64	178	352	407	297	127	31	5	1461
Frequency(%)	4.38	12.18	24.09	27.86	20.33	8.69	2.12	0.34	100

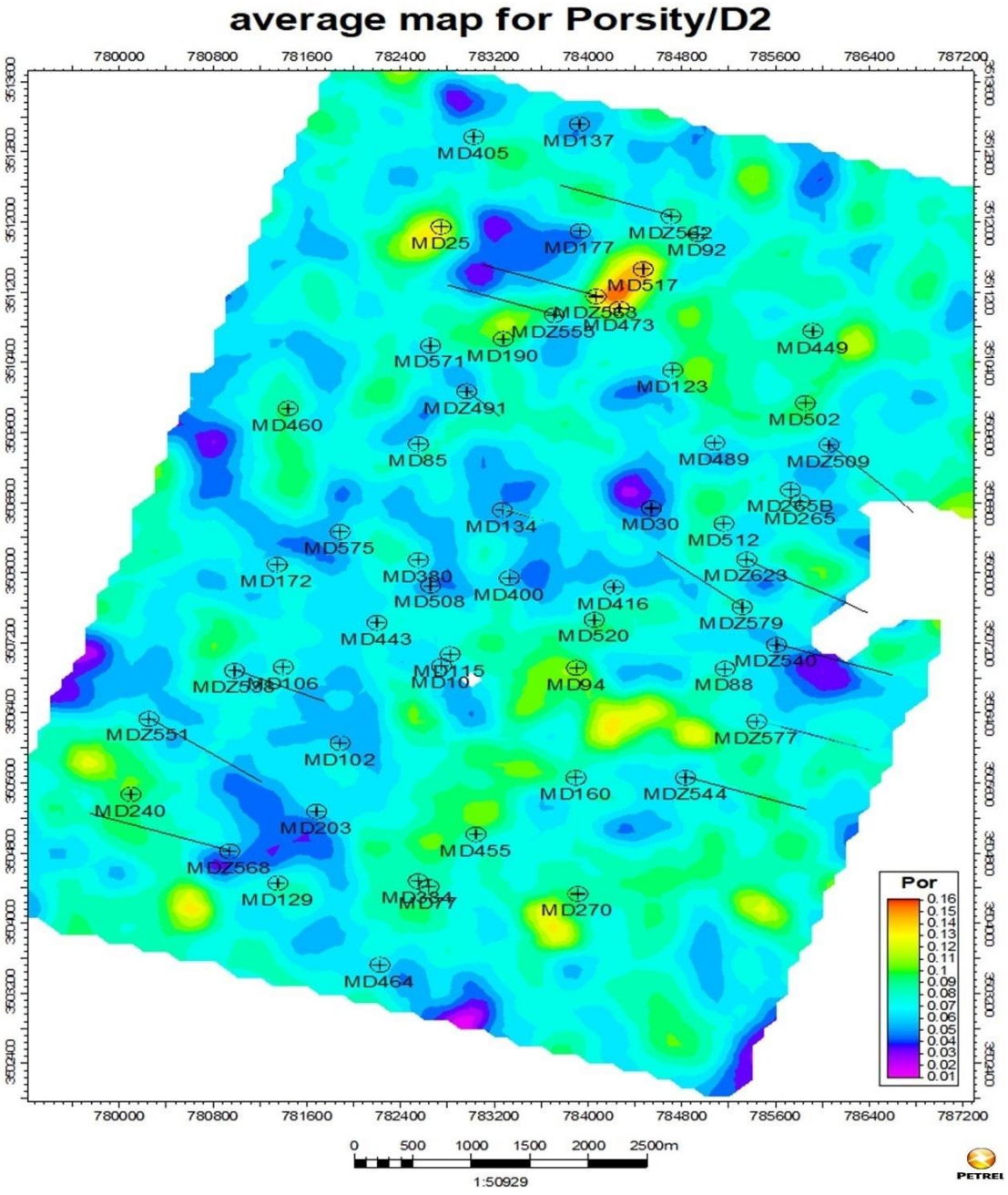

Figure 29. Isoporosity map of D2.

The isoporosity map shows that the good values are located in the NE, NW, and in the southern half of the zone, while in the central and SW areas, the porosities remain low.

2. Permeability:

Table 3: Permeability distribution histogram parameters of D2.

Classes	0.1-0.4	0.4-0.8	0.8-1.6	1.6-3.2	3.2-6.4	6.4-12.8	12.8-25.6	25.6-51.2	51.2-102.4	102.4-200	Total
Samples Nb.	354	171	165	185	204	149	140	111	82	41	1602
Frequency (%)	22.10	10.67	10.30	11.55	12.74	9.30	8.74	6.93	5.12	2.60	100

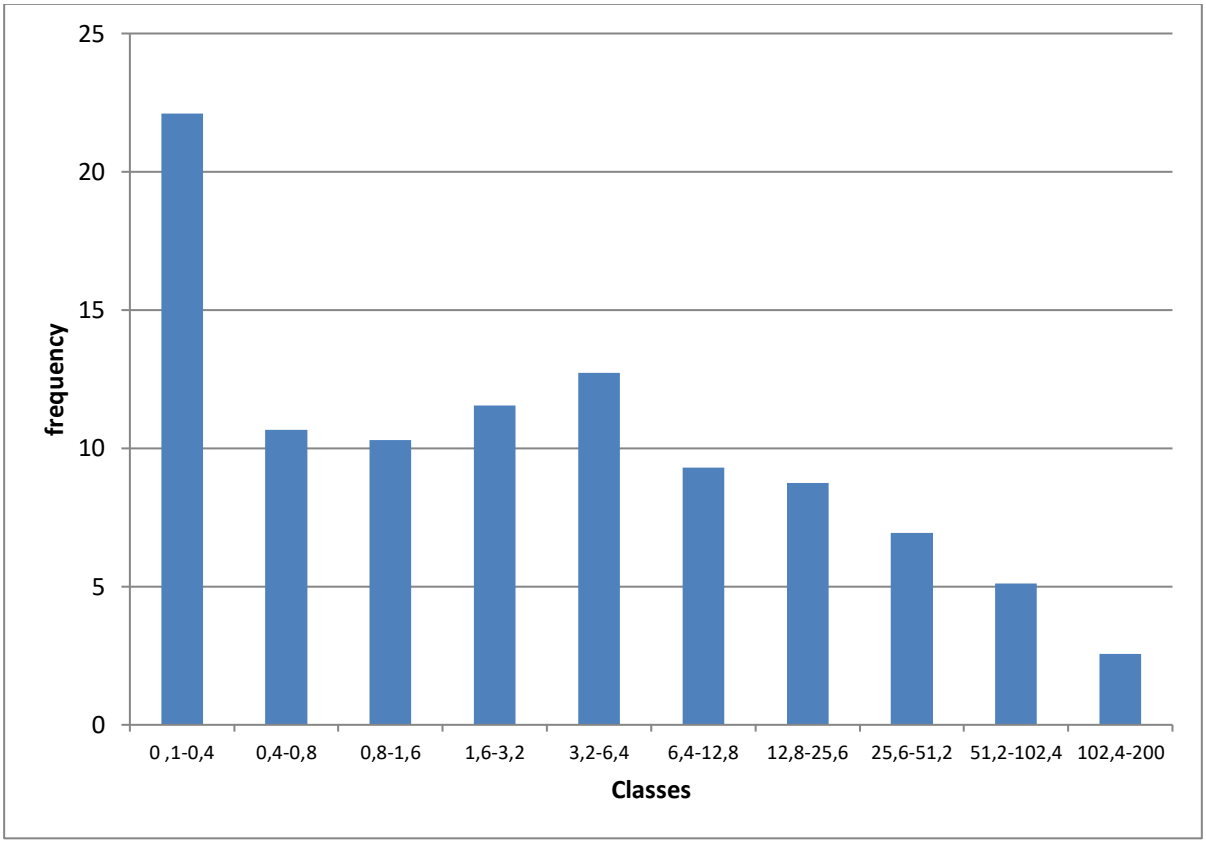

Figure 30: Histogram of permeability distribution of D2

The histogram of permeability distribution (Figure 30), based on 1602 samples, shows a bimodal distribution with a geometric mean of (1.65 mD). One mode is at 22.5% for the class of 0.1-0.4 mD and another mode (13% for the class 3.2 mD - 6.4mD.

Table 4: Summary of statistical calculations of D2

Observations	Minimum	Maximum	Moyenne	Ecart-type
1602	0,100	199,830	14,327	29.272

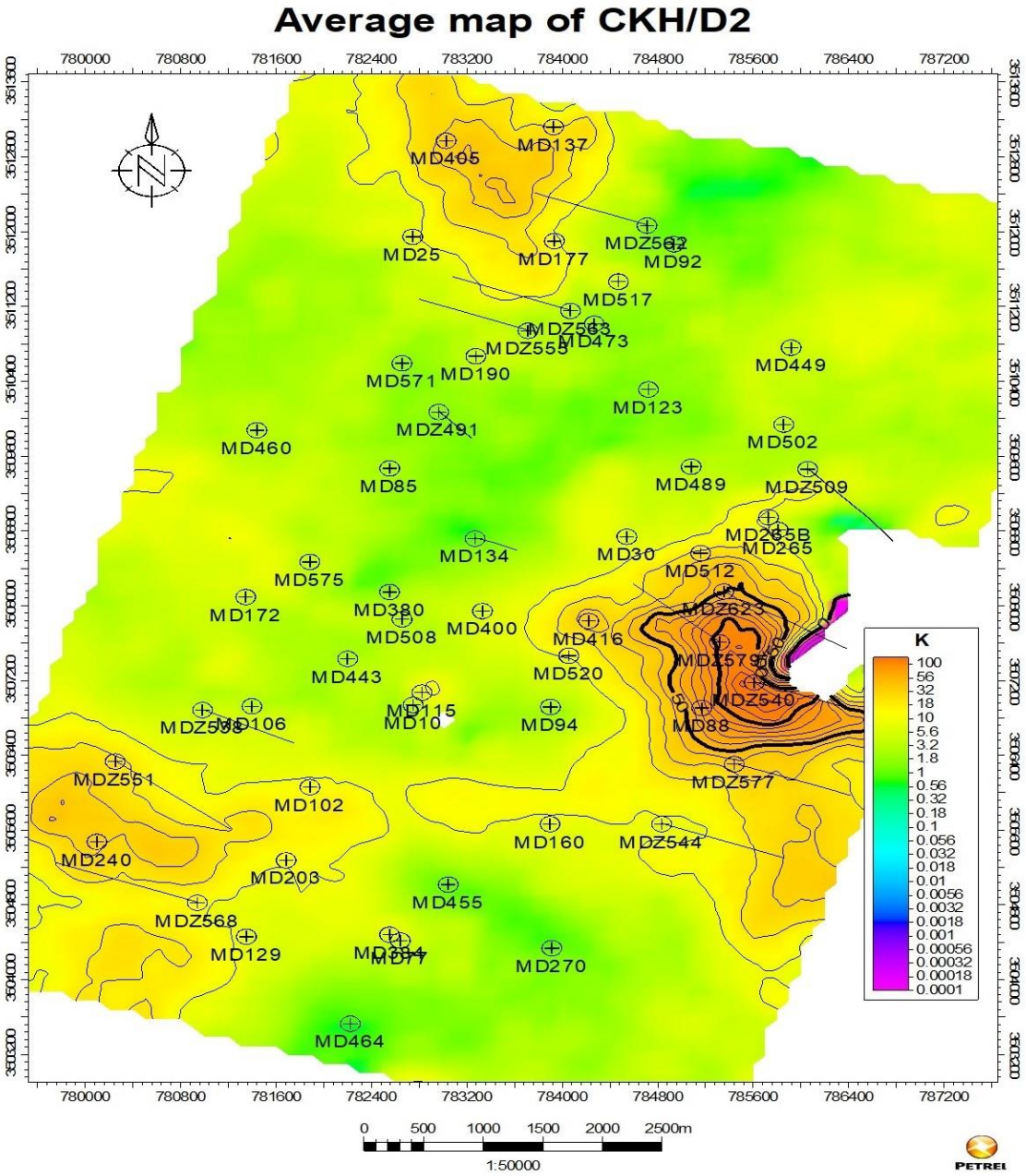

Figure 31: Permeability map of D2

The permeability map reveals the presence of large sectors with high permeabilities, especially in the southwest and southeast regions. Overall, the permeability distribution is fairly homogeneous across the zone, although slightly less pronounced in the central-north and south regions.

5.2. Inter Drain (ID)

- Porosity:

Table5: Porosity parameters distribution of ID

Classes	0-2	2-4	4-6	6-8	8-10	10-12	12-14	14-16	**Total**
Samples Nb.	68	188	473	737	547	200	41	6	2260
Frequency(%)	3,00	8,32	20,93	32,61	24,20	8,85	1,85	0,266	100

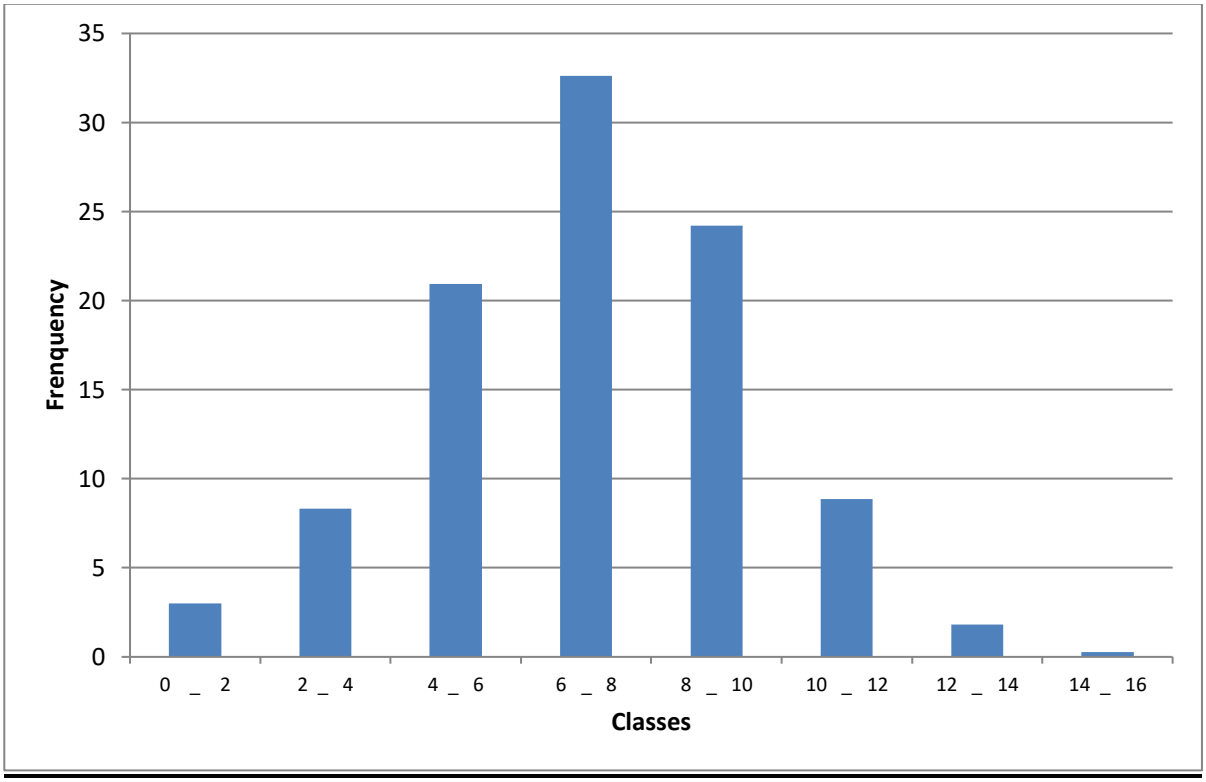

Fig.32: Distribution histogram of ID porosity

The porosity frequency histogram (Fig32), compiled from 2260 samples, indicates a unimodal distribution, suggesting the homogeneity of porosity distribution. The arithmetic mean is 7.0884%.

Table 6: Summary of statistical calculations of ID

Observations	Minimum	Maximum	Moyenne	Ecart-type
2260	0,100	25,700	7,081	2,542

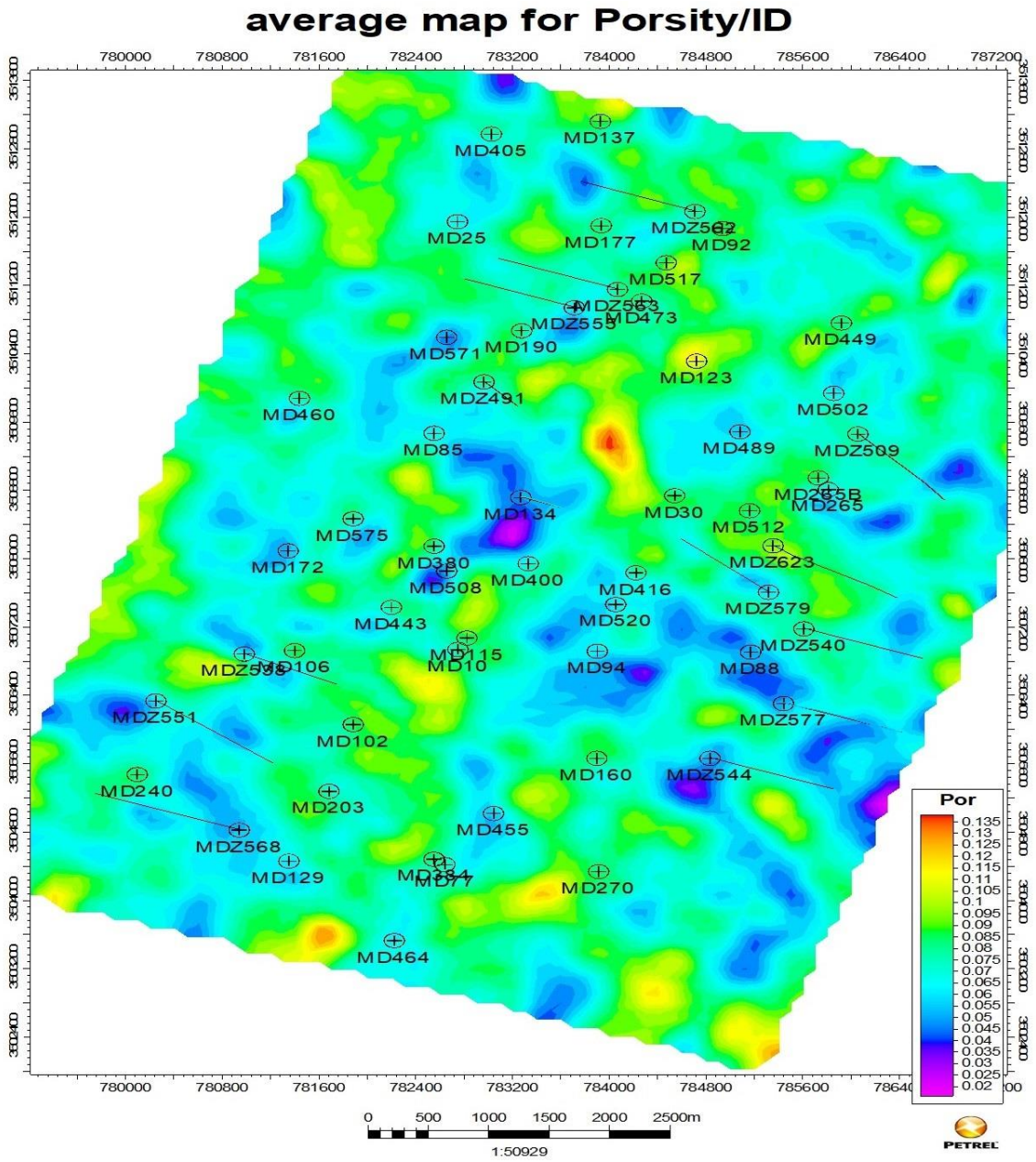

Figure 33: Porosity map of ID

The spatial distribution of porosity (Fig. 33) reveals that the best values are generally located in the central, southern, northwestern, and northeastern areas.

- Permeability:

Table 7:Permeabilityparameters distribution of ID

Classes	0.1-0.4	0.4-0.8	0.8-1.6	1.6-3.2	3.2-6.4	6.4-12.8	12.8-25.6	25.6-51.2	51.2-102.4	102.4-200	**Total**

Samples Nb.	464	247	282	280	302	274	180	125	74	38	2266
Frequency (%)	20,48	10,90	12,45	12,36	13,33	12,09	7,94	5,52	3,27	1,68	100

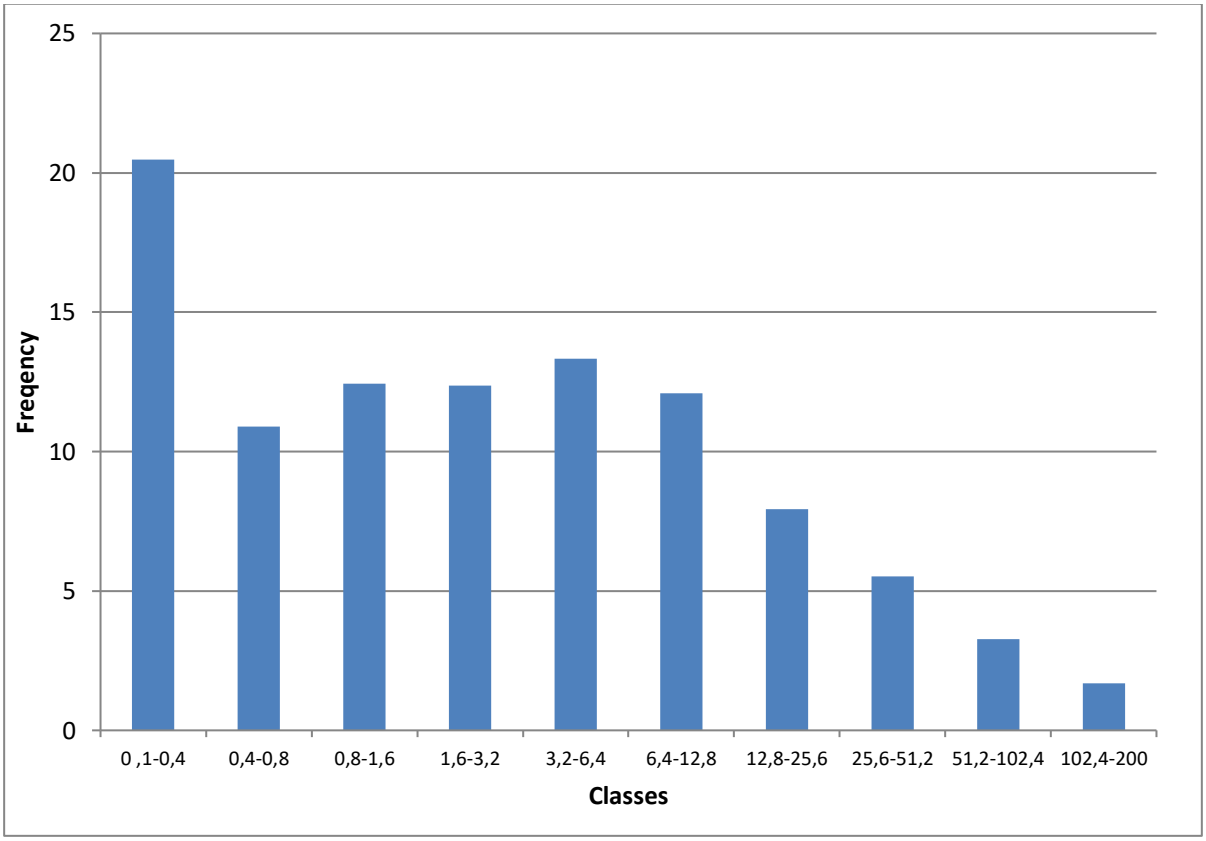

Fig.34-Distribution histogram of ID permeability

The frequency histogram (Fig34), developed from 2266 samples, shows that the distribution of permeability is bimodal with one mode (21%) around values of 0.1 – 0.4 mD and another less significant mode (14%) around values of 3.2 – 6.4 mD. The geometric mean is 1.38 mD.

Table 8: Summary of statistical calculations of ID permeability.

Observations	Minimum	Maximum	Moyenne	Ecart-type
2260	0,100	195,710	10,448	23,123

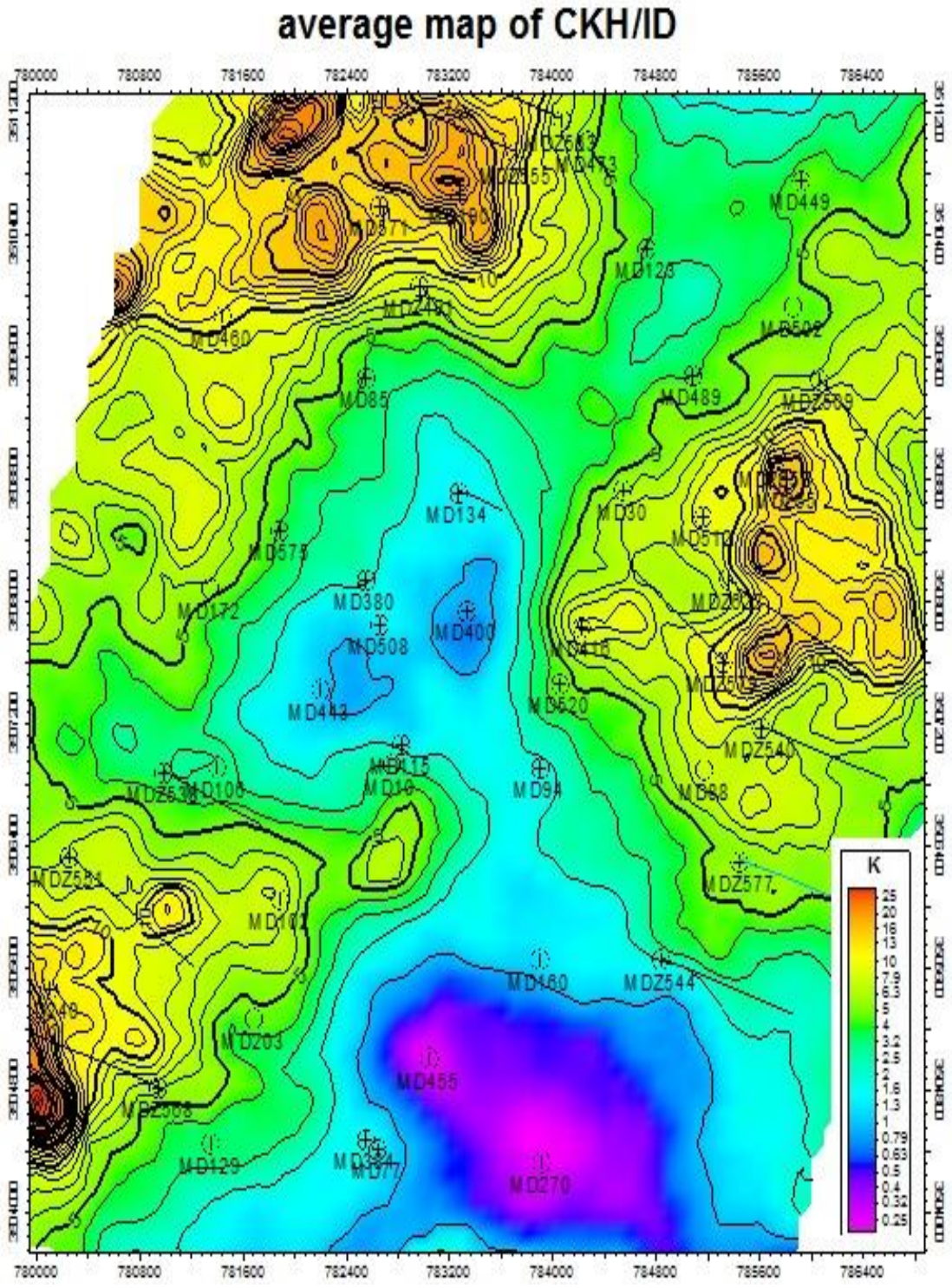

Figure 35: Isopermiability map of ID.

The permeability map of the Inter-Drain (ID) reveals a spatial distribution that is concentrated in the north, west, southwest, and east of the area. In contrast, permeability values are low in the center, southeast, and north. This distribution can be explained by the lithology and

sedimentological characteristics of the ID, which consists of alternating thin layers of sandy clay and more frequent intercalated silty layers.

5.3. D1 Drain

Porosity:

Table 9: Porosity parameters distribution of D1

Classes	0-2	2-4	4-6	6-8	8-10	10-12	12-14	14-16	16-18	18-20	**Total**
Samples Nb.	27	96	298	520	517	351	157	51	13	5	2035
Frequency(%)	**1,33**	**4,72**	**14,64**	**25,55**	**25,41**	**17,25**	**7,72**	**2,51**	**0,64**	**0,25**	100

- Number of samples: 2035
- Porosity distribution: Unimodal
- Arithmetic mean of porosity: 8.4072%.

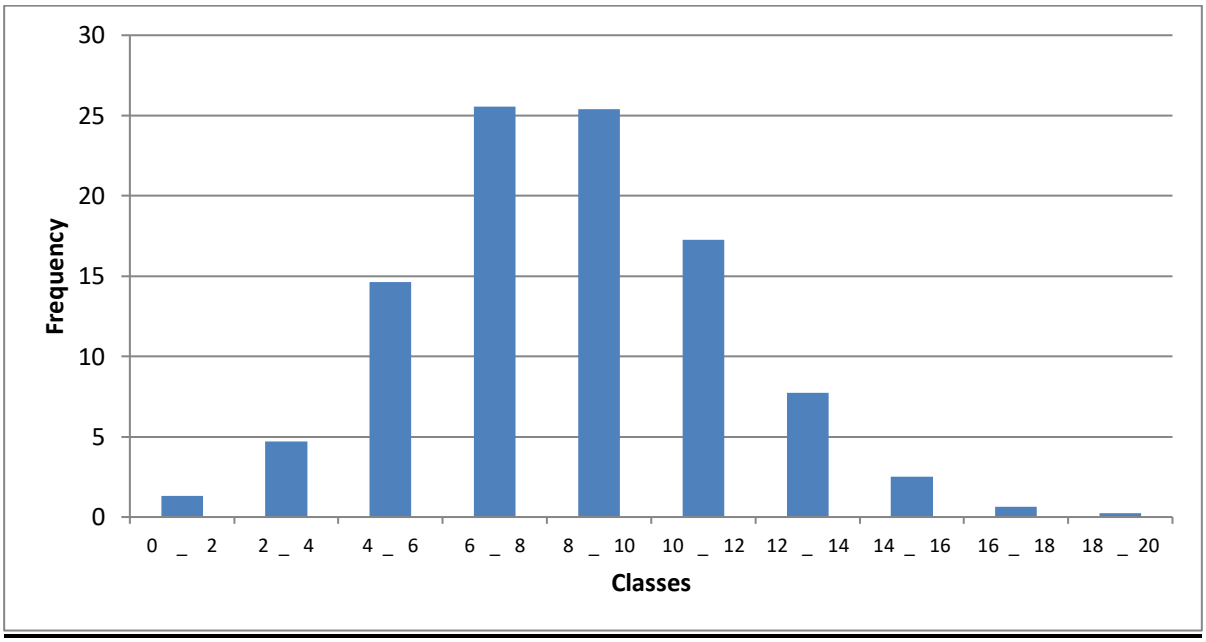

Figure 36 - Porosity Distribution Histogram of D1

Table 10: Summary of statistical calculations of D1 porosity.

Observations	Minimum	Maximum	Moyenne	Ecart-type

2035	0,100	193,200	13,171	26,252

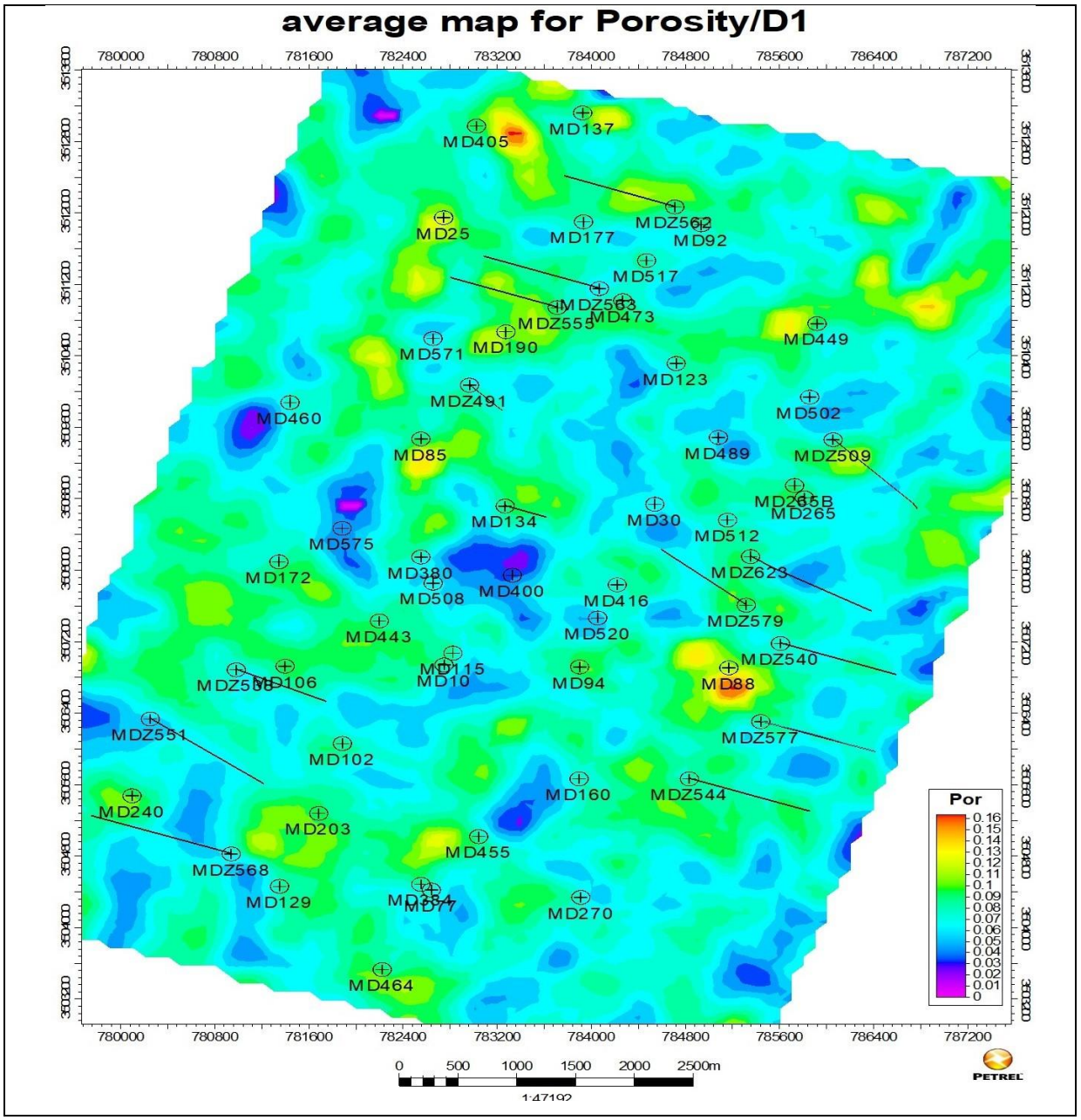

Fig: 37 - Map of the porosity of D1.

The porosity map shows that the best values are located to the East and Northwest of the area, while in the center and even to the South, porosities remain low.

- Permeability

Table 11: Permeability parameters distribution of D1

Classes	0.1-0.4	0.4-0.8	0.8-1.6	1.6-3.2	3.2-6.4	6.4-12.8	12.8-25.6	25.6-51.2	51.2-102.4	102.4-200	Total
Samples Nb.	333	194	269	280	275	221	192	135	112	47	2058
Frequency (%)	16,18	9,43	13,07	13,61	13,36	10,74	9,33	6,56	5,44	2,28	100

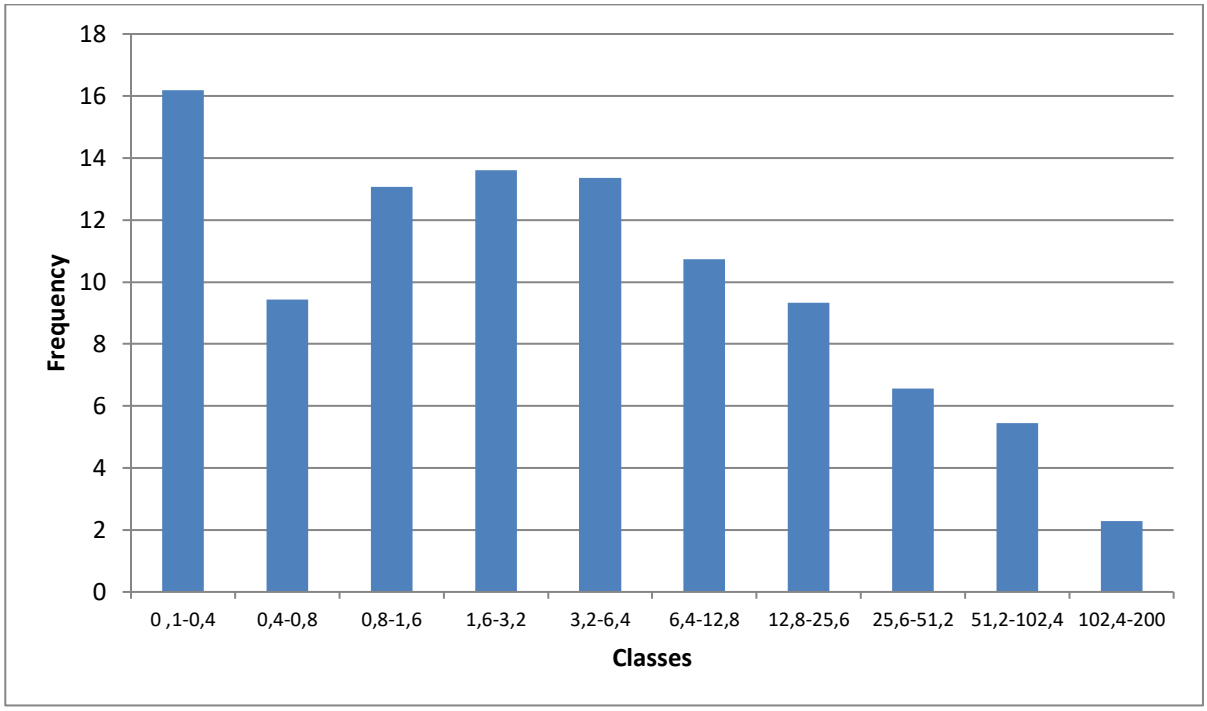

Fig. 38 - Histogram of the permeability distribution of D1. The frequency

Histogram (Fig. 38), based on 2058 samples, shows that the porosity distribution is bimodal with a geometric mean of 1.56 mD.

Table 12: Summary of statistical calculations of D1 permeability

Observations	Minimum	Maximum	Moyenne	Ecart-type
2058	0,400	57,900	8,656	3,720

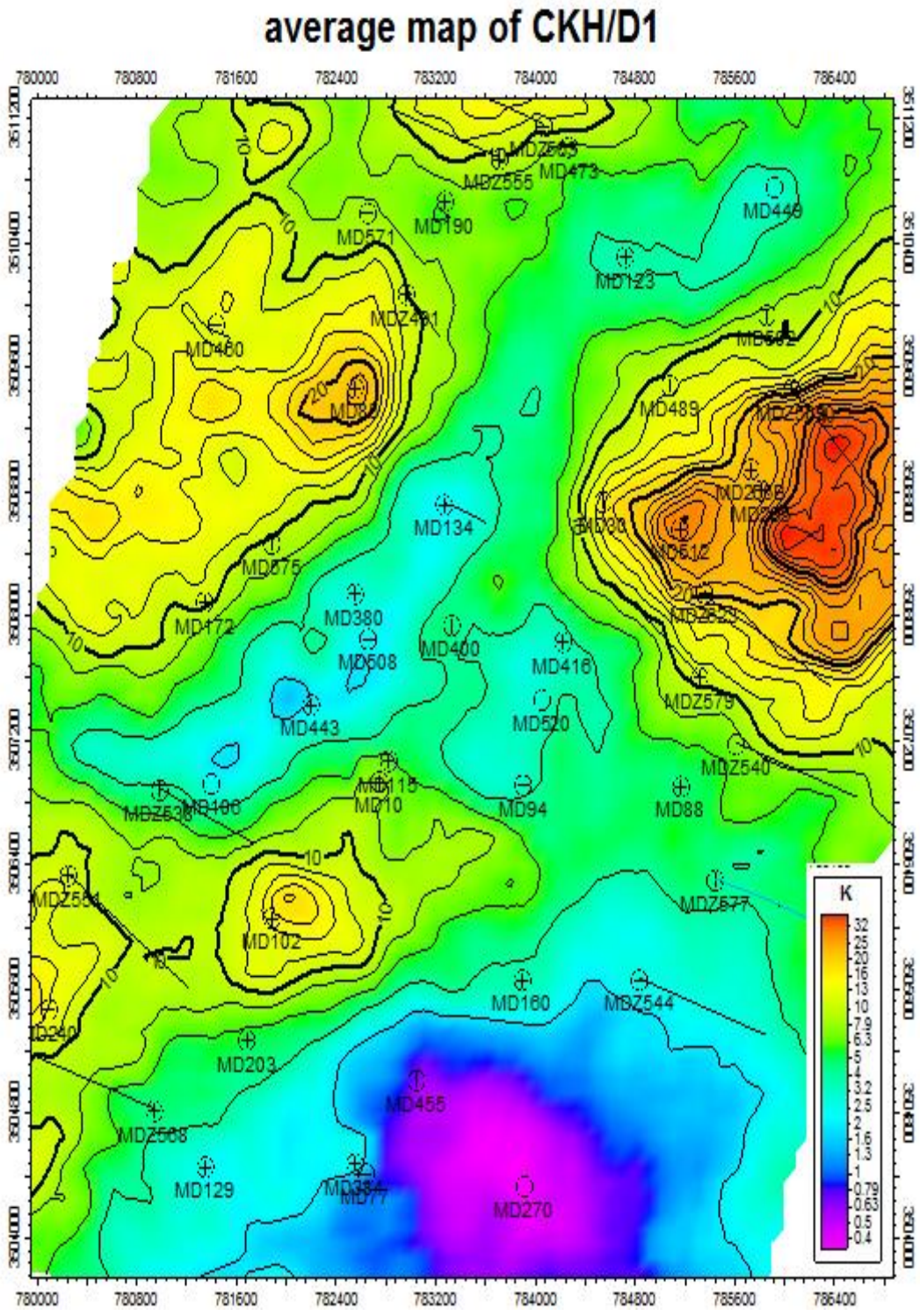

Fig. 39 - Isopermeability map of D1

The impermeability map established in D1 reveals the presence of three sectors of good permeability: one to the east, another to the north and northwest, and the third to the southwest. Less favorable impermeability values are found to the south and southwest of the area.

5.4. Cambrian R2ab:

Note: The R2AB is located between the log markers R200 and R250. Its average thickness is approximately 35 meters.

1-Porosity statistics

Table 13: Porosity parameters distribution of R2

Classes	0-2	2-4	4-6	6-8	8-10	10-12	12-14	14-16	16-18	18-20	**Total**
Samples Nb.	52	70	112	186	294	335	307	259	129	45	1789
Frequency (%)	**2,91**	**3,91**	**6,26**	**10,40**	**16,43**	**18,73**	**17,16**	**14,48**	**7,21**	**2,51**	100

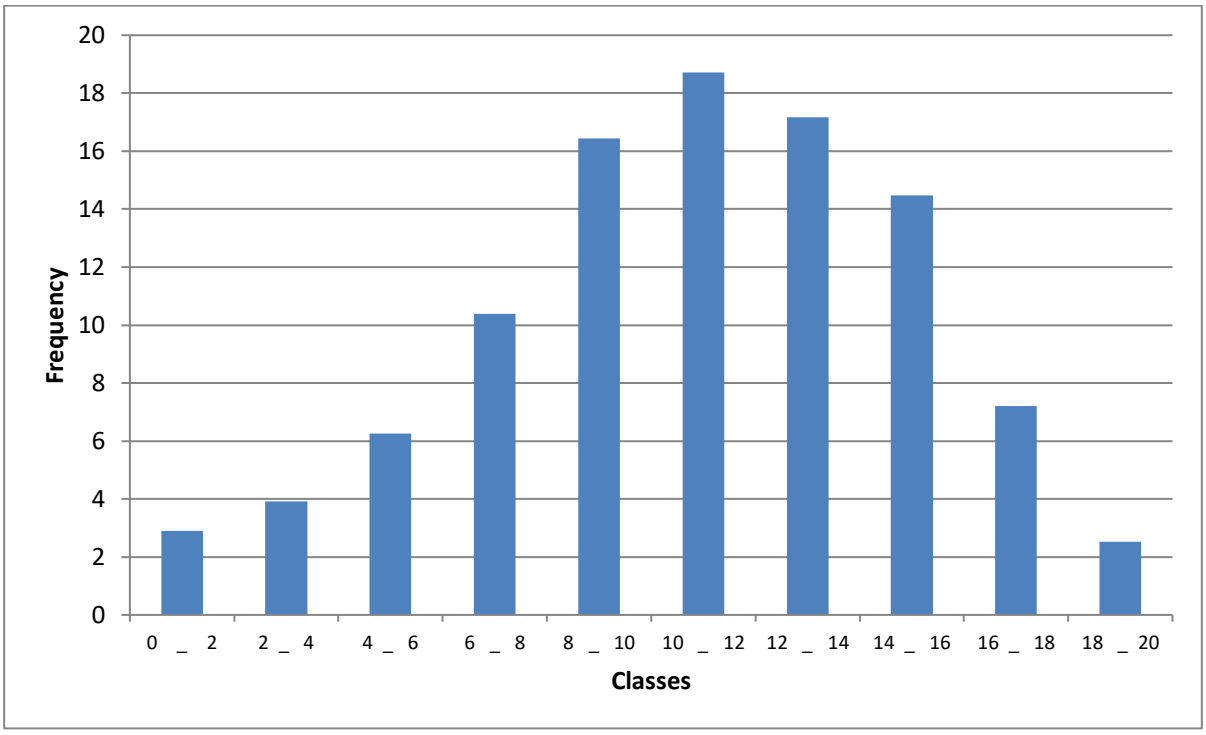

Fig. 40: Histogram of Porosity Distribution of R2

The frequency histogram (Fig. 40), constructed from 1789 samples, indicates that the porosity distribution is unimodal. The peak of the samples (19%) is observed around the 10-12% class, indicating the homogeneity of the samples with an arithmetic mean of 10.864%.

Table 14: Summary of statistical calculations of R2porosity

Observations	Minimum	Maximum	Moyenne	Ecart-type
1789	0,100	21,900	10,941	4,163

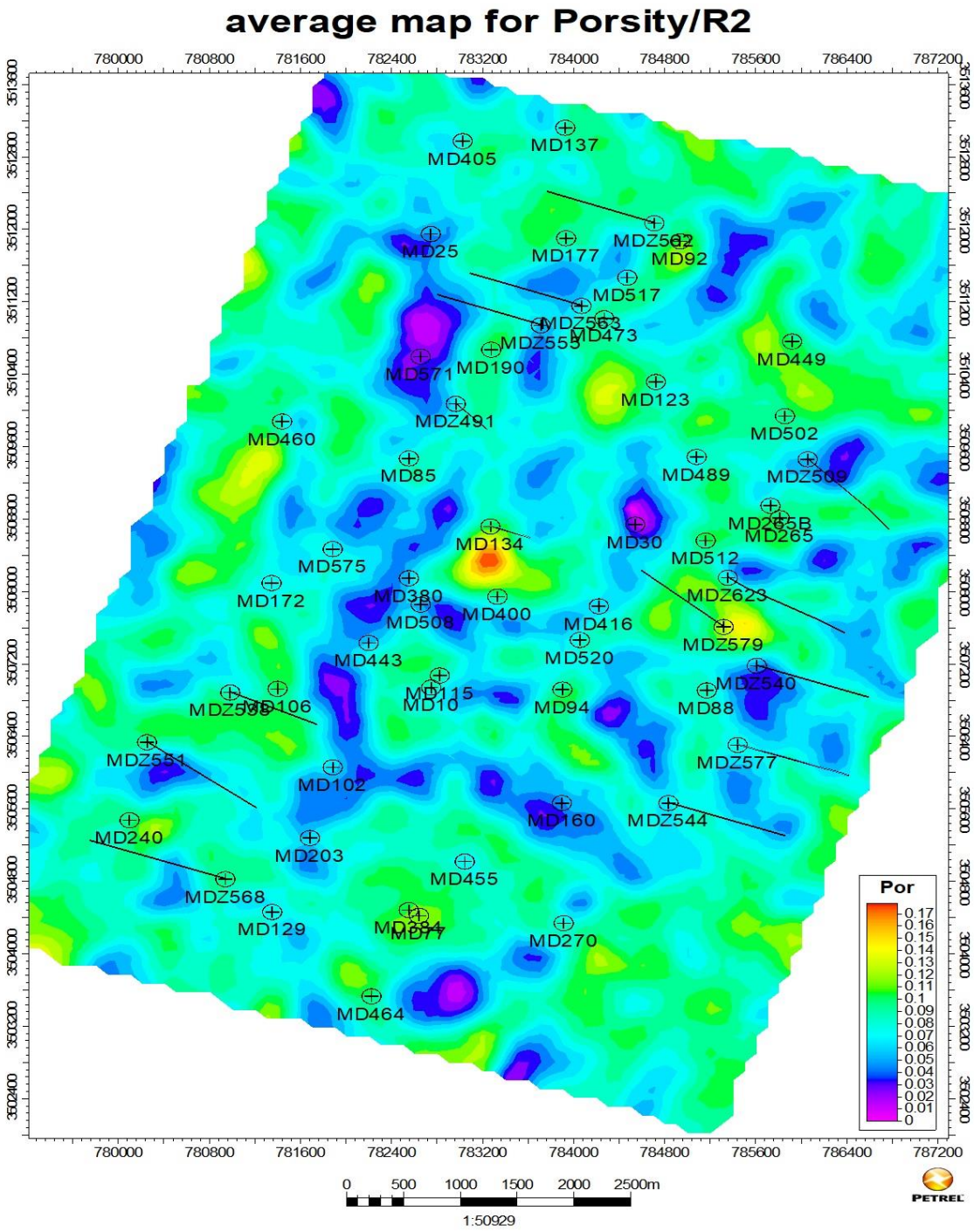

Fig. 41: Porosity Map of R2

The isoporosity map reveals that both high and low values are dispersed throughout the area. Generally, high values are observed in the center, west, south, southwest, north, and northeast. Mediocre values are recorded between sectors of good values.

2-Permeability statistics

Table 15: Permeability parameters distribution of R2

Classes	0.1-0.4	0.4-0.8	0.8-1.6	1.6-3.2	3.2-6.4	6.4-12.8	12.8-25.6	25.6-51.2	51.2-102.4	102.4-200	Total
Samples Nb.	545	281	348	342	197	71	44	18	14	13	1873
Frequency (%)	29,10	15,00	18,58	18,26	10,52	3,79	2,35	0,96	0,75	069	100

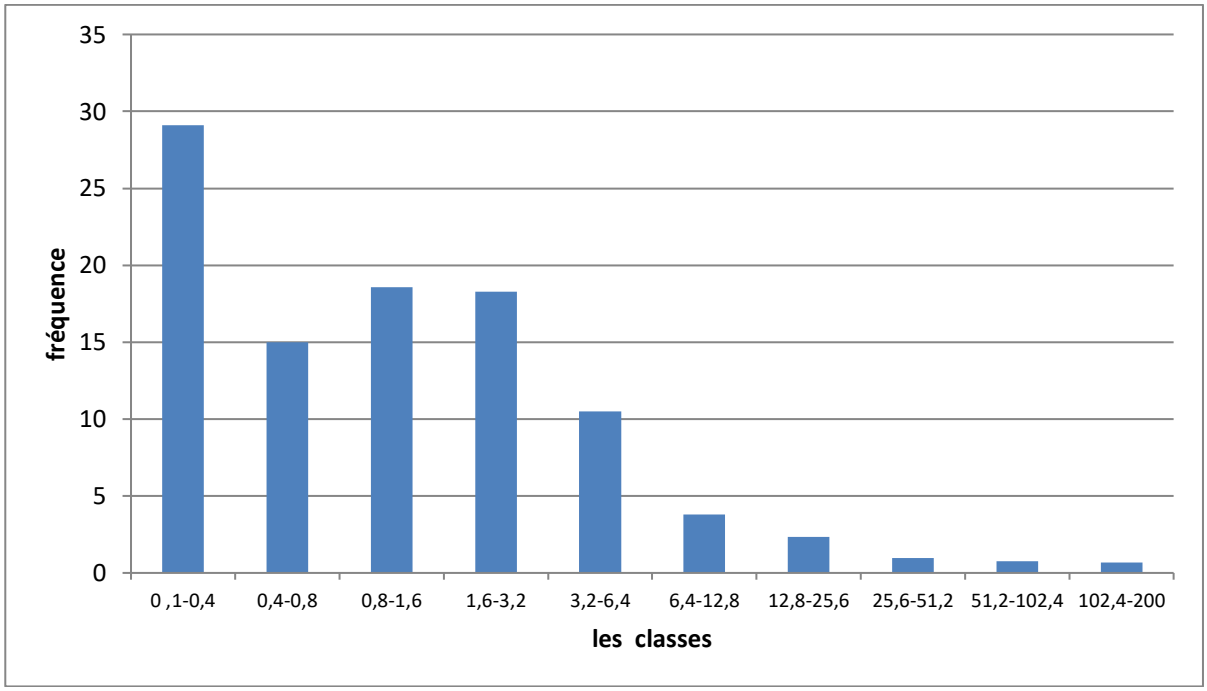

Fig. 42: Histogram of Permeability Distribution of R2

The frequency histogram (Fig. 42), based on 1873 samples, shows a bimodal distribution of permeability. Approximately 30% of the values are clustered between 0.1 and 0.4 mD, and 36% between 0.8 and 3.2 mD. Only 10% of the values fall between 3.2 and 6.4 mD.

Beyond 6.4 mD, the number of samples is very low (<5%). The geometric mean of permeability is 1.053 mD.

Table 16: Summary of statistical calculations of R2permeability

Observations	Minimum	Maximum	Moyenne	Ecart-type
1873	0,100	189,60	4,054	14,752

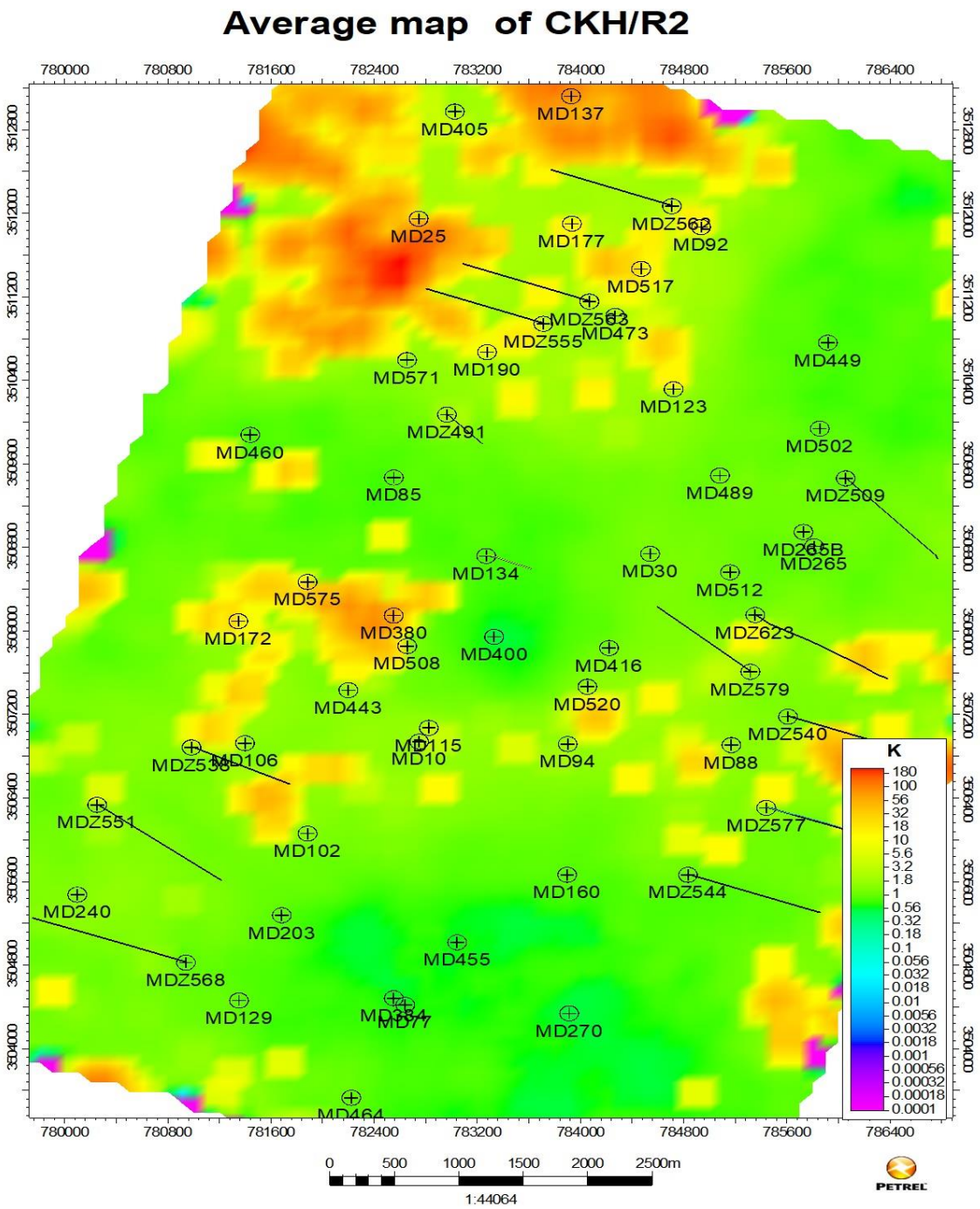

Fig. 43: Permeability Map of R2

Partial Conclusion

The geostatistical analysis yielded valuable insights into the reservoir properties:

- Porosity Distribution: Porosity exhibits a normal (unimodal) distribution across all drains, indicating a single dominant pore size range.
- Porosity Values: The median and arithmetic mean porosities are very similar in all drains. The slight deviations observed in D2, ID, and D1 may be attributed to geological factors like anisotropic grain size (Ra) or presence of natural fractures.
- Permeability Distribution: Permeability shows greater heterogeneity compared to porosity, characterized by a bimodal distribution in all drains. This suggests the presence of two distinct permeability ranges within the reservoir.
- Reservoir Quality: Overall, porosity in the Cambrian reservoir can be classified as moderate, ranging between 5% and 11%. Permeability varies spatially, with Ra classified as low to moderate, and R2 exhibiting very low permeability. Matrix permeability values range from 0.1 mD to 100 mD. However, fractured zones can exhibit significantly higher permeability, exceeding 1000 mD, suggesting that fracturing plays a key role in hydrocarbon production from the HMD reservoir.

6. Influence of Petrophysical Parameters on Petrographic Properties

Introduction:

This excerpt aims to explore potential correlations between the physical and geological characteristics of oil reservoirs to better understand the impact of geological features on petrophysical properties and their implications.

Among the geological characteristics, significantly influencing reservoir properties are grain size, morphology, sorting, and various types of cements present. Our study focuses on the relationships between these characteristics individually. However, in reality, diagenetic processes may amplify petrophysical properties are influenced by all these geological parameters simultaneously, and locally, these influences.

It is important to note that concerning the study of the impact of clay cements, we used the total clay content for both the Ra and R2 reservoirs, due to a lack of specific data on the two main types of clay cements present in the Cambrian reservoir of the HMD field, namely kaolinite and illite.

1. Methodology

The adopted methodology focuses on correlating each petrographic component, such as silica and the two types of clay, kaolinite and illite, which constitute the main cements of the Cambrian sandstones in the Hassi-Messaoud reservoir. The objective is to evaluate the impact of each petrographic element constituting the rock matrix of the reservoir on its petrophysical properties.

To do this, we used a mathematical approach to establish correlations between permeability (K in mD) and porosity (Φ in %) with each petrographic component, in order to derive a mathematical function whose coefficient reflects the type and degree of influence of these components on petrophysical properties.

This analysis relied on creating partial scatter plots between petrographic parameters (clay, silica) and petrophysical parameters (permeability and porosity) using Excel software.

6.1. Drain D2

- Permeability - Porosity Correlation (Fig. 44)

The figure below shows that the relationship between permeability and porosity is directly proportional. The correlation coefficient is 0.262.

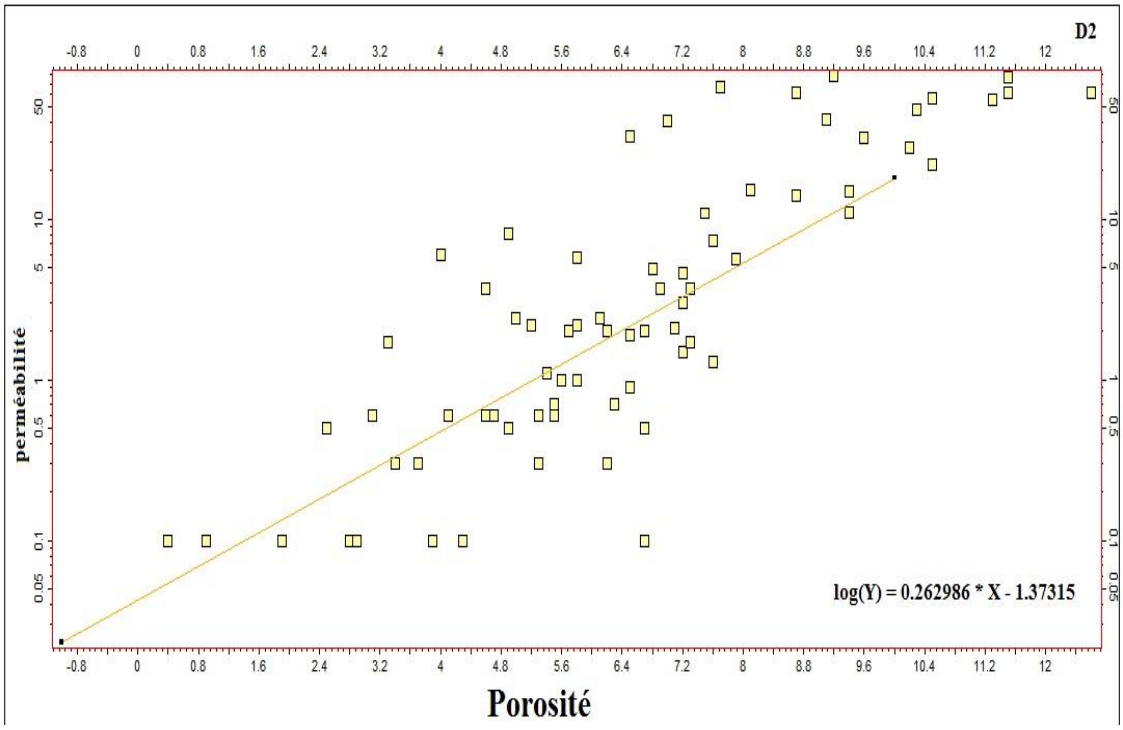

Fig. 44: Permeability-Porosity Correlation

- Correlation Permeability - Clay Cement (Fig. 45)

The correlation analysis between clay content and permeability reveals a significant inversely proportional relationship between these two parameters. The obtained correlation coefficient is approximately -0.0709. This result indicates that the increase in clay cement content has a negative impact on permeability, highlighting that an excess of clay in the reservoir rock matrix hinders its ability to allow fluid flow.

- Correlation Porosity - Clay Cement (Fig. 46)

The correlation analysis between clay percentage and porosity highlights a moderately proportional relationship vertically between clay cement and porosity. The obtained correlation coefficient is approximately 0.08. This suggests that there is a tendency for porosity to increase with increasing clay cement content, although this relationship is not very strong.

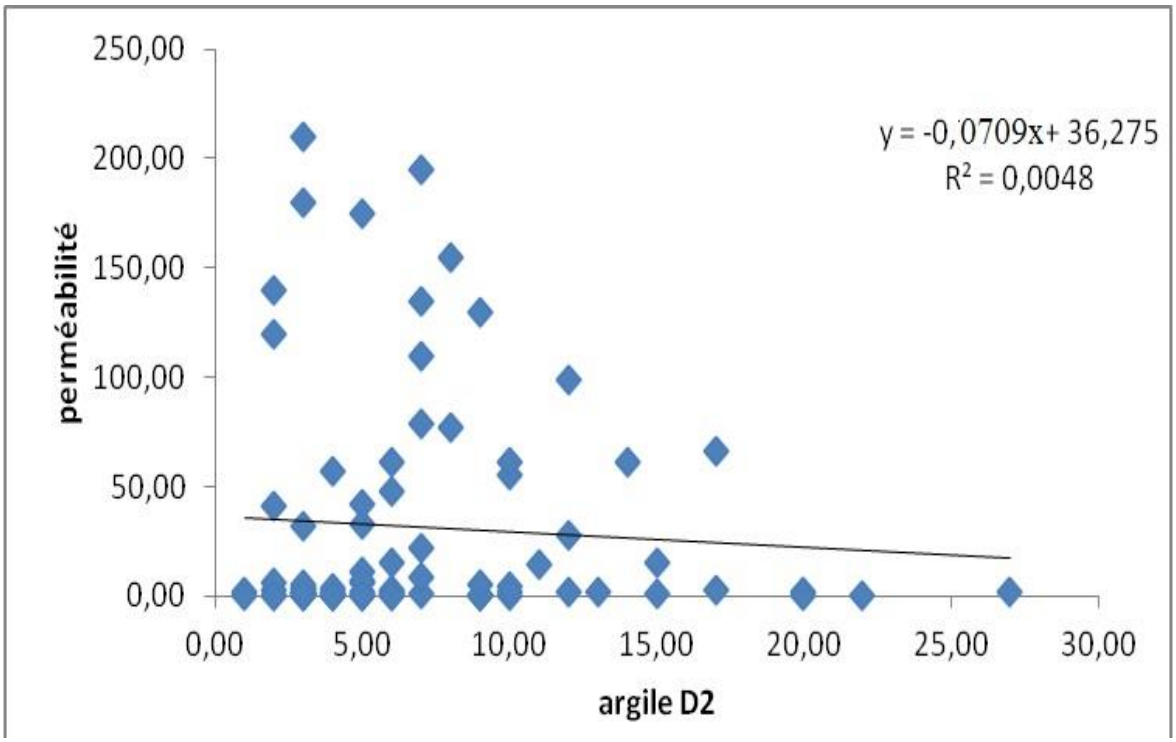

Fig. 45: Permeability-Clay Cement Correlation for Drain D2

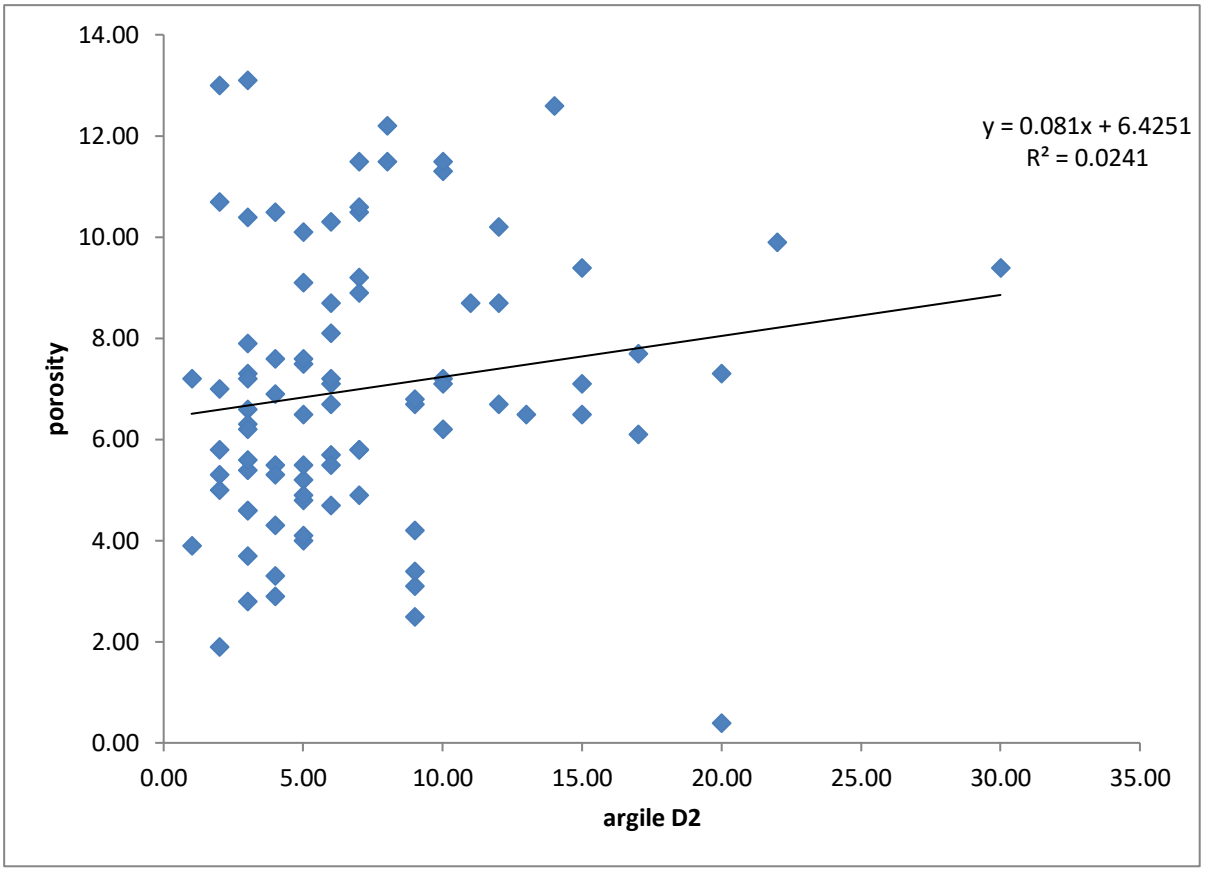

Fig. 46: Porosity-Clay Cement Correlation for Drain D2

- *Corrélation Perméabilité - Silice Cement (Fig. 47)*

The correlation analysis highlights a marked inverse relationship between permeability and silica cement, the latter being predominantly derived from secondary salinization. The correlation coefficient is approximately -2.014. This value suggests a strong association between an increase in the presence of silica cement due to secondary salinization and a decrease in permeability, indicating that the formation of this type of cement significantly deteriorates the reservoir's ability to allow fluid flow.

- *Corrélation Porosité - Silice Cement (Fig. 48)*

The figure below shows a weak inverse relationship between porosity and silica with a correlation coefficient of approximately -0.158.

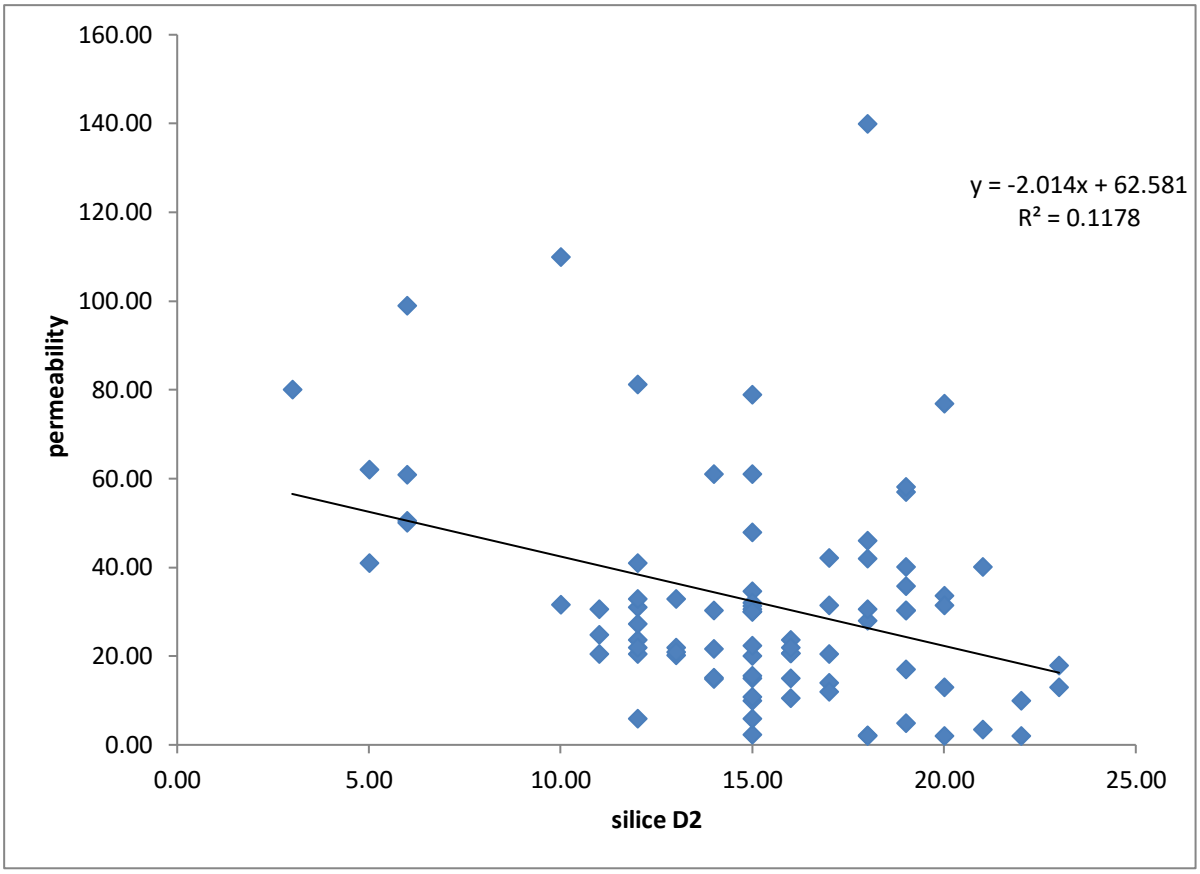

Fig. 47: Permeability-Silica Cement Correlation for Drain D2

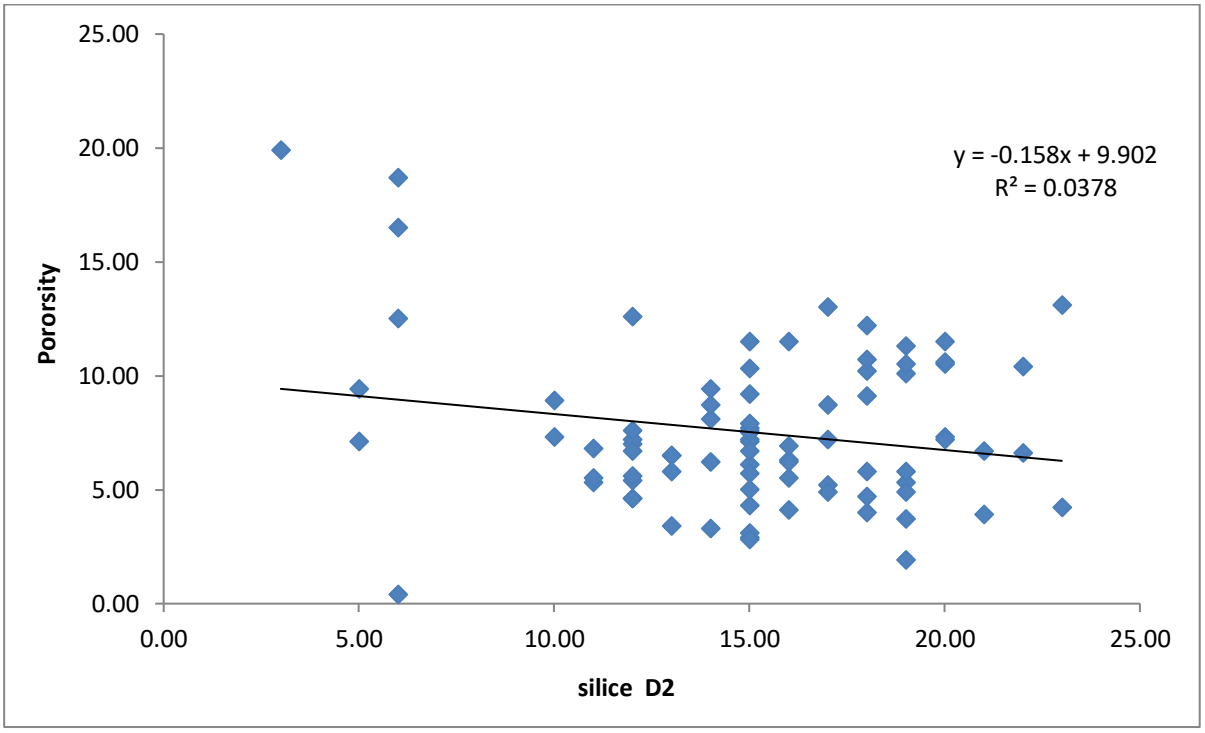

Fig. 48: Porosity-Silica Cement Correlation for Drain D2

6.2. Inter-Drain (ID)

- Corrélation Perméabilité - Porosité (Fig. 49)

In this figure depicting the correlation graph between KmD and Φ (%), it is observed that the relationship between these two parameters is directly proportional with a correlation coefficient of approximately 0.232.

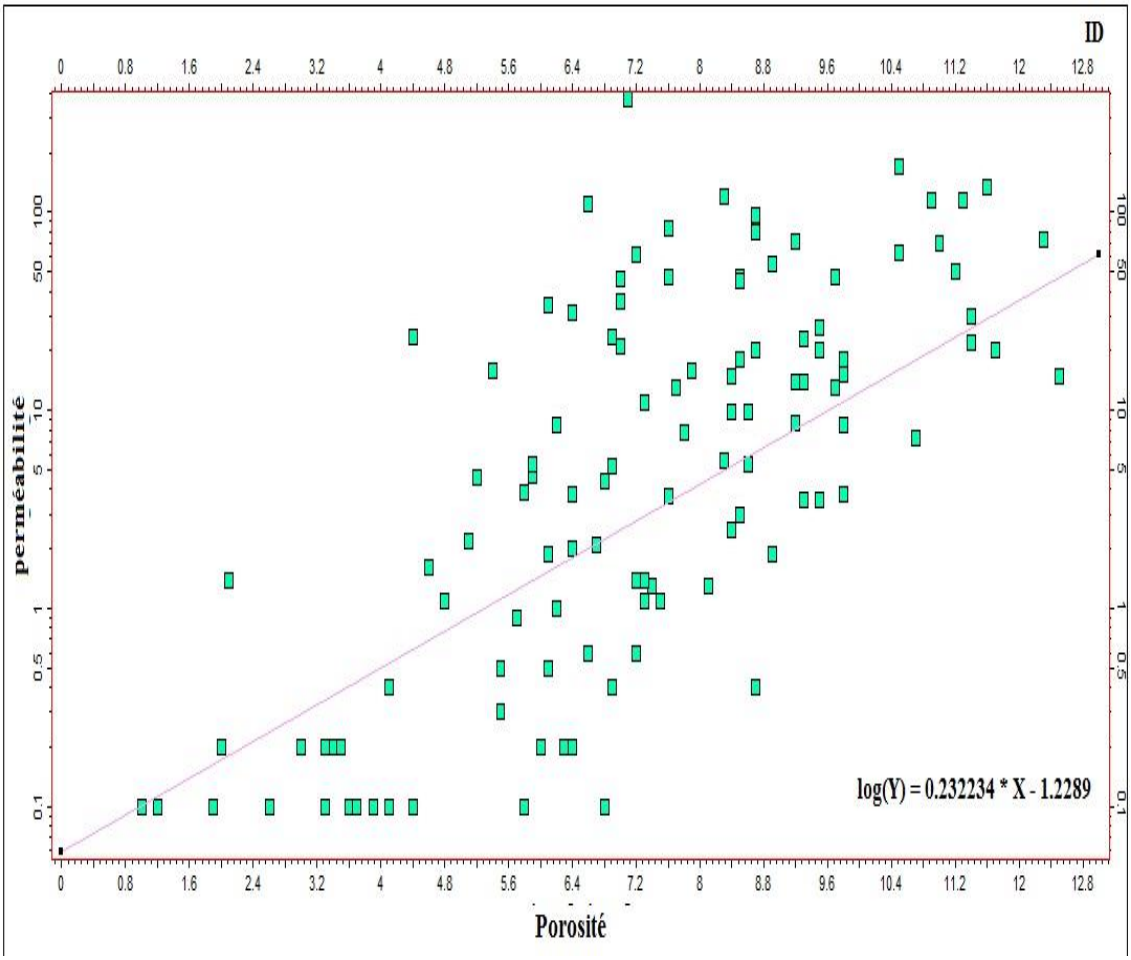

Fig. 49: Permeability-Porosity Correlation

- Corrélation Perméabilité - Ciment Argileux (Fig. 50)

In the figure illustrating the correlation between clay content and permeability, a slight inverse relationship is observed between these two parameters. The correlation coefficient is approximately -0.685. This suggests a moderate association between an increase in clay content and a decrease in permeability, indicating that the increased presence of clay in the reservoir rock matrix tends to reduce its ability to allow fluid flow.

- Corrélation Porosité - Ciment Argileux (Fig. 51)

The correlation analysis between clay volume and porosity reveals a weak inverse correlation vertically between these two parameters. The correlation coefficient is approximately -0.063. This indicates that there is a slight tendency for porosity to decrease with increasing clay volume, although this relationship is weak.

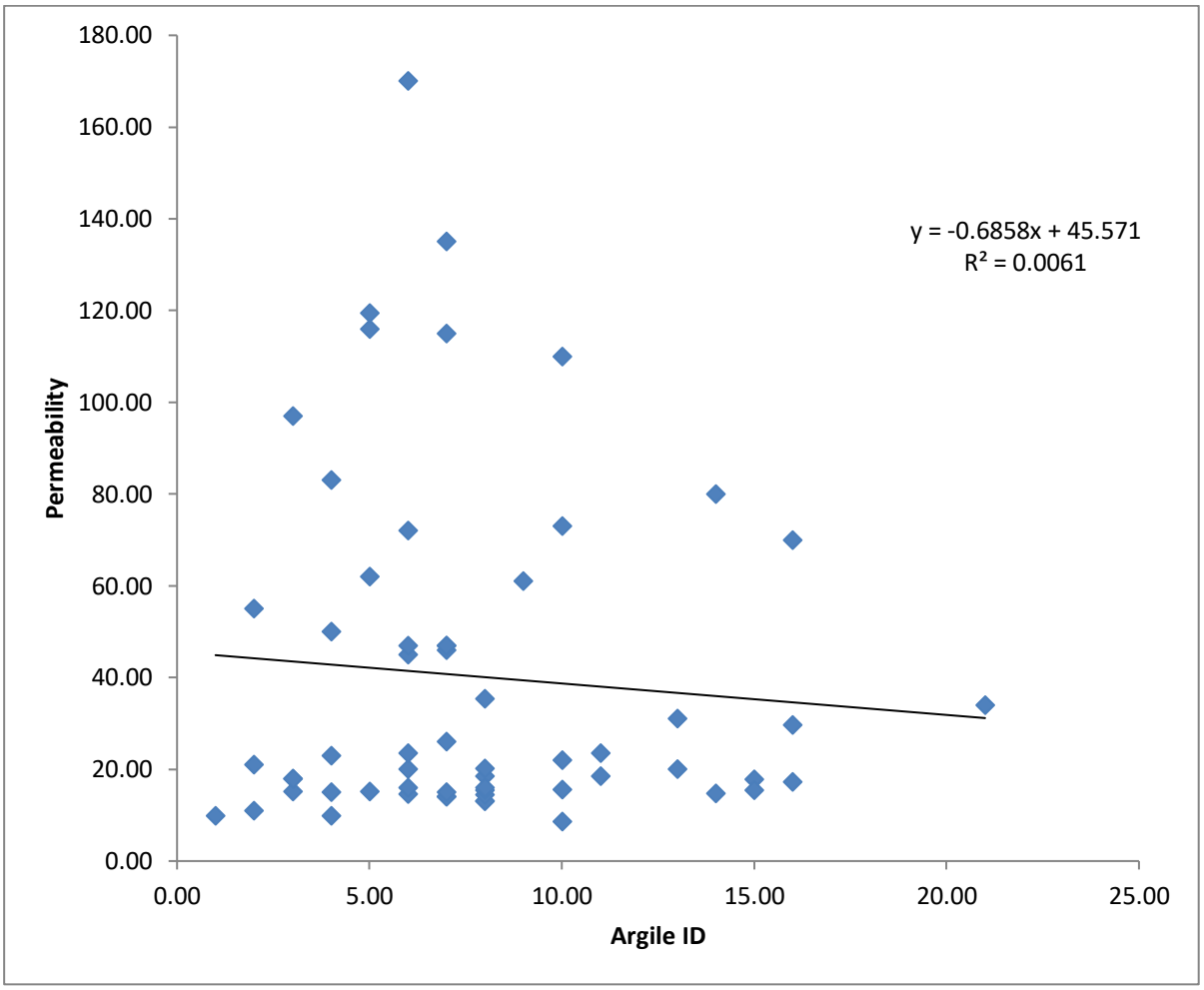

Fig. 50: Permeability-Clay Cement Correlation for Inter-Drain (ID)

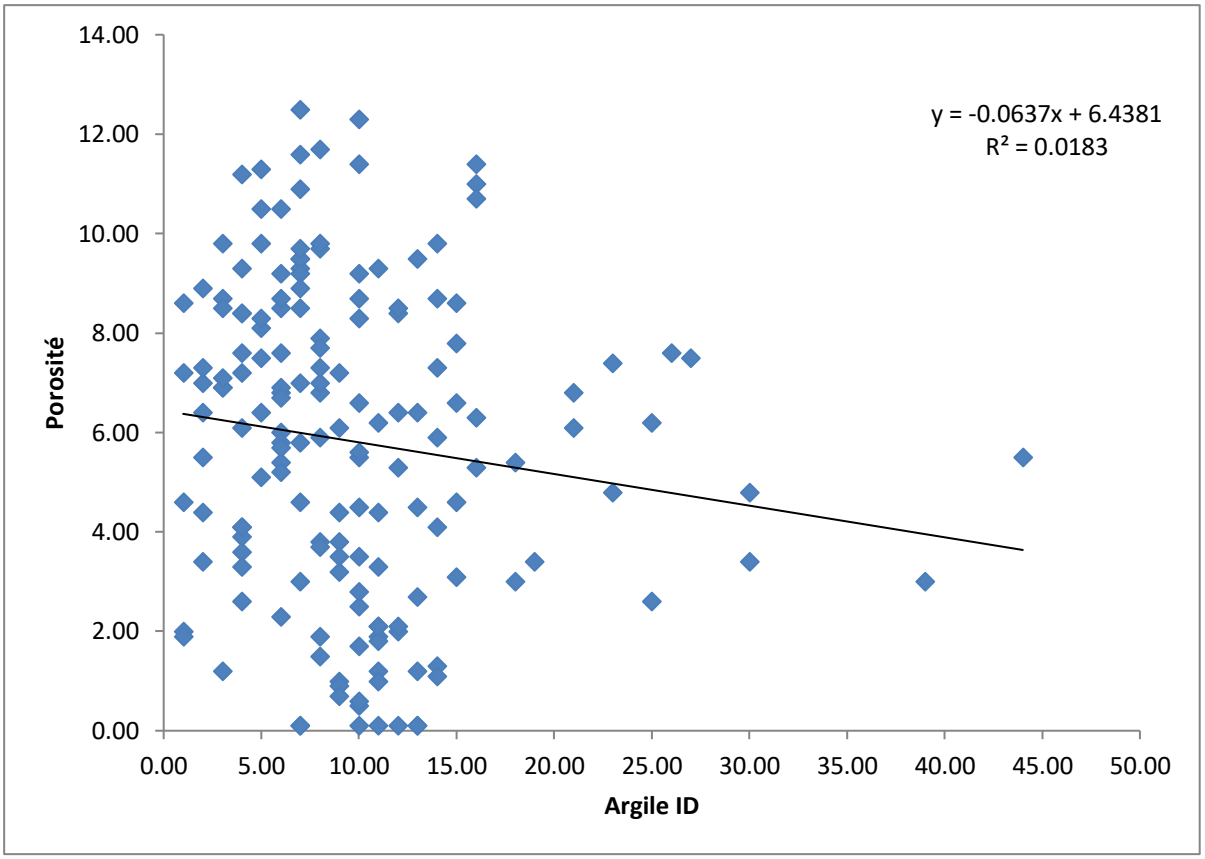

Fig. 51: Porosity-Clay Cement Correlation for Inter-Drain (ID)

Permeability - Siliceous Cement Correlation (Fig. 52):

In the correlation graph between permeability and siliceous cement presented below, a strong inverse relationship between these two parameters is clearly observed. This is reflected by a correlation coefficient of approximately -1.72. This value indicates a significant association between an increase in the presence of siliceous cement and a decrease in permeability, emphasizing that the accumulation of this type of cement, likely derived from secondary salinization processes, significantly impairs the reservoir's ability to allow fluid flow.

Porosity - Siliceous Cement Correlation (Fig. 53):

Similarly, in the presented graph, we observe an inverse relationship between siliceous cement and porosity, although the correlation coefficient is less significant, around -0.210. This correlation suggests a moderate association between increased siliceous cement and decreased porosity, indicating that the increased presence of this type of cement, likely associated with secondary salinization processes, reduces the amount of void spaces in the reservoir rock.

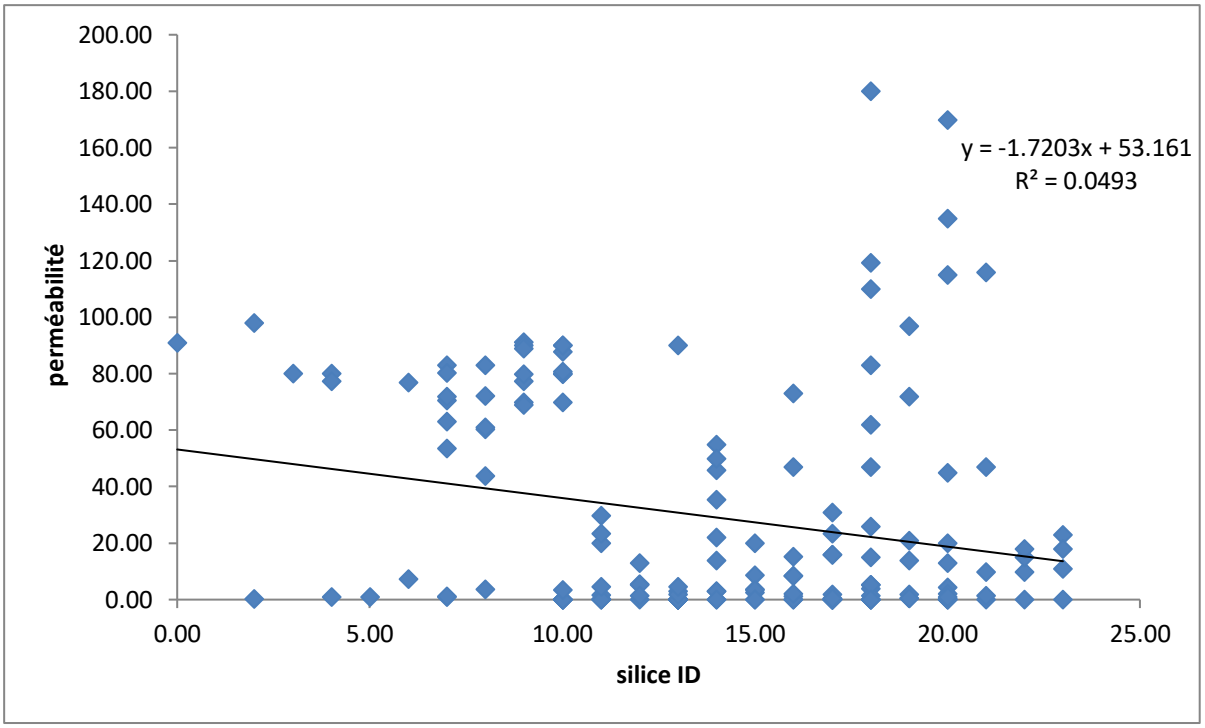

Fig. 52: Permeability-Silica Cement Correlation for Inter-Drain (ID)

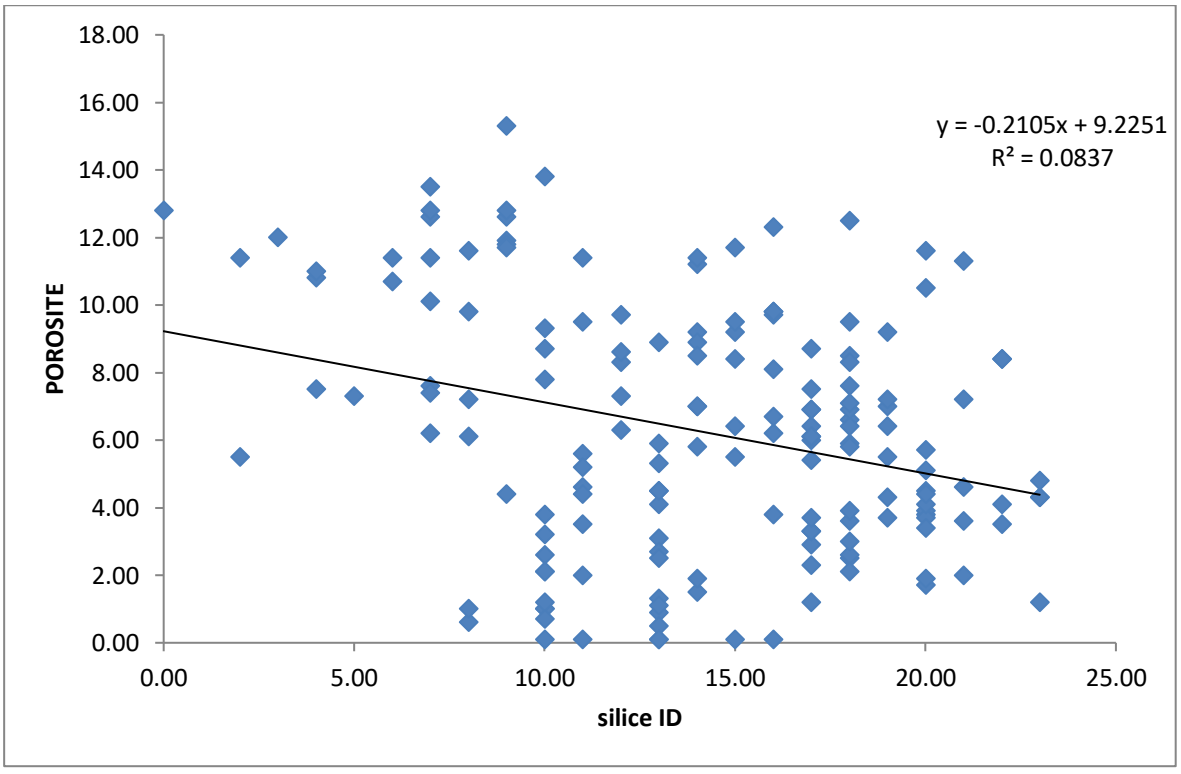

Fig. 53: Porosity-Silica Cement Correlation for Inter-Drain (ID)

6.3. D1 Drain

Permeability - Porosity Correlation (Fig. 54)

The correlation presented in the figure below (Fig. 54) highlights a moderate relationship between permeability (K in mD) and porosity (Φ in %). The correlation coefficient is 0.131. This indicates a moderate tendency for permeability to increase with increasing porosity, although this relationship is not very strong.

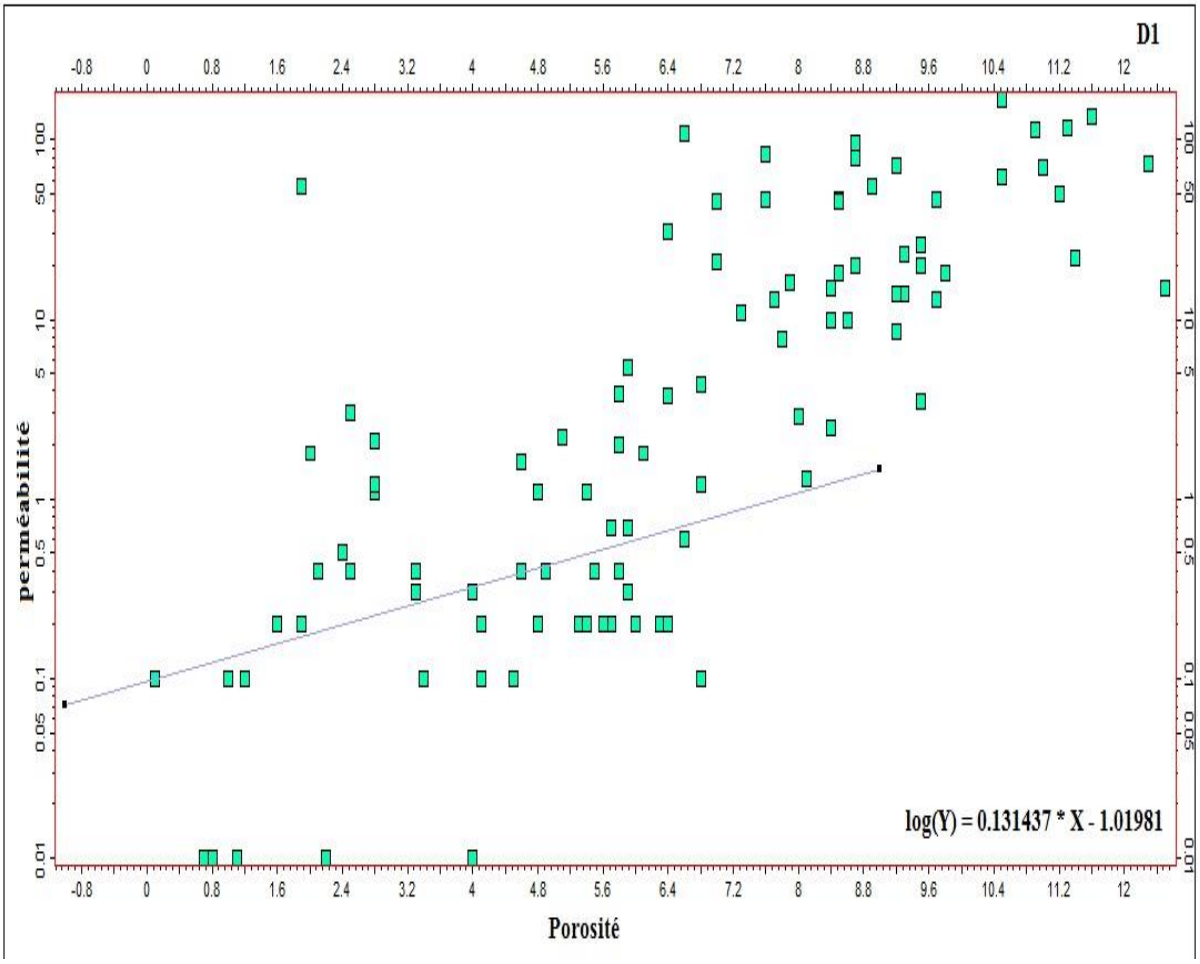

Fig. 54: Permeability-Porosity Correlation

2.3 Permeability - Clay Cement Correlation (Fig. 55)

The figure below illustrates an inverse relationship between permeability and clay cement, with a moderately high correlation coefficient of approximately -0.138. This correlation suggests a moderate association between increased clay cement and decreased permeability,

indicating that the increased presence of this type of cement, likely resulting from diagenetic processes, reduces the reservoir's capacity to allow fluid flow.

2.4 Porosity - Clay Cement Correlation (Fig. 56)

The correlation graph between porosity and clay cement reveals an inverse relationship between these two parameters. The correlation coefficient is weak, approximately -0.189. This indicates a moderate association between increased clay cement and decreased porosity, suggesting that the increased presence of this type of cement, likely resulting from diagenetic processes, reduces the amount of void space in the reservoir rock.

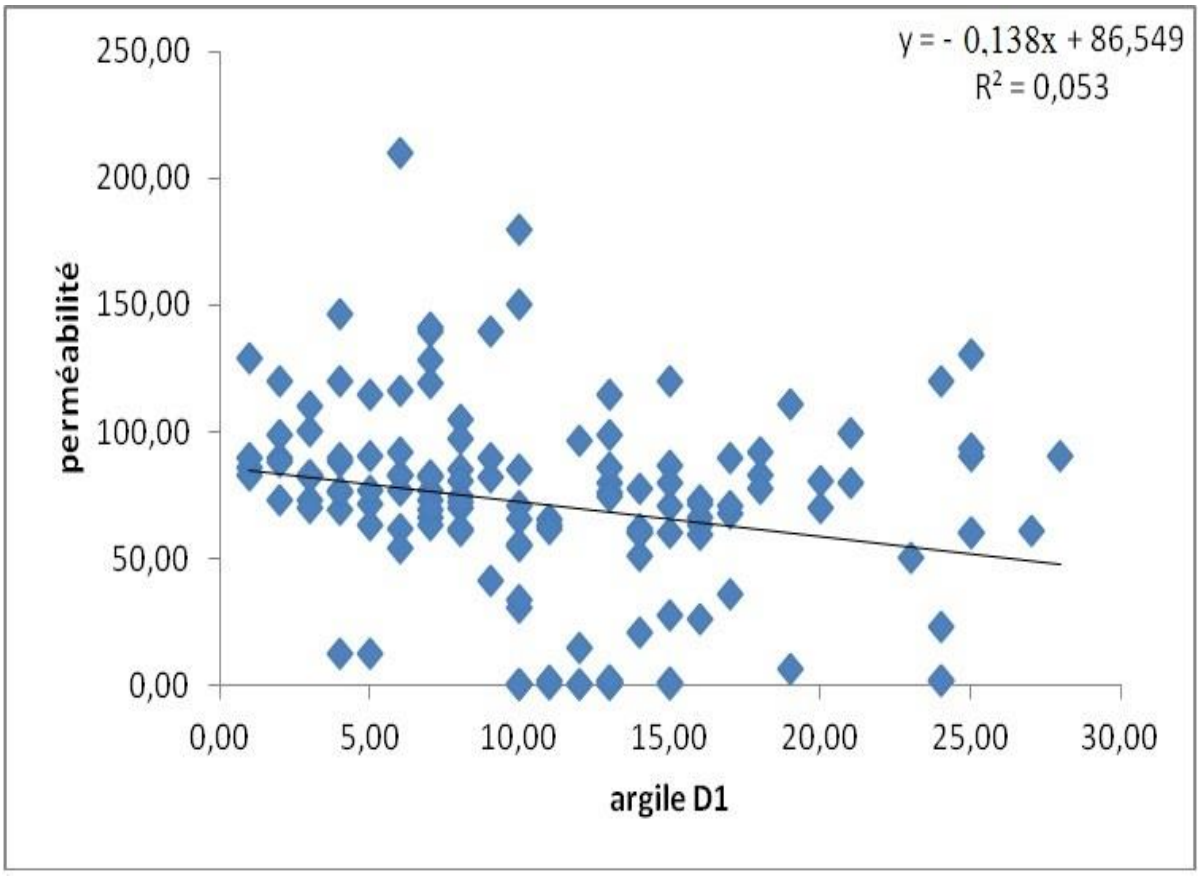

Fig. 55: Permeability-Clay Cement Correlation for Drain D1

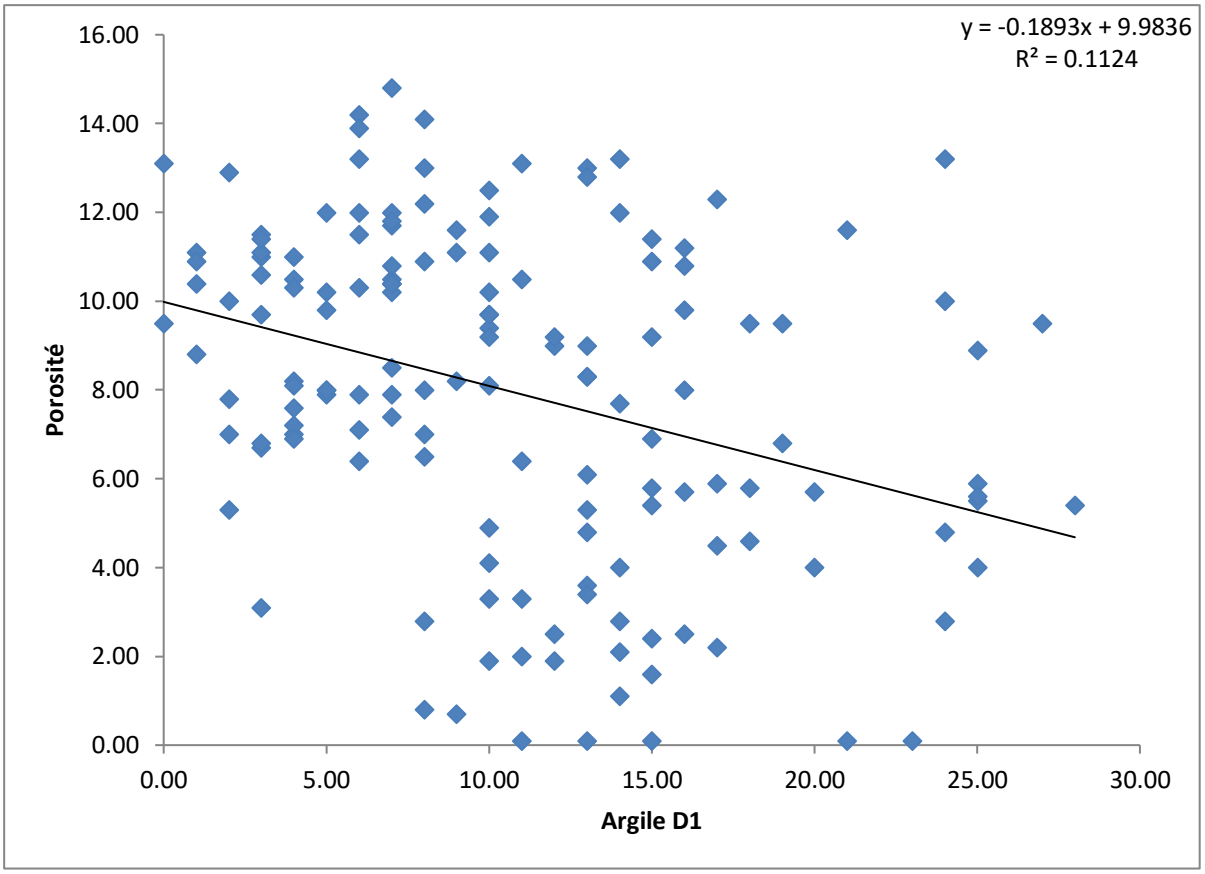

Fig. 56: Porosity-Clay Cement Correlation for Drain D1

2.5 Permeability - Siliceous Cement Correlation (Fig. 57)

The correlation between these two parameters, represented by the graph below, indicates a weak inverse correlation between them. The correlation coefficient is -0.111. This suggests a moderate association between increased D1 siliceous cement and decreased permeability, meaning that the increased presence of this type of cement tends to reduce the reservoir's capacity to allow fluid flow.

2.6 Porosity - Siliceous Cement Correlation (Fig. 58)

The correlation analysis between silica percentage and porosity reveals a favorable proportional relationship between siliceous cement and porosity. The correlation coefficient obtained is approximately 0.256. This value suggests a moderate to strong association between increased siliceous cement and increased porosity, indicating that the increased presence of this type of cement promotes an increase in the quantity of void spaces in the reservoir rock.

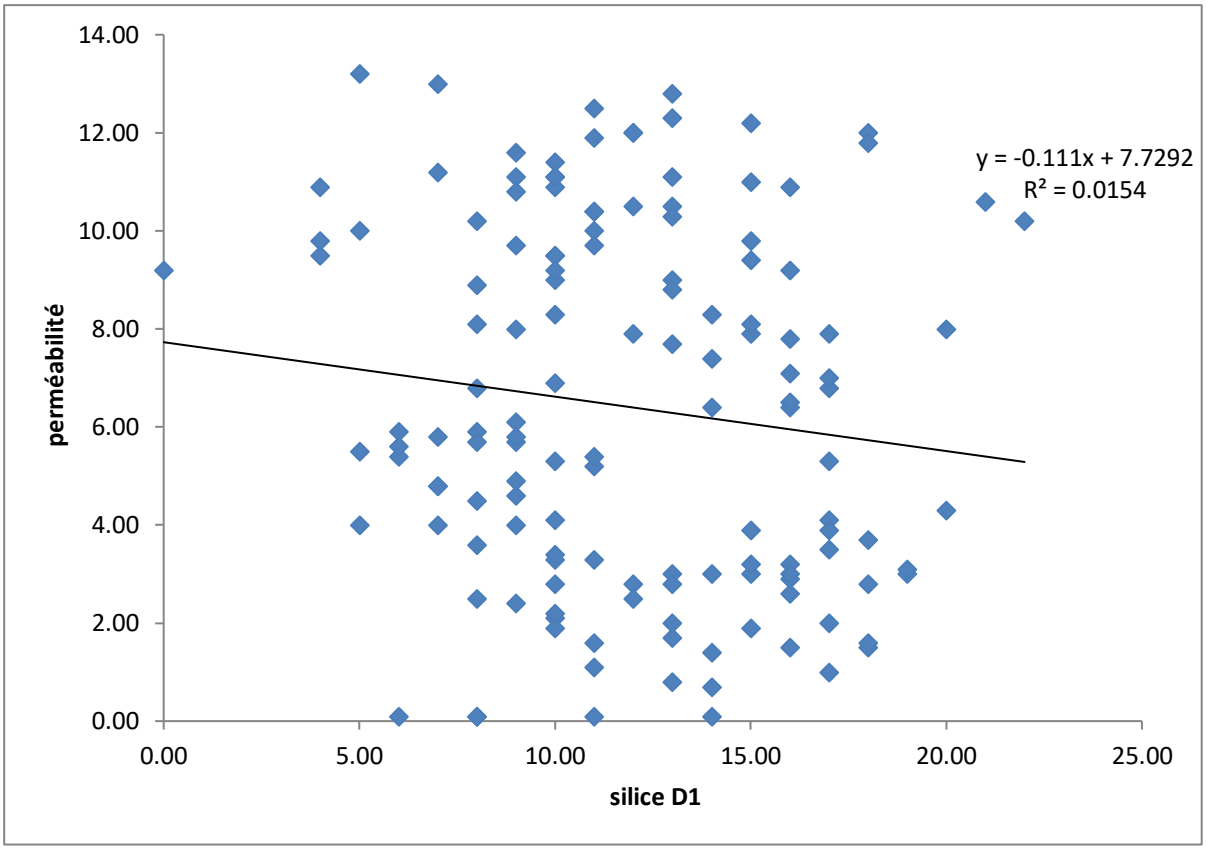

Fig. 57: Permeability-Silica Cement Correlation for Drain D1

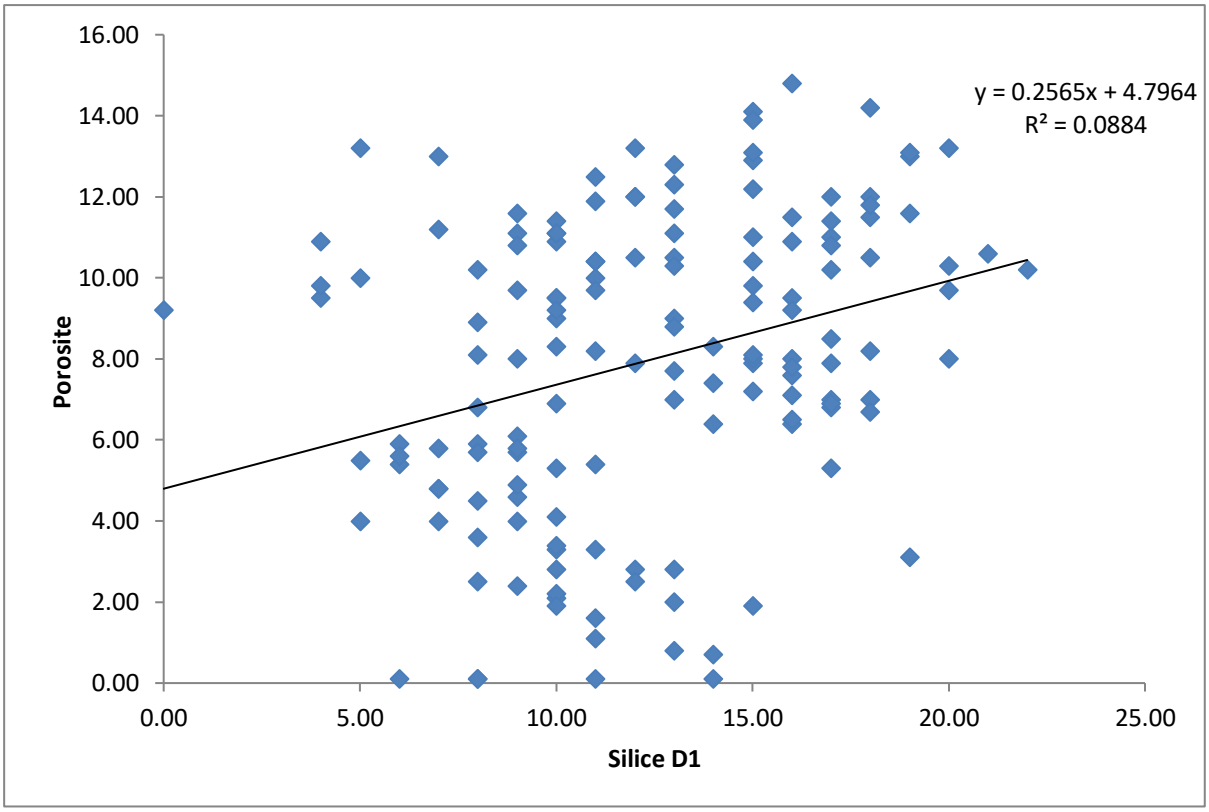

Fig. 58: Porosity-Silica Cement Correlation for Drain D1

6.4. Lithozone R2ab

2.7 Permeability - Porosity Correlation (Fig. 59)

The figure below illustrates a weak relationship between permeability (KmD) and porosity (Φ in %). The correlation coefficient is approximately 0.095. This indicates a slight association between increased permeability and increased porosity, although this relationship is not very strong..

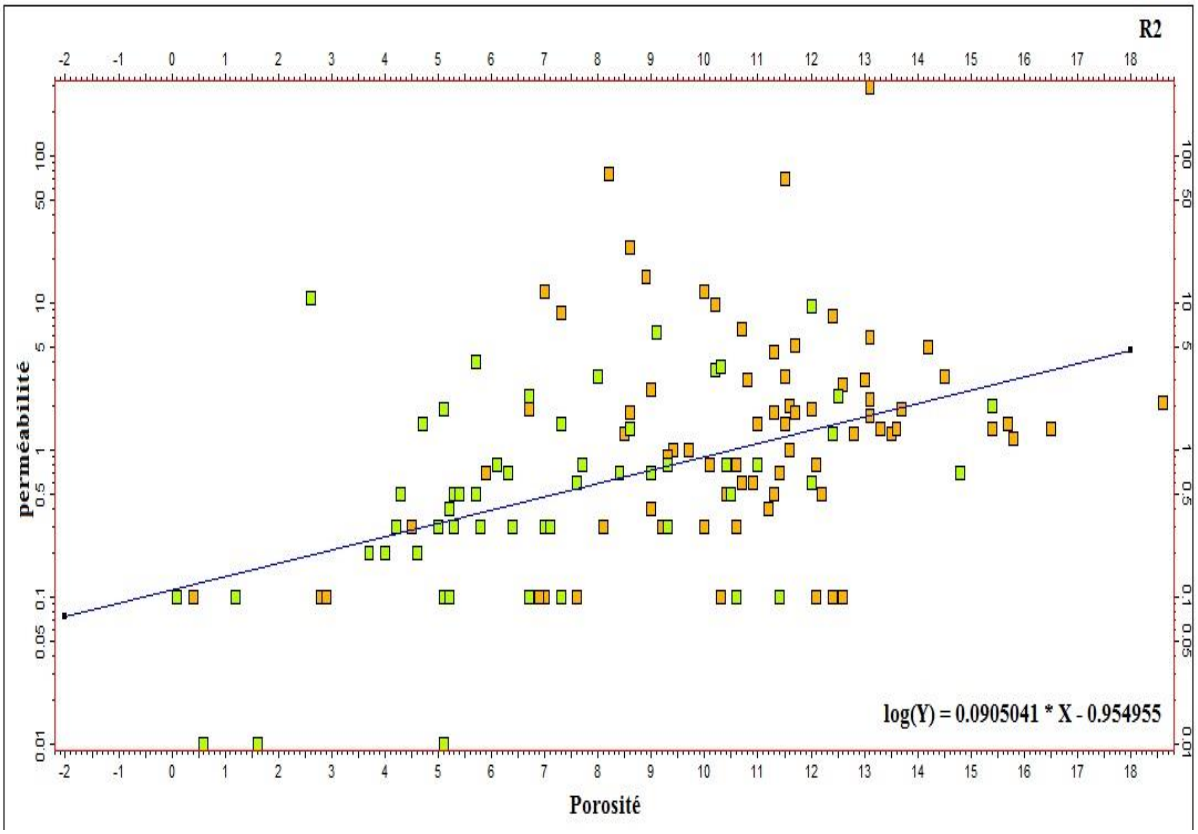

Fig. 59: Permeability-Porosity Correlation

2.8 Permeability - Clay Cement Correlation (Fig. 60)

The graph below, representing the correlation between permeability and clay cement, demonstrates an inverse relationship between these two parameters. The correlation coefficient is -0.458, indicating a moderate relationship between them. This suggests that an increase in the presence of clay cement generally leads to a decrease in permeability, meaning

that the reservoir's capacity to allow fluid flow is reduced when clay cement is more abundant.

2.9 Porosity - Clay Cement Correlation (Fig. 61)

The relationship between porosity and clay cement, as indicated by the correlation between these two parameters, demonstrates a direct and proportional relationship. The correlation coefficient is 0.090. This suggests a slight association between increased clay cement and increased porosity, indicating that when the proportion of clay cement increases, the porosity of the reservoir rock tends to increase as well, although this relationship is not very strong.Fig. 60: Permeability-Clay Cement Correlation for Lithozone R2

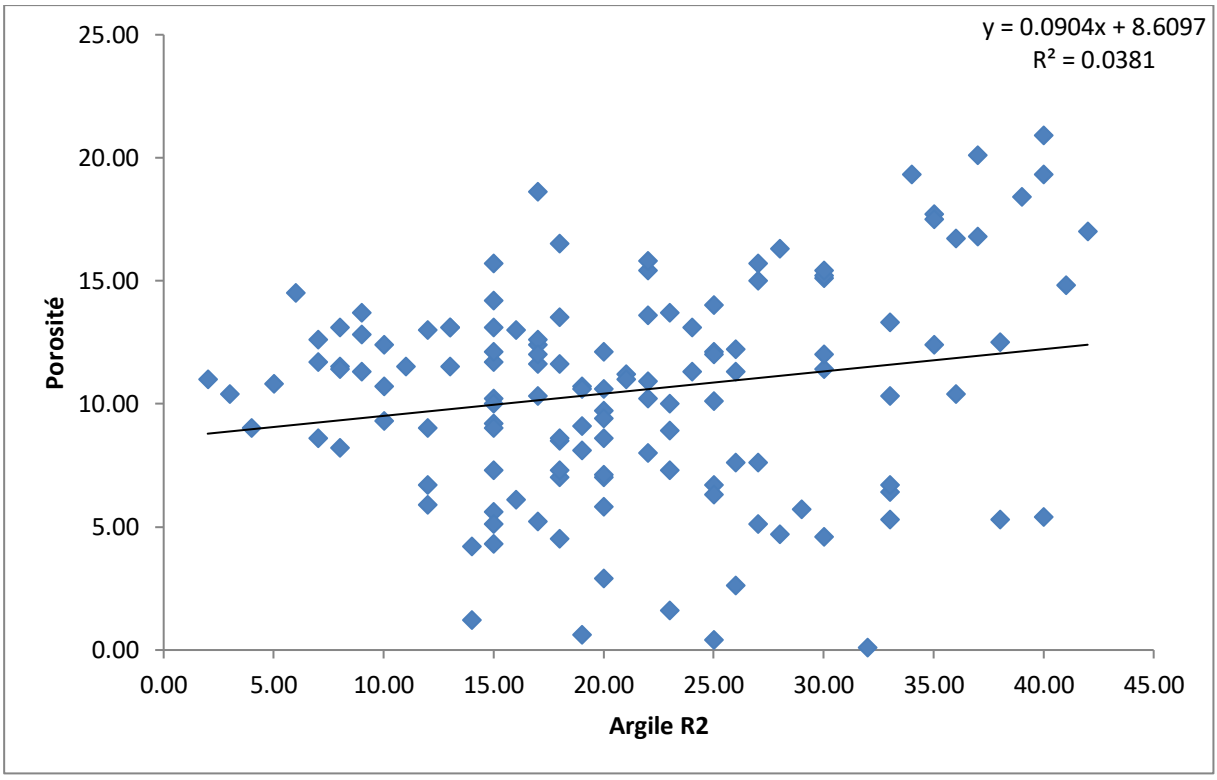

Fig. 61: Porosity-Clay Cement Correlation for Lithozone R2

Permeability - Siliceous Cement Correlation (Fig. 62):

The figure below, illustrating the correlation between permeability and siliceous cement, highlights the detrimental role of silica in permeability evolution. Their variation is inversely proportional, with a correlation coefficient of approximately -0.519. This correlation indicates that an increase in the presence of siliceous cement generally leads to a decrease in

permeability, meaning that the reservoir's ability to allow fluid flow is reduced when siliceous cement is more abundant.

Porosity - Siliceous Cement Correlation (Fig. 63):

The graph below, illustrating the correlation between porosity and siliceous cement, reveals a moderate inverse relationship between these two parameters, with a correlation coefficient of -0.390. This correlation underscores the detrimental effect of silica on porosity. It suggests that an increase in the presence of siliceous cement is generally associated with a decrease in reservoir rock porosity, reducing the amount of void space available for fluid storage.

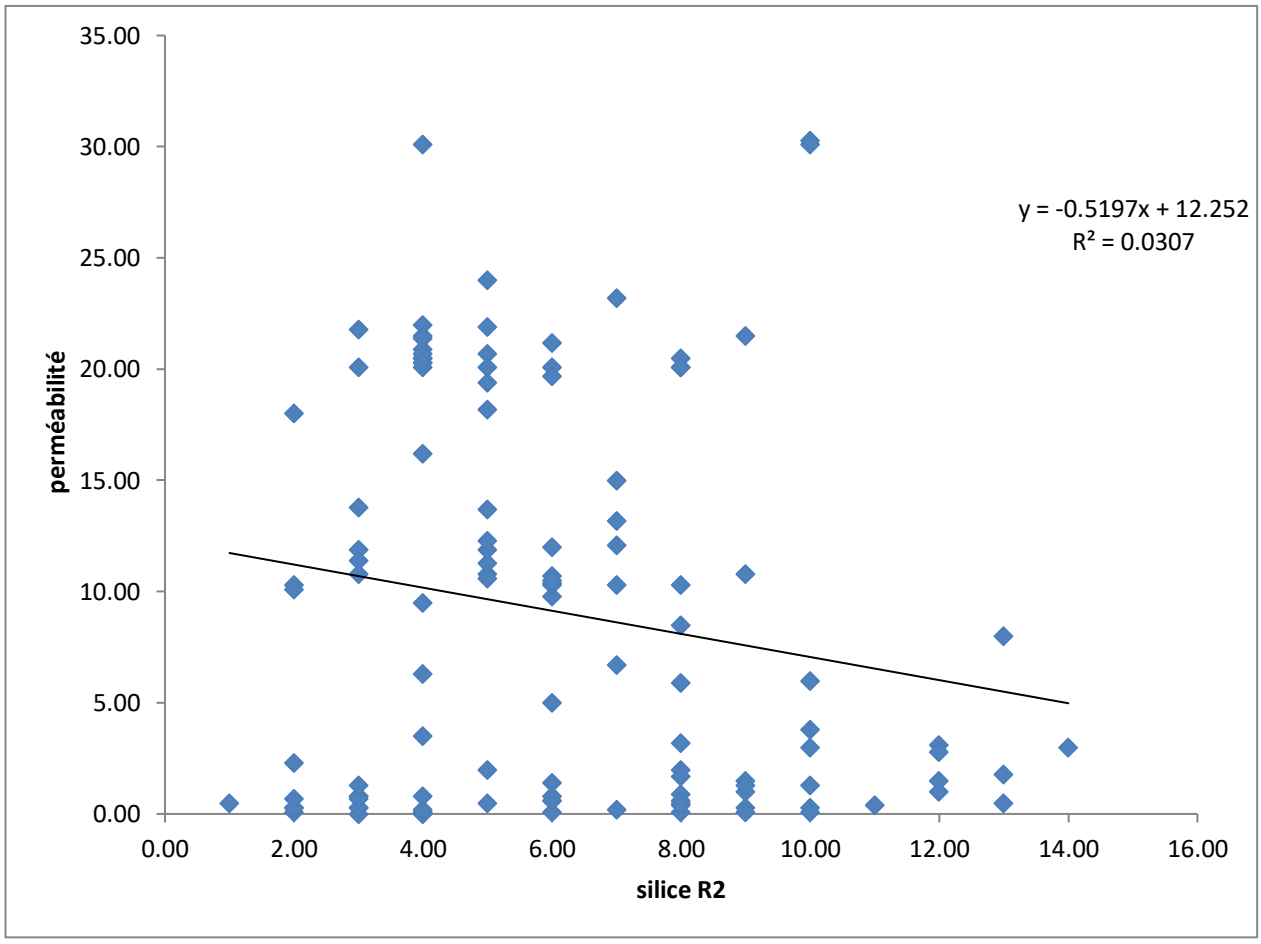

Fig: 62 - Permeability - Siliceous Cement Correlation in R2

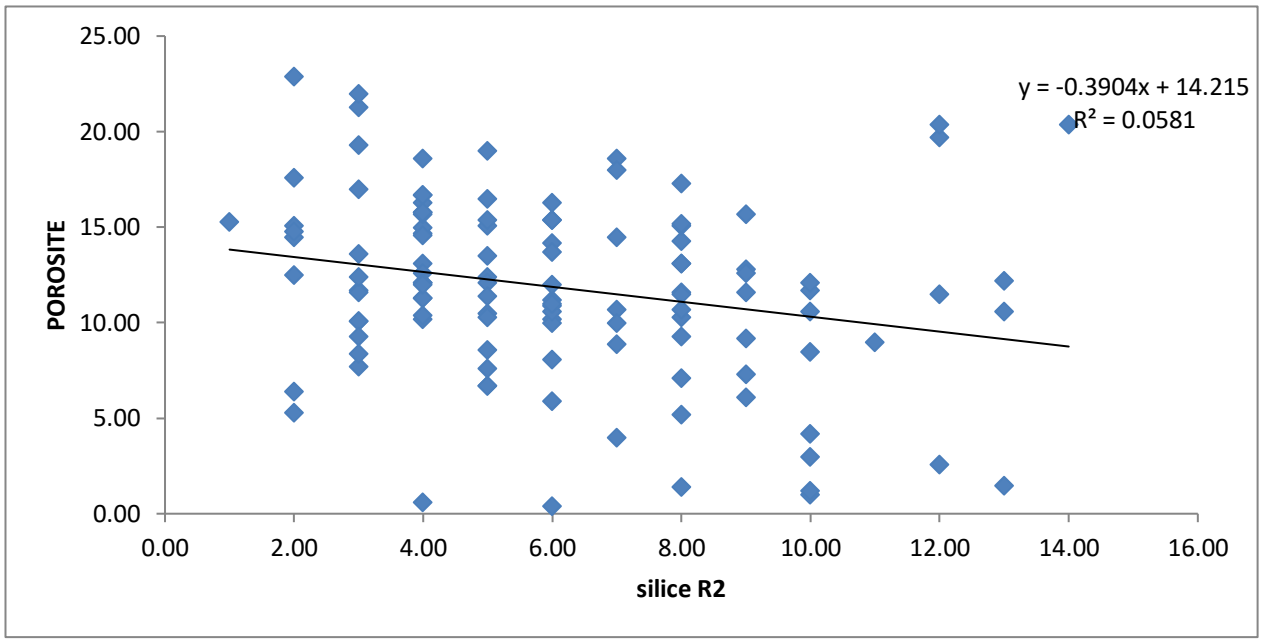

Fig: 63 - Porosity - Siliceous Cement Correlation in R2

Conclusions

Through this study, we have identified the types of relationships between petrographic parameters and petrophysical characteristics. Here are the key points summarizing these relationships:

Permeability (KmD) - Porosity (Φ %) Relationship:

- There is a linear proportional relationship between permeability and porosity. This relationship varies in intensity depending on the studied zones, being weak in R2ab, moderate in D1, and quite strong in D2 and ID. Thus, these two properties generally evolve in the same direction.

Clay Cement:

- The relationship between permeability and clay cement is inverse in all drains, especially in R2ab and D1. In ID and D2, its effects are less pronounced. This difference can be attributed to the composition of the clay, which is mainly illitic in R2ab and probably kaolinitic in the other zones.

- The relationship between porosity and clay cement varies among drains. In R2ab and D2, it is weakly proportional, while in D1 and ID, it is inversely proportional.

Siliceous Cement:

- The relationship between permeability and siliceous cement is inverse in all drains, but with different correlation coefficients. This relationship is stronger in D2 and ID due to the increased presence of secondary silicification phenomena in these areas.

- The relationship between porosity and siliceous cement is generally inverse and linear but varies in intensity among zones. In D1, there is a weak directly proportional relationship between these two parameters.

In summary, these results highlight the importance of different types of petrographic cements in determining the petrophysical properties of reservoirs, as well as the variability of these relationships across the studied geological zones.

2. Partial Conclusions

At the end of this study, several observations were formulated, summarized as follows:

- **Structural and stratigraphic model*:***

- Presence of major faults, notably a SW-NE direction, affecting Paleozoic series with a northern uplifted part and a southern depressed part.

- Pronounced Hercynian erosion, even affecting locally the D2 level, with valleys filled with eruptives on the southern border.

- Four wells reached the water zone, with a sw65% surface at an absolute elevation of -3273m.

- **Property model:**

- Porosity follows a normal distribution, suggesting homogeneity in its distribution.

- Permeability varies rapidly vertically and horizontally, showing a bimodal distribution, indicating heterogeneity.

- The best reservoir properties are found in the north, northwest, southwest, and east sectors.

- The best drainage areas are drains D2 and ID, while R2 is characterized by poor to low properties.

- Gas breakthroughs are mainly observed in drains D2 and ID, while drain D1 primarily produces oil with a small amount of gas.

- Siliceous cement, derived from secondary silicification, degrades reservoir properties in almost all drains.

- The relationship of clayey cement with permeability varies among drains: linearly proportional in R2ab and D2, and inverse in D1 and ID.

- Interpretation of imaging logs reveals a dominant NE-SW fracture direction, likely closed, and a secondary NNE-SSW and N-S direction, potentially open and beneficial for fluid flow.

These observations provide a comprehensive understanding of the geology and reservoir properties, essential for the evaluation and efficient exploitation of petroleum resources.

Recommendations

- Based on the observations resulting from this study and considering the production challenges encountered in zone 20a, several solution proposals have been formulated, including:

- Conducting Production Logging Tool (PLT) operations on other wells to monitor gas evolution in the reservoir and identify breakthrough zones more accurately.

- Investigating the possibility of sealing gas leaks if technically feasible.

- Proposal for converting a well to Short Radius drilling:

- Well MD134 was drilled and completed in October 1970 with 2’’7/8 x 2’’3/8 casing suspended and a 5’’ Hyd. position gravel pack.

- From its production start until 1988, MD134 underwent wireline checks 3 to 4 times per year and water shut-offs for maintenance. During this period, the oil flow from the well showed instability contrary to the Gas-Oil Ratio (GOR).

- Samples taken in 1973 revealed primarily sedimentary deposits, but samples from 1996 showed a predominantly saline composition.

- MD134 underwent two stimulation operations:

- Hydraulic fracturing in February 1995, which had no significant effect. Perforations were made at the following depths: 3300m-3306m, 3312m-3324m, 3332m-3338m.

- Acidizing in September 2002, which also had no effect.

- After the negative results of the previous operations, the well was re-entered in Short Radius drilling mode in zone D1, between 24/05/2007 and 03/07/2007, with the following parameters:

- Target: Depth between 3343m and 3357m

- Azimuth: North 109°

- Vertical depth: 368.28m

- After drilling in Short Radius (SR) mode, the well was completed with 4"1/2 Anchored Reservoir casing, covered with a pre-perforated Liner.

4. Analysis of MD134 Production Results after Conversion to Short Radius.

Formation Test Results for this Well are as Follows:

Type de Test	Date	Pression (kg/cm²)			Débit (m³/h)		Index Prod.|Inj.	HK			Skin	Duse	Remarque
		Gisement	Fond Dyn.	Tete				Proche	Lointain	(Hw * Kyz)			
DST	10/07/2007	254.49	211.18	138	Huile	2.11	.056	-	90	-	2.2	9.53	Repris en short radius dans le D1, Vs 368 m, Az N109, Inc 91

Table No. 9: Formation Test Results Conducted on this Well

The petroleum results obtained are significantly unsatisfactory, primarily due to the well encountering a fault, resulting in the displacement of the drain out of the initially targeted zone, from the base of D1 to an area with poor reservoir properties. This is clearly illustrated in Figure...

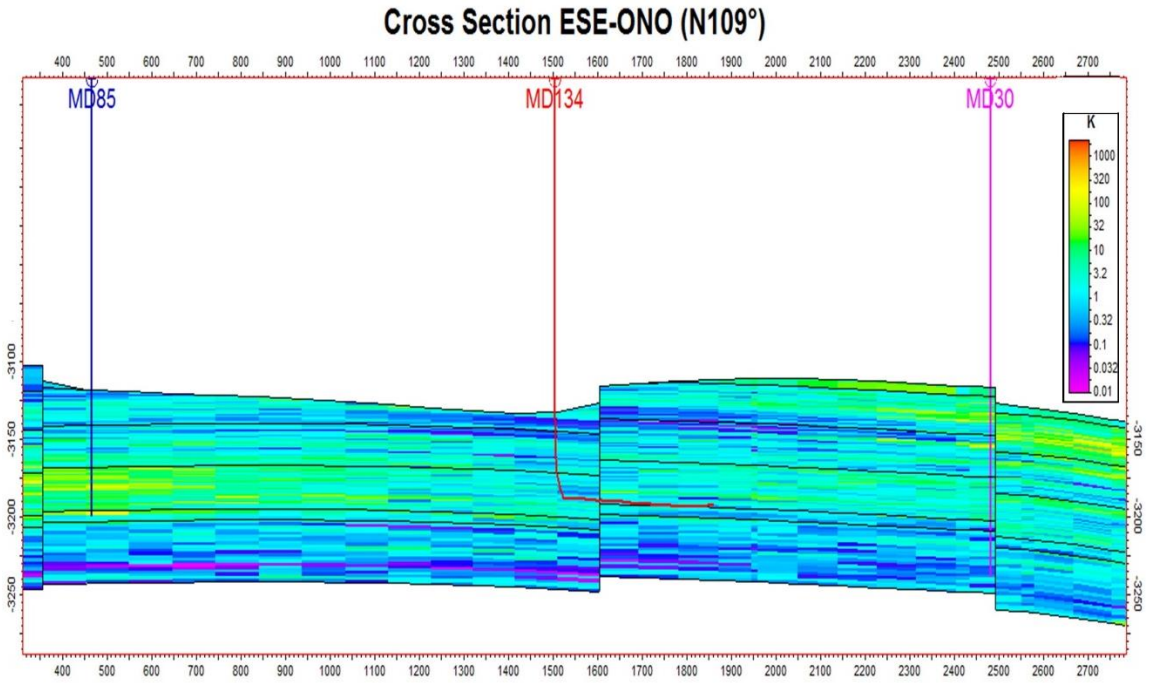

Figure 64: Cross-section ESE-ONO (N109°).

The new proposal is as follows:

The selected target is Drain D1, while zones D2 and ID represent gas breakthrough areas. Since the reservoir properties are significantly better in the opposite direction to the current one, and there is no fault in that direction, it is wiser to reorient well MD134 in this same direction, towards N292º. MD134 is located in an area with unfavorable petrophysical characteristics. Therefore, to surpass this zone, it is necessary to move more than 350 meters away from the well to reach an area with more advantageous properties towards the west-northwest, between MD85 and MD575 (see Fig... and Fig...).

- Good permeability to the North, Northwest, Southwest, and East.

- Poor permeability to the South and along the WSW-ENE axis.

A cross-section depicting the permeability profile, the direction of the first drain, as well as the target and direction of the projected new drain.

Figure 64 shows a cross-section from one to the east-southeast (N292°).

New conversion parameters:

Objective: D1

Target: 3348m – 3353m

Azimuth: N292º

Vs: 350m

Note:

- VS: Vertical Section corresponds to the projection of the drain onto a horizontal plane. Its length equals the distance measured from the vertical to the total depth in TVD (True Vertical Depth).

- Target: Targeted formation and interval.

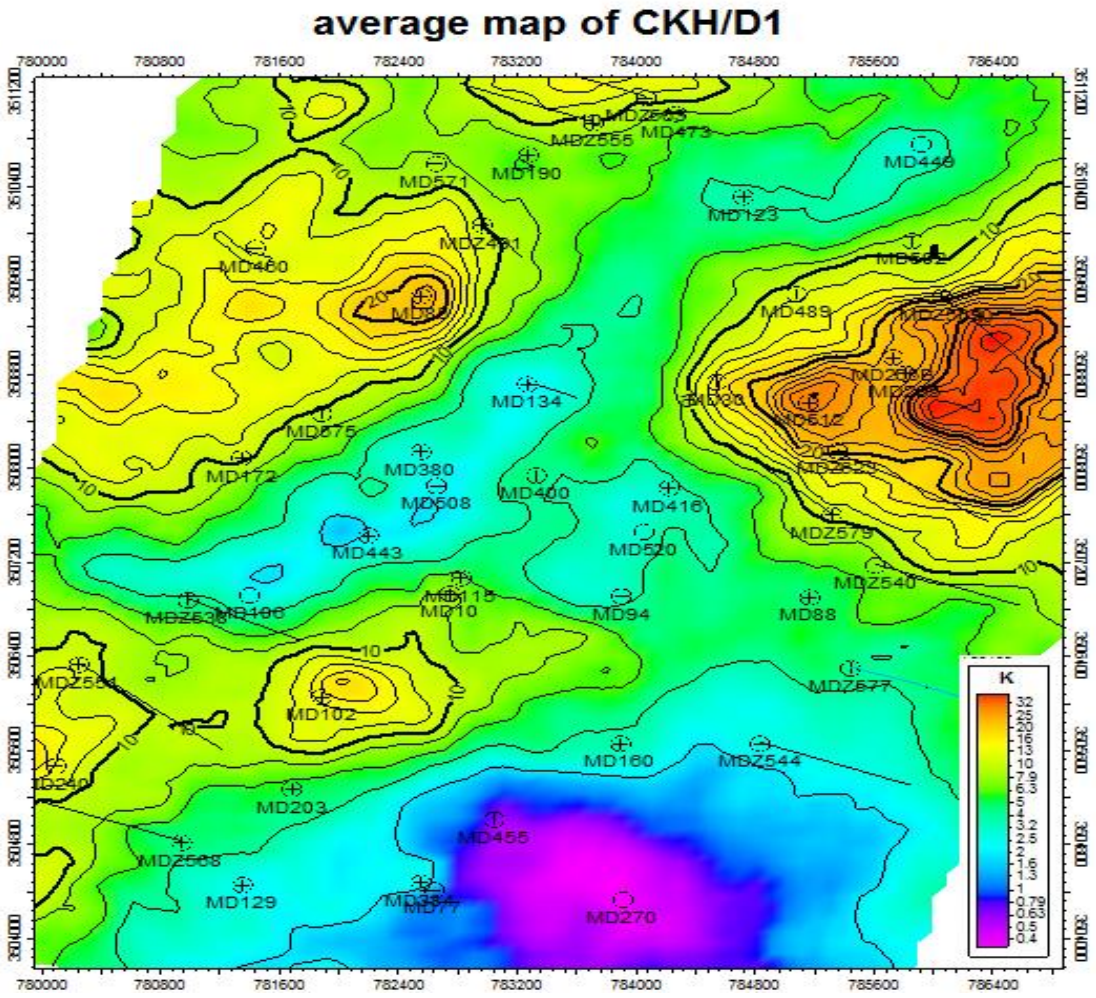

Fig. 65: The permeability contour map shows the spatial distribution of K (mD).

General conclusion

The overall geology and reservoir characteristics of Zone 20a in the Hassi Messaoud Field are the subject of this study. The first part of the work examines the geological makeup and reservoir properties of Zone 20a within the Hassi Messaoud field. Zone 20a is situated in the central region of the field, displaying intricate geological characteristics and a stage of production that is gradually approaching maturity.

The following section will present the key geological aspects of the area under consideration.

The Zone 20a is situated along a significant northeast-southwest trending fault, which has resulted in the division of the zone into uplifted and subsided regions. Furthermore, the structure is further complicated by the presence of various faults with varying orientations and magnitudes. The Hercynian erosion phase had a profound impact on the zone, creating deep valleys and exposing underlying formations.

The primary reservoir units in Zone 20a are Drains D1, ID, D2, and R2ab, which are encountered by the majority of wells. Drains D4 and D5 are present only in the southernmost part of the area. Erosion has differentially affected the various drains, with the upper sections (D3, D4, D5) being more susceptible.

The substantial erosion, particularly in the northern part of the zone, has significantly altered the original structural configuration and reservoir thickness. The southern portion of the reservoir exhibits a less eroded structure with a southward dip.

The water level is as follows: The water table (SW = 65%) is of paramount importance for the optimal production of hydrocarbons. The average water table depth, as estimated from well data, is -3273 meters in absolute elevation.

The stratigraphy of the area in question is as follows: The principal reservoir units, arranged from the lowest to the highest point, are as follows:

R2ab (secondary reservoir) is composed of coarse sandstone with micro-conglomerates and oblique bedding. The Drain D1 is composed of coarse sandstone with a dominant arched oblique bedding pattern, which is often micro-conglomeratic at the base. The Drain ID: This is a transitional zone between D1 and D2, characterized by an increased silt content and the presence of Tigillites. The Drain D2 is characterized by well-sorted coarse sandstone with dominant tabular oblique bedding and interspersed silt layers. The Drain D3 (present in southern and central parts) is composed of fine to medium sandstone, which is rich in silt beds and bioturbations.

Drains D4 and D5 (minimal presence) are composed of fine-grained sandstones with a limited lateral extent.

The diagraphic correlations (well log analysis) demonstrate a clear trend of increasing erosion from the southeast to the northwest, which corresponds to the structural uplift in the same direction. Conversely, minimal thickness variations are observed laterally within the uneroded drains.

Zone 20a presents a complex geological setting, with a faulted structure and significant erosion impacting the reservoir. The zone is currently undergoing depletion and requires production maintenance strategies such as gas injection. Future exploitation efforts may benefit from a characterization of petrophysical properties to identify zones with higher reservoir quality for potential infill drilling or well conversion.

The second part of this work presents a sedimentological analysis of six core drillings from Zone 20a of the Hassi Messaoud field. The core descriptions provide detailed information about the encountered rocks, including their lithology, grain size, color, and the presence of specific elements and structures. These observations are crucial for understanding the depositional environment of the reservoir.

The key findings include:

• Variations in grain size and composition were observed, with sandstones ranging from fine to very coarse-grained and quartzites exhibiting varying degrees of silicification.

• The presence of clay minerals was noted, suggesting a clayey composition in some zones.

• Color variations were identified, ranging from reddish-brown and gray to light and dark gray, which may indicate differences in weathering conditions.

The presence of fractures, often filled with minerals such as anhydrite, calcite, or pyrite, suggests diagenetic alterations and potential fluid flow paths. The identification of sedimentary structures, such as stratification and brecciation, aids in the reconstruction of depositional processes.

This work also highlights the results of Production Logging Tool (PLT) interpretation, which indicates that oil production is primarily concentrated in Drain D1, while gas breakthroughs are more frequent in Drains D2 and Inter-Drain (ID). Of interest is the observation that wells with high Gas-Oil Ratios (GOR) are situated in the central northern region with higher elevations relative to the main fault, suggesting a potential correlation between structural position and reservoir quality.

This work studies the petrophysical parameters of the reservoir, the correlations between them, and their impact on the reservoir.

• This study examines the petrophysical properties (porosity and permeability) of the Cambrian reservoir in the Hassi-Messaoud field, Algeria, with the objective of understanding how these properties influence hydrocarbon production.

• Petrophysical properties are measured in the laboratory using core samples and estimated using well logging tools.

The distribution of porosity across all drains (D2, ID, R2ab, and D1) is unimodal, indicating a single dominant pore size range. The median and average porosities are similar across the drains, with slight variations attributed to geological factors. In contrast, permeability exhibits greater heterogeneity compared to porosity, showing a bimodal distribution in all drains. This suggests the presence of two distinct permeability ranges within the reservoir, likely due to variations in grain size and the presence of natural fractures. Overall, reservoir quality can be classified as moderate, with porosity ranging between 5% and 11% and permeability varying spatially. Matrix permeability ranges from 0.1 mD to 100 mD, but fractured zones can exhibit significantly higher permeability. Fractures are believed to play a key role in hydrocarbon production.

The study also examines the impact of geological characteristics (grain size, sorting, and cementation) on petrophysical properties. Clay and silica cements are the primary components influencing porosity and permeability in Cambrian sandstones. An increase in clay cement content is associated with a reduction in both porosity and permeability, while an increase in silica cement (likely due to secondary salinization) is linked to a significant decrease in permeability and a moderate decrease in porosity.

Bibliographicreferences

[1] F. Baadi, H. Boughebache, Etude et Analyse des Paramètres Pétrophysiques de la Zone 14 (Hassi Messaoud), in: Département des Sciences de la Terre et de l'Univers, Université de Kasdi Merbah, Ouargla, Algérie, 2023, pp. 101.

[2] R. Lasmi, Caractérisation des Quartzites de Hamra dans les gisements de Hassi Terfa, Hassi D'zabat et Hassi Guettar : Pétrophysique, Fracturation et Modélisation, in: Faculté des Hydrocarbures et de la Chimie, Université M'hamedBougara, Boumerdès, Algerie, 2013, pp. 151.

[3] H. Aït-Salem, Le Trias détritique de l'Oued Mya (Sahara algérien) : sédimentation estuarienne, diagenèse et porogenèse, potentialités pétrolières, in, Université Lyon-1, France, 1990, pp. 1 vol. (162 p.-[110] p. de pl.-[162] dépl.).

[4] O. Bachi, A. Rebih, A. Benglia, Evaluation des Paramètres Pétrophysiques de la Zone N°13 (Région Hassi Messaoud), in: Département des Sciences de la Terre et de l'Univers, Universite Kasdi Merbah, Ouargla, Algerie, 2021, pp. 84.

[5] SONATRACH, Découpage en drain du Cambrien de Hassi Messaoud in, CRD, Internal Report 2005.

[6] S. Zerroug, Bounoua, N., Lounissi, R., Zeghouani, R., Djellas, N., Kartobi, K., Etchecopar, A., Tchambaz, M., Abadir, S., Simon, P., Fuller, J.,, Well Evaluation Conference Algeria, in: Schlumberger (Ed.), Schlumberger, 2007, pp. 489.

[7] A. DokkaMurty, Sedimentological study of cores: Methodology and Eléments of Study, in: SéminaireGéologiepétrolier SONATRACH.

[8] H. Benessam, Caractérisation et modélisation du réservoir cambro-ordovicien de la zone 23 du champ de Hassi Messaoud, in: Département des Sciences de la Terre et de l'Univers, Département des sciences de la terre et de l'univers, Faculté des sciences de la nature et de la vie et sciences de la terre et de l'univers, Université Abou Bekr Belkaid-Tlemcen, 2016.

[9] A. L'Homer, Bull. Ser Géol. Algérie, Alger, 35 (1967).

[10] A. Trabelsi, N. Kriker, A. Ghedairi, Caractérisation Pétro-physique d'un Réservoir cambro-ordovicien de la zone 13 du champ HMD Par l'utilisation de Diagraphies et des Mesures sur Carottes, in: Département des Sciences de la Terre et de l'Univers, Université de Kasdi Merbah, Ouargla, Algérie, 2019, pp. 93.

[11] Beicip-Franlab, Révision du modèle géologique du champ de Hassi Messaoud, in, CRD-SONATRACH, Internal report 1995.

[12] Beicip-Franlab, Caractérisation et évaluation des réservoirs ordoviciens de pourtours de Hassi Massaoud in, DEP-SONATRACH, Internal report 2007.

[13] BEICIP-FRANLAB, Petrophysical characterization of the Cambrian reservoir of the Hassi Messaoud field, in, Production Division of Sonatrach, Internal report 1995.

[14] Petrophysical technologies (Trytecompany).

[15] Petrophysical technologies (Weatherford company).

[16] Petrophysical technologies (Soxheletcompany).